Design and Experimental Evaluation of Compact RFID Tags for UHF RFID Applications

Abdulhadi E. Abdulhadi

Department of Electrical and Computer Engineering

McGill University

Montréal, Québec

August 2014

A thesis submitted to McGill University in partial fulfilment of the requirements of the degree of Doctor of Philosophy

© A. E. Abdulhadi, 2014

ACKNOWLEDGEMENTS

I would like to thank Professor Ramesh Abhari for all the guidance and advice she has given and continues to give me. I also would like to thank my family in Libya for their continued support, and for all the help they provided throughout my study. I am grateful to all my friends in Montréal for all the great times we had together. Thank you, Khaled Aljahime, Wadah Munner, Essa Hawassh, and all the others who make life here fun and interesting. Thank you to my family in Canada for always being by my side. Thank you my childern, Shahed, Arwa, Mohamed and Sufyan. Finally, I want to thank my parents, sisters, and brothers without whose support nothing would have been possible.

ABSTRACT

Radio frequency identification (RFID) has become one of the fastest growing wireless technologies. An RFID system is a real-time processor that enables the information stored on a tag to be tracked and exchanged remotely with an RFID reader. The RFID tag plays a critical role in determining the overall performance of the entire system, as well as its size, cost and detection range. In this thesis, various miniaturized RFID tag antennas are investigated and implemented for conventional and emerging passive ultra high frequency (UHF) RFID applications. First, the design and experimental evaluation of three compact printed tag antennas including folded, 2D and 3D meander monopoles are presented. Next, designing a new miniaturized tunable passive UHF RFID tag is undertaken with the operation frequency covering the entire range of the UHF RFID regulated bands (840-960 MHz). This design method not only can be used in tags targeting the global RFID market, but also is crucial for the successful implementation of an RFID system that is tolerant of detuning due to fabrication process variations and loading of deployment environment. As well, a low profile RFID tag consisting of a compact microstrip patch antenna backed by a mushroom-type Electromagnetic Band Gap (EBG) structure is proposed. This design which achieves an area reduction of 29.11% compared to a conventional patch yields a maximum reading range of around 11 m as a free standing tag and when attached to a metallic surface.

To extend the reading range of the RFID tag, a solar panel is integrated with the patch antenna to boost the RFID chip's operating power. Furthermore, new aspects

of antenna and RFID chip integration in multi-port/antenna arrangements are explored through the design and measurement of tag prototypes.

RFID technology has recently been employed in sensor applications for low-cost low-power wireless sensor node implementation. This thesis also presents novel dual-port UHF RFID tag antennas for simultaneous wireless identification and sensor applications. Special RFID tag antennas are designed and integrated with passive resistive sensors demonstrating detection of sensor data by utilizing a commercial RFID reader. Finally, another RFID-tag-sensor for transmission of generic sensor data is implemented, which also includes solar energy harvesting. This design is further improved by employing a novel two-port patch antenna that collects the ambient RF energy through its second port. A reliable RFID communication range of up to 27 m was achieved in an indoor measurement scenario, which represents, to the author's knowledge, the longest distance ever reported for similar sensor-enhanced RFID tags.

ABRÉGÉ

L'identification par radiofréquence (RFID) est devenue l'une des technologies sans-fil qui évoluent le plus rapidement. Un système RFID est un processeur en temps réel qui permet que l'information stockée sur une étiquette soit suivi et remplacée à distance à l'aide d'un lecteur RFID. L'étiquette RFID est un facteur déterminant pour la performance d'un système ainsi que pour sa taille, son prix et sa portée. Dans cette thèse, plusieurs antennes d'étiquette RFID miniatures sont évaluées et mises en uvre pour des applications RFID à ultra haute fréquence (UHF RFID) conventionnelles et émergeantes passives. Premièrement, la conception et l'évaluation expérimentale de trois antennes d'étiquette compactes imprimées, incluant une antenne unipolaire en serpentin pliée, 2D et 3D, sont présentées. Ensuite, la conception d'une nouvelle étiquette UHF RFID miniature accordable est menée avec une fréquence d'opération couvrant l'intervalle entier des bandes UHF RFID (840-960 MHz). Cette méthode de conception peut non seulement être utilisée pour les étiquettes visant le marché RFID global, elle est cruciale pour le succès d'un système RFID qui est tolérant envers les désaccords dû à la fabrication et son chargement dans l'environnement de déploiement. De plus, une étiquette RFID à profile bas consistant en une antenne compact à microbande avec une structure de bande interdite électromagnétique (EBG) de type champignon est proposé. Cette conception qui a une aire 29.11% plus petite que les microbandes conventionnelles démontre un intervalle de lecture maximum de 11 m lorsque l'étiquette tient par elle-même et lorsqu'elle est attachée à une surface métallique.

Pour augmenter l'intervalle de lecture de l'étiquette RFID, un panneau solaire est

intégré à la microbande de l'antenne pour amplifier la puissance d'opration de la puce RFID. Plus encore, l'intgration de nouveaux aspects de l'antenne et de la puce RFID dans un système d'antenne multi-étiquettes est explorée par la conception et l'évaluation de prototypes d'étiquette.

La technologie RFID a été employée récemment pour l'implantation de capteurs sans-fil à faible consommation d'énergie et à faible coût. Cette thése présente aussi de nouvelles antennes pour étiquette RFID UHF à double port pour l'identification sans-fil et les applications de capteurs simultanément. Des antennes à étiquette RFID spéciales ont été conues et intégrées à des capteurs de résistance passive pour démontrer la détection de données provenant d'un capteur en utilisant un lecteur RFID commercial. Finalement, un autre capteur à étiquette RFID pour la transmission de donnée générales utilisant l'énergie solaire est implanté. Cette conception est améliorée en utilisant une nouvelle antenne à bande à deux ports qui canalise l'énergie des radiofréquences ambiantes par son second port pour fournir la puissance nécessaire à l'étiquette. Un intervalle de communication RFID fiable allant jusqu'à 27 m a été obtenu dans un contexte de mesures à l'intérieur, ce qui représente, selon les connaissances de l'auteur, la plus grande distance jamais reportée pour des capteurs à étiquettes RFID similaires.

TABLE OF CONTENTS

LIST OF FIGURES

LIST OF TABLES

List of Acronyms

2D Two-Dimensionalo

3D Three-Dimensional

AMC Artificial Magnetic Conductor

EIRP Effective Isotropic Radiated Power

EM Electromagnetic

EPT Enhanced Passive Tag

HF High Frequency

IC Integrated Circuit

IOT Internet Of Things

LF Low Frequency

MBS Modulated Backscattring Signals

MCU Microcontroller Unit

RCS Radar Cross Section

RFID Radio Frequency Identification

UHF Ultra High Frequency

WSN Wireless Sensor Networks

Chapter 1

Introduction

1.1 Overview

Automatic identification technologies, such as Signature Capture, Magnetic Stripe Readers, Optical Character Recognition, Biometric Technologies, Barcodes and Radio Frequency Identification (RFID) have become the critical components in the operation of various industries and business processes. These technologies are able to identify people, products, codes, serial numbers, rapidly and accurately. Due to their low cost and ease of implementation, barcodes have been the primary means of identifying products in retail industry. However, the main disadvantage of barcode technology is the limited information capacity, very short reading range and the need for a line-of-sight reading arrangement. In fact, due to the line-of-sight requirement, reading barcodes is a time-consuming process. As well, the printed barcode sticker must be placed on the outside of a product, where it is subject to wear and tear. Barcode tags also have no read/write capability, thus the information written on a printed barcode sticker cannot be changed. These drawbacks make barcode technology unsuitable for many modern applications.

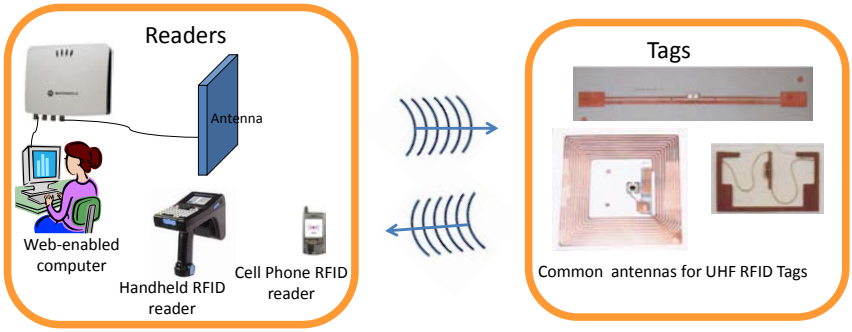

Figure 1–1: The main components of a typical RFID system [1].

Significant reduction in the manufacturing costs of integrated circuits in the past decade has resulted in the explosive growth of an alternative automatic identification technology, i.e Radio Frequency Identification (RFID) [1–3]. An RFID system enables people and products to be uniquely identified without the need for a line-of-sight reading arrangement. Indeed, many industries have entered into a new business process stage as a result of the rapid development of RFID systems. Currently, RFID systems play an important role in various industries. Emerging applications of RFID technology extend from security access control, healthcare and patient identification, and smart space allocations [4,5] to internet of things (IOT) and wireless sensor networks (WSN). A typical RFID system is composed of tag and reader components as shown in Fig. 1–1. In almost all of RFID applications an RFID integrated circuit (IC) is attached to the tag antenna to store identification data and respond to the reader. RFID tags can be classified into active, semi-active and passive tags based on the source of power supply of the chip [6]. Active and semi-active tags have their own power source for powering the microchip. An active tag also contains a transmitter that is always on and powered by a battery to communicate with the reader. While the semi-active tag uses the battery only for powering up the microchip, it

relies on backscattering (like a passive tag) to transmit data back to the reader. A passive tag is the least complex and hence the cheapest. It has no built-in power supply, but uses the electromagnetic (EM) field transmitted by a reader to power up the mircochip and transmit its information back. Because the passive tag has a limited supply of power, typically no more than a simple ID number is transmitted in a limited reading range. The allocated operation frequencies of RFID systems are low frequency (LF), high frequency (HF), ultra high frequency (UHF) and microwave frequency(MW), which may slightly vary from region to region. The UHF band is among the most popular spectra for RFID applications, due to the availability of mature low cost electronics, reasonable reading range (few meter and above) and the relatively small tag footprint in comparison to lower frequency designs). Table 1–1 presents the various UHF frequency bands used for RFID applications across the globe [7].

Table 1–1: UHF RFID frequency bands [7]

Country/ Region	Frequency	Power
North America	902-928 MHz	4 W EIRP
Europe	866-869 MHz	2 W ERP
China	917-925 MHz and 840-845 MHz MHz	2 W ERP
Japan	950-956 MHz	4 W EIRP

In general, the cost of a passive tag depends on its operation frequency, the amount of needed RFID chip memory, the design of the antenna, substrate material and tag's packaging. Normally, the cost of passive tags ranges from 12 cents for the simplest tag antenna design to several dollars for tags that are designed for placement on special materials (e.g. a metallic object) or tags that are covered with special coating materials for protection from heat, cold, moisture or chemicals. The

average prices of ordinary passive UHF RFID tags are presented in Table 1–2 for 2009 and 2010. Table 1–3 presents the cost of RFID tags that are specifically designed to survive harsh conditions [8].

Table 1–2: Ordinary UHF RFID tags pricing in 2009 and 2010 operating at UHF band [8]

Tag	Low	High	Average 2009	Average 2010	Reduction
10K	$ 0.12	$ 0.18	$ 0.1448	$ 0.1510	↑ 4.28 %
100K	$ 0.11	$ 0.14	$ 0.1235	$ 0.1235	↔ No change
1M	$ 0.09	$ 0.13	$ 0.1100	$ 0.1088	↓ 1.09 %

Table 1–3: Speciality UHF RFID tags designed for harsh conditions pricing in 2009 and 2010 operating at UHF band [8]

Size (sq mm)	Low	High	Average 2009	Average 2010	Reduction
Small<1000	$ 3.09	$ 4.65	$ 3.52	$ 3.21	↓ 8.8 %
Mde. 1000-2500	$ 2.29	$ 4.32	$ 4.32	$ 3.82	↓ 11.57 %
Large>2500	$ 3.50	$ 6.50	$ 5.01	$ 4.69	↓ 6.38 %

Despite the popular use of RFID technology in industry, still many design challenges remain to be addressed to allow its widespread adoption in many existing and emerging applications. The first design challenge is tag miniaturization without compromising RFID system performance. For example, a miniaturized RFID system can be easily integrated with a mobile phone to make electronic payments (similar to a smart card) or to place calls based on the RFID tags it encounters. Also, in order to place an RFID taged product in the global market, the RFID tag needs to be tunable or wideband enough to cover the entire RFID band for the intended applications. In addition, the RFID performance, specially that of its antenna, is subject to detuning due to the loading of identification object (which could be liquid, metal, chemicals, etc.). Therefore, it is often desired to create a compact tag that

is not susceptible to detuning, while extending its reading range without increasing the reader's power. A Tag's or reader's power sensitivity dramatically influences the maximum achievable reading range. The power sensitivity of an RFID tag is determined by the power sensitivity of its RFID IC as well as the gain (and efficiency) of tag antenna. The optimal design of tag antenna for obtaining the highest gain and maximum power transfer extends the reading range and relaxes the power sensitivity requirement of the RFID chip. Thus, a lower cost RFID chip can be selected for the tag.

The new frontiers of RFID applications extend beyond the mere identification and retrieval of data stored in the internal memory of RFID chip. In the past few years, RFID technology has been chosen as a viable low-cost technique for the deployment of sensor networks to communicate the dynamic data created by sensors [9, 10]. These emerging applications require the best use of a link's power budget. Innovative design of tag antennas and use of multiport measurements and multi antenna arrangements are the promissing techniques that can address the power and cost limitations RFID-tag-based sensor.

1.2 Thesis Rationale and Contributions

In this thesis, a number of new UHF RFID tag antennas (a total of 16 prototypes) for emerging identification and sensor applications have been designed, fabricated and experimentally evaluated. Addressing, the key challenges in tag antenna design and deployment, namely miniaturization, tunability, resilient operation on metal and lossy objects, and enhanced sensitivity via the integration of power scavenging techniques, have been the central goals of this thesis. In this endeavour

other engineering challenges, such as the development of a systematic way for RFID tag evaluation via measurement, and the implementation of a sensor system with RFID technology have been undertaken as well. Few enhanced RFID tags have been designed and integrated with passive and active sensors. A new multi-port patch antenna is designed and incorporated with a passive sensor to provide environmental information such as (humidity, and temperature) along with the identification number. In addition, a novel long-range solar cell-assisted RFID tag-enabled sensor incorporating an active sensor and a microcontroller unit (MCU) to write sensor data in the RFID chip memory have been developed and experimentally evaluated. More specifics about the achievement of these objectives and the thesis contributions are described as follows.

Miniaturized Monopole UHF RFID Tag Antennas:

When a passive tag enters the radiation field of an RFID reader, the tag antenna harvests the RF energy from the signal transmitted by the reader antenna. The amount of power required to turn the chip on strongly depends on the performance of the tag antenna [11, 12]. Due to their simplicity and omni directional radiation pattern, dipole antennas are commonly used as passive tag antennas [13, 14]. In RFID applications it is strongly desired to maintain a minimal footprint for the tag. The methods most commonly used to minimize antenna size are folding and meandering [7, 14–18]. A meander dipole can achieve resonance at a much lower frequency compared to straight dipoles, due to its compact increased length as well as the resultant inductive loading of the meander turns. In order to further reduce the footprint of meander or folded dipoles, monopole versions of these antennas should be investigated. Therefore, the design and experimental evaluation of three compact

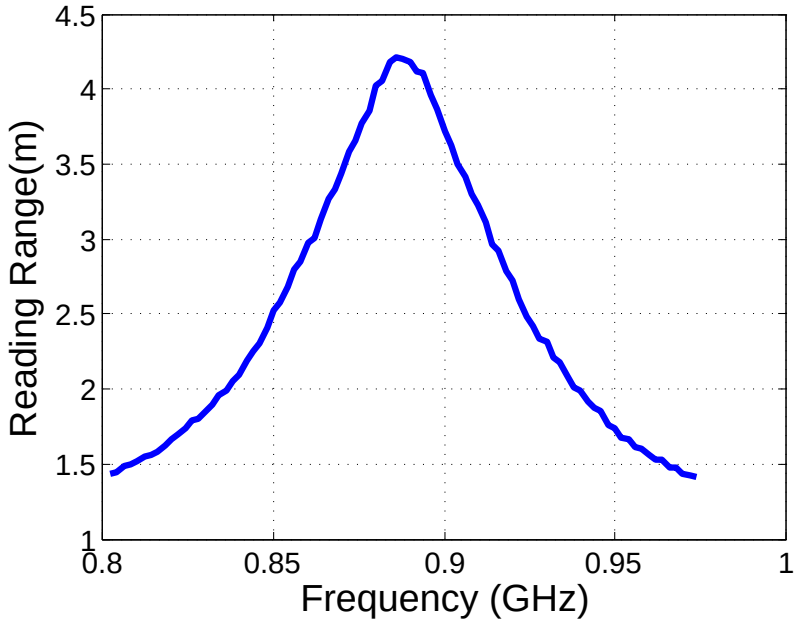

Figure 1–2: Reading Range of a Commercial RFID Tag [19]

printed monopole antennas for UHF RFID applications have been proposed in this thesis. In this endeavor, the problem of designing a matching network for connecting an antenna to an RFID chip with a complex output impedance (with small real part and relatively large reactive part) is addressed via inductive loop coupling. The antennas that include folded, 2D meander and 3D meander monopole designs, were fabricated using a 1.524mm-thick Rogers RB4350B substrate with a relative permittivity of 3.66. Experimental results reveal that these tags cover the worldwide UHF RFID operation band (860-960 MHz) with a maximum readable range of 6.3 m for the folded monopole, 5.39 m for the 2D, and 5.24 m for the 3D meander monopole designs with an effective isotropic radiated power of 3.28 W by the reader.

Compact Tunable Passive UHF RFID Tag Prototype for Global Operation:

As indicated earlier the licensed frequency bands for the operation of UHF RFID systems are different in various regions in the world. In China UHF RFID systems are required to operate at 840-845 MHz and 920-925 MHz bands, while in Europe, North America and Japan 866- 869 MHz, 902-928 MHz, and 950-956 MHz bands are respectively designated for UHF RFID applications [7, 17]. This means that a UHF RFID tag intended for the global market should operate efficiently across multiple bands from 840 MHz to 960 MHz. One solution is to utilize broad band RFID tag antennas. However, these designs usually occupy a larger area than the narrow band structures reported in literature, e.g [18], and do not achieve comparable levels of performance at different UHF RFID frequency bands. Fig. 1–2 shows the reading range versus frequency of a commercial passive UHF RFID tag. It is clearly shown that the maximum reading range achieved by this tag is 4.3 m at 886 MHz band, which drops to 1.6 m at Japan's UHF RFID band, and to 2.09 m at the 840MHz UHF RFID operation frequency band in China [19]. To address this problem, a compact tunable passive UHF RFID tag whose operation frequency covers the entire range of the UHF RFID regulated bands (840-960 MHz) is designed and experimentally evaluated in this thesis. To reduce the size of the printed folded monopole tag antenna and to tune its resonance frequency, a tunable inductor is integrated in its layout, resulting in an area reduction of 36.5% in comparison with a conventional non-tunable monopole tag antenna. Measurements using a commercial reader demonstrate that a global maximum reading range of at least 5.9 m and at most 6.1 m is achieved by this low-cost tunable passive RFID tag.

Testing Methods for the Evaluation Passive RFID Tags:

The commercial RFID readers that are available only operate at specific frequency bands. For example, our RFID reader, i.e., GAO 216010 reader [20], only covers 865-868 MHz (European band) and 902-928 MHz (North America band). With this commercial reader, the optimum operation frequency of a tag (especially a tunable tag) cannot be detected if it is shifted out of the reader's operational bands. Therefore, a simple measurement method is proposed in this thesis to obtain the antenna mode frequency response of a tunable tag [21]. Using a wide band horn antenna and a Vector Network Analyzer (VNA), the frequency response of the tunable tag can be obtained by determining a calibrated reflection coefficient (S_{11}). To measure the radiation pattern of tag antennas, matching circuits and feeding wires are necessary when a conventional radiation pattern measurement system is used. These additional components, which do not exist when the tag is deployed in practice, influence the radiation pattern, especially for miniaturized tag antennas. Thus, a method for measuring the radiation pattern of an assembled UHF RFID tag without the use of any additional matching circuits or feeding wires is also presented in this thesis.

Miniaturized Passive UHF RFID Tag Antennas for Identification of Metallic Objects:

Many objects that require identification with passive RFID technology contain or are totally made of conductive materials. Most of the RFID tag antennas in the market are dipole, loop, and monopole type antennas [7, 14–18, 22]. These types of antennas due to their omnidirectional radiation are influenced by the characteristics of the identification object, and their resonance frequency, input impedance,

radiation pattern and efficiency degrade, especially when they are mounted on conductive materials. To avoid this, patch antennas that are backed by a ground plane and thus exhibiting less sensitivity to the characteristics of identification object can be used. Their main drawback is their larger footprint compared to the the dipole type candidates. The most common techniques used for patch antenna miniaturization are employing higher-permittivity material for the antenna substrate and incorporating slots on the patch [23, 24]. However, increasing the permittivity is often associated with higher dielectric loss. Also, incorporating slots on a patch, only results in about $10\% - 20\%$ size reduction while compromising gain, bandwidth, and efficiency [25]. Another technique that is used for this purpose is utilizing an electromagnetic bandgap structure (EBG) as the patch substrate. An EBG structure supports slow-wave propagation; thus, the size of a patch antenna can be significantly reduced by simply integrating it above an EBG substrate [21]. A low profile RFID tag consisting of a compact microstrip patch antenna for operation from 860-960 MHz is proposed in this thesis. The patch, which is backed by a mushroom-type EBG structure, achieves an area reduction of 29.11% in comparison with a conventional patch design. The RFID chip is integrated on the patch via an inset feed line that is positioned in a way to deliver the conjugate impedance matching between the antenna and the chip. The maximum reading range of the tag is found to be around 11 m in two test scenarios of free standing tag and tag attached on a metallic surface.

Another solution for reducing the impact of identification object on tag antenna performance is by using an artificial magnetic conductor (AMC) as the ground plane of printed dipoles and monopoles. The AMC prevents short-circuiting of the antenna

by the metallic identification object while improving its directivity. Therefore, a UHF printed meander monopole RFID tag antenna incorporating an AMC as the reflector is presented in this thesis. The proposed antenna is designed to operate with a chip having an input impedance of $8.2 - j61\Omega$. For maximum power transfer between the chip and the antenna, the T-Matching technique is implemented. The fabricated assembled tag is evaluated in both free-space and when attached to a metal plate. Measurements demonstrate achieving a maximum readable range of 10 m in free space and 8.3 m when the tag is placed on a metal sheet.

RFID Tag Antenna for Enhanced Power Sensitivity:

As mentioned earlier the reading range of an RFID system is determined by reader's sensitivity and the power sensitivity (threshold power to activate the circuit) of tag's RFID chip [26]. Therefore, the main concern in designing the passive RFID tags is reducing the power consumption of the integrated circuit and increasing the amount of the collected RF power to increase power sensitivity and thus the operating reading range. There are several research efforts that address reducing the required minimum power to activate the chip. Most of these studies are directed towards enhancing the rectifier efficiency using Schottky diodes [27–29]. The other studies focus on reducing power consumption by selecting optimum communication protocols [30] or using multiple unmodulated waves to illuminate a passive tag at a cost of increased complexity [31, 32]. Yet, the limited reading range problem has not been completely solved using these methods. Thus, in this thesis, design and implementation of an enhanced-range passive tag that utilize solar energy to provide a portion of tag's operating power (in addition to harvesting RF energy) is presented. Moreover, a second design is proposed for extending the reading range that uses a

multiple-port RFID chip with multiple antennas or multi-port antennas in order to receive more than one copy of reader's signal that can be used for additional RF energy harvesting.

RFID Tag-Enabled Sensors:

RFID tag-enabled sensors, have several key features, such as low cost, zero power backscatter communication, and standardized identification of nodes (tags), that make them an attractive candidate to complement the currently existing wireless sensor networks (WSN). In this thesis, an RFID tag is integrated with a passive resistivitve humidity/temperature sensor to design a low-cost solution for detecting heat or humidity exposures of sensitive items that could be used in several applications including supply chains, manufacturing, pharmaceutical or construction industries. Few dual-port UHF RFID tag antennas for wireless identification and sensing applications are implemented as well as one dual-band prototype. Two RFID chips, one with and the other without an attached sensor, are incorporated in a single tag antenna with two excitation ports. One of the RFID chips serves as the reference signal (reference port) transmitter in the sensing process, while the other chip with the integrated sensor (sensor port) transmits a signal impacted by the sensed temperature or humidity. The measured results demonstrate that the sensed data can be extracted using a commercial RFID reader by recording and comparing the power required to active RFID chips.

Another design of an RFID tag-based sensor incorporating an active sensor for transmitting a generic sensor data is also proposed in this thesis. This RFID sensor relies on a new generation RFID chip with two communication interfaces: a wired I^2C interface connected to a microcontroller unit (MCU) [33] and a wireless UHF

interface for transferring identification and data to standard Gen2 readers [10]. In addition, the required power for the active sensor and the MCU is supplied via solar energy by adding a layer of solar cells on the top of the tag antenna. Furthermore, a novel approach using a multi-port UHF RFID tag with two energy harvesting strategies, i.e. solar and RF, to enable self-powered operation of the RFID tag-based sensor is implemented.

1.3 Publications

The contributions of this thesis are summed up in the following journal and conference papers:

1. A. E. Abdulhadi and R. Abhari, "A Solar-Energy-Assisted Sensor-Enhanced UHF RFID Patch Antenna for Wireless-Sensor Network Applications" Submitted to *IEEE Transactions on Industrial Informatics Special Issue on Industrial Wireless Networks*.
2. A. E. Abdulhadi, D. Yi, M. Parvizi, and R. Abhari, "Multi-port UHF RFID tag antenna for enhanced energy harvesting of self-powered wireless sensors," *in Microwave Symposium (IMS), 2014 IEEE MTT-S International, 2014*,pp. 1-3.
3. A. Abdulhadi and R. Abhari,"Design and experimental evaluation of miniaturized monopole UHF RFID tag antennas," *Antennas and Wireless Propagation Letters, IEEE*, vol. 11, pp.248-251, 2012.

4. A. E. Abdulhadi, H. M. Tehran, and R. Abhari, "Design and characterization of a miniaturized patch antenna for passive UHF RFID applications," *in Microwave Symposium Digest (MTT), 2012 IEEE MTT-S International, 2012*, pp. 1-3.
5. A. E. Abdulhadi and R. Abhari, "Tunable compact printed monopole antenna for passive UHF RFID tags," *in Antennas and Propagation Society International Symposium (APSURSI), 2012 IEEE, July 2012*, pp. 1-2.
6. A. E.Abdulhadi and R. Abhari, "Passive UHF RFID printed monopole tag antenna for identification of metallic objects," *in Antennas and Propagation Society International Symposium (APSURSI), 2012 IEEE, July 2012*, pp. 1-2.
7. A. E. Abdulhadi and R. Abhari, "Dual printed meander monopole antennas for passive UHF RFID tags," *in Antennas and Propagation (APSURSI), 2011 IEEE International Symposium on, 2011*, pp. 988-991.
8. A. E. Abdulhadi and R. Abhari, "Compact printed monopole tag antennas for UHF RFID applications," *in Antennas and Propagation Society International Sympo-sium (APSURSI), 2010 IEEE, 2010*, pp. 1-4.
9. A. E. Abdulhadi, A. Suntives, and R. Abhari, "Design of a SIW-based data communication system using a SIW six-port receiver," *in Electrical Performance of Electronic Packaging and Systems, 2009. EPEPS '09. IEEE 18th Conference on, Oct 2009*, pp. 151-154.

1.4 Thesis Outline

An introduction to RFID system is presented in Chapter 2, which includes the principles of an RFID system and the operating mechanism of passive RFID tags

that communicate with the reader via a zero-power backscattering technique. The applications of traditional as well as modern RFID tags, which convey information beyond the identification data stored in an RFID chip and that are used to send data created dynamically by onboard sensors are also discussed in this Chapter.

Chapter 3 reports on the design and experimental evaluation of three compact printed monopole antennas, i.e. folded, 2D meander and 3D meander, for UHF RFID applications. The tags are measured via a special RFID testing system (Tag-Formance) along with an in-lab commercial RFID reader and a Vector Network Analyzer. This chapter also presents a method for measuring the radiation pattern of an assembled UHF RFID tag without the use of any additional matching circuits or feeding wires.

Chapter 4 focuses on the design of a compact tunable passive UHF RFID tag prototype for global operation. A survey of existing tunable RFID tags is presented, followed by a detailed description of the design of the proposed tunable tag. In this chapter, the equivalent lumped element circuit to model the integrated chip inductor in Ansoft HFSS is also presented. Finally, a tag incorporating a tunable inductor that is adjusted by changing the height of its aluminum core is also presented.

Design and characterization of a miniaturized passive UHF RFID tag antenna for the identification of metallic objects is discussed in Chapter 5. First, the design of a miniaturized UHF tag antenna consisting of a microstrip patch backed by an EBG structure is presented. The measured results of its antenna mode frequency response, radiation pattern and reading range in the two cases of a stand alone tag and tag mounted on a metallic sheet are reported. A UHF printed meander monopole RFID tag antenna incorporating an AMC reflector is then presented. Finally, the

experimental evaluation of the antenna backed by a 4 cells × 4 cells AMC surface is also discussed in this chapter.

Design of RFID tag antennas for enhanced power sensitivity and extended reading range is studied in Chapter 6. First, the reader is provided with a survey of the published papers on enhanced passive RFID tags (EPT). Then, the design and implementation of a patch antenna incorporating a new generation of RFID IC (Monza X) is proposed to improve the reading range. Solar cell strips are glued onto the top of the tag antenna and connected to the DC lines of the RFID IC with small wires to provide a portion of IC's operating power to extend the reading range. Fullwave simulation and power sensitivity results, along with the reading range measurements, are provided in this chapter. To design a miniaturized tag with a longer reading range, integration of a multi-port RFID chip with multi-antennas is also proposed in this chapter.

In Chapter 7, single and dual band patch antennas are proposed for UHF RFID tag-based sensor. A prototype example using a passive resistive sensor is presented. To improve the reading range of the prototype, solar energy harvesting is integrated in the design. Fullwave simulation and power sensitivity test results, along with antenna pattern measurements are provided in this chapter.

Another approach of an RFID tag-enabled sensor for transmission of generic sensor data is investigated and implemented in Chapter 8. Single and two-port patch antennas integrated with the new generation UHF I^2C-RFID chip and an external thermal/humidity sensor are described, along with elaboration on employing a hybrid energy harvesting strategy. Finally, an experimental evaluation of the RFID sensor in a climate chamber is also presented.

Chapter 9 summarizes this work and reports conclusions. Future work recommendations are also provided to further improve UHF RFID tags and RFID sensor system designs.

Chapter 2

Introduction to RFID Technology

2.1 Introduction

Radio frequency identification (RFID) is one of the hottest technologies in recent years. A simple explanation of a radio frequency identification system is that it is a two-way radio communication that offers advanced solutions for a variety of applications in the domains of tracking, security, ticketing, electronic payment, etc [34–36]. Most of the RFID systems that are currently available operate at one of the following frequency ranges: low frequency band (LF) (125 KHz to 134 KHz), high frequency (HF) (13.56 MHz), ultra high frequency band (UHF) (860 to 960 MHz) and (2.4 GHz to 2.4835 GHz), and microwave frequency bands (MW) (5.8 GHz). Globally, each country has its own frequency allocation for RFID systems. For instance, in North and South America UHF RFID system band is from 902-928 MHz with 4 watts maximum power that can emanate from an RFID reader, while European UHF RFID system band is 865-868 MHz with 2watts of allowed maximum power. In Japan and few Asian countries UHF RFID system band 950-956 MHz.

As shown in Fig. 2–1, RFID systems are composed of two basic components: a reader and a tag. The tag, which is affixed to the objects to be identified, consists of a combination of two parts a chip and an antenna printed on a substrate. The size of the tag, therefore, is definitely dependent on the antenna size. For certain applications of RFID systems, such as electronic payments, ticketing, supply chain management, security, and health monitoring, a small, light and efficient printed antenna is required. Furthermore, it should be environmentally friendly and inexpensive. The second part of an RFID system is the reader, which has its own antenna and communicates with the tag via radio frequency. The reader consists of a transmitter, receiver and control units. The design and implementation of a successful RFID reader should incorporate the consideration of many technical issues such as gain and polarization of the antennas, power consumption of the over-all system, and isolation between an RFID reader's transmitting and receiving paths.

2.2 RFID Tag

The RFID tag is composed of an antenna and a microchip. As indicated in Chapter 1, based on the way the tag is powered, RFID tags can be classified into three different categories: active, semi-active and passive RFID tags. Active and semi-active RFID tags that have their own power source for powering the microchip, manufacturing cost is higher compared to passive tags. As a tradeoff, passive RFID tags have limited readable ranges and only operate in the presence of the electromagnetic field of the RFID reader. Also, like a semi-active tag, it communicates passively and uses the incident radio wave to draw power for its modulated backscattering signals (MBS) [37, 38]. In this thesis the focus is on various aspects of tag design and

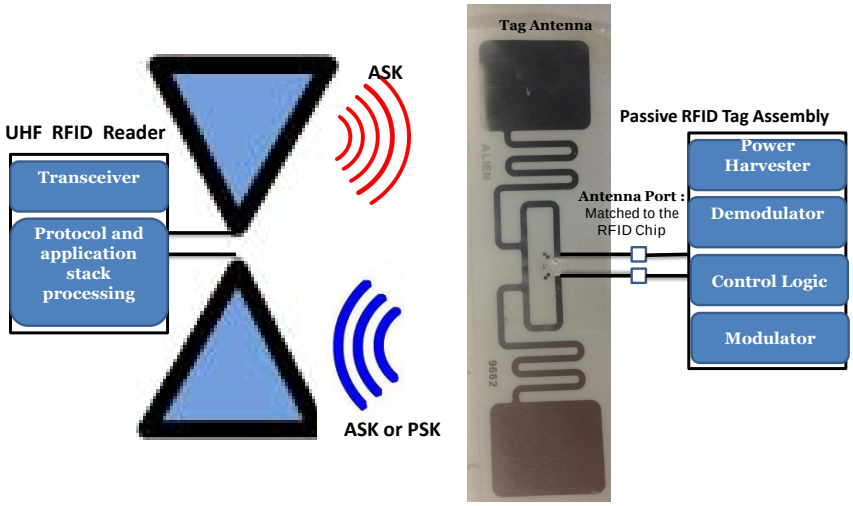

Figure 2–1: RFID system configration [32].

RFID reader design; discussion on communication protocols and modulations are not within the scope considered here. More information about the these areas can be found at [39, 40].

2.3 Passive Tag Implementation

The block diagram of a passive RFID tag is shown in Fig. 2–2. A passive tag consists of an antenna and an integrated circuit chip. The tag chip contains an RF-analog front end and control logic blocks. The RF-analog front end includes a voltage rectifier, a demodulator, and a modulator. There is no internal power source and the required power is generated from the RF signal transmitted by the reader using the power harvester circuitry. This power should be higher than the threshold needed to turn the chip on. The passive RFID tag operates in the following

way: The power harvester circuitry produces the power from an incident radio wave and converts the RF power into DC power to provide the required power of the tag IC. The demodulator is used to demodulate the reader commands. The logical controller is the central part of the tag's IC, and it decodes a reader command and selects the corresponding response according to the Electronic Product Code (EPC) Generation-2 air interface protocol [37–39]. The modulator is then used to generate the tag's response to the reader by launching its modulated backscattering signal (MBS) to the antenna. A typical tag's response and continuous wave (CW) query from the reader are shown in Fig. 2–3. The tag sends its response using an unmodulated continuous wave (CW) from the reader by varying its input impedance between two states Z_{C1} and Z_{C2}, effectively changing its radar cross-section (RCS) and modulating the backscattered signals. The magnitude of vector differential radar cross section,$\Delta\sigma$, of the tag can be obtained as follows [41]:

$$\Delta\sigma = \frac{\lambda^2 G^2}{4\pi} \left|\rho_1 - \rho_2\right|^2 \tag{2.1}$$

where G is the tag antenna gain, $\Delta\sigma$ is a parameter used for tag evaluation, and ρ_1 and ρ_2 are complex power wave reflection coefficients derived from:

$$\rho_{1,2} = \frac{Z_{c1,2} - Z_a^*}{Z_{c1,2} + Z_a} \tag{2.2}$$

where Z_a is the antenna's input impedance. Realization of conjugate matching between the tag antenna and the chip improves the received power budget (reader $\rightarrow$ transponder). However, if tag's impedances are switched between short and open circuit, the modulation efficiency of backscattering signals is improved (transponder

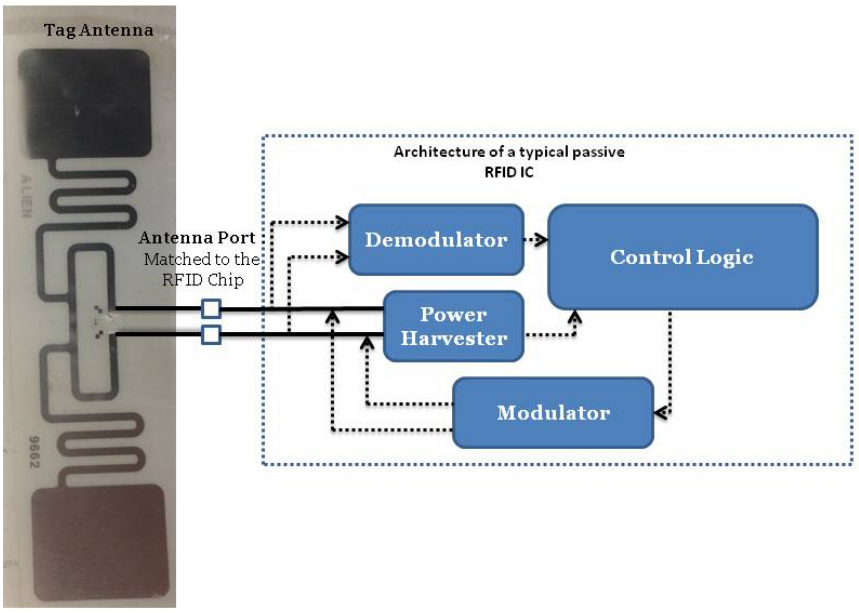

Figure 2–2: Pssive RFID tag configurations [32].

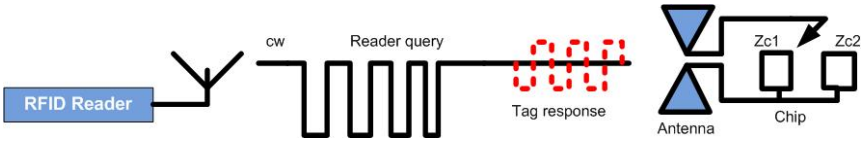

Figure 2–3: A sample diagram showing passive RFID system's reader and query response [41].

→ reader). Conjugate matching techniques are used in this thesis to improve the reading range of the proposed tags.

2.4 Performance Limitations of the Passive UHF RFID System

The most important RFID system performance characteristic is the reading range. There are different factors that determine the reading range of a tag such as tag's characteristics, propagation environment, and reader's operational characteristics. The prominent factors pertaining to the RFID system design are described as follows.

A. Chip Power Sensitivity

This is the minimum power required to activate an RFID chip. In a passive system, this amount of power is generated from the RF signal. The lower it is, the longer distance at which the tag can be detected. Thus, RFID chips with several RF inputs connected to different antenna ports are proposed to improve the power sensitivity and increase the reading range [42–44]. As mentioned in Chapter 1, another technique uses an additional source, such as solar power, to improve the power sensitivity [10, 31, 32]. Unlike a semi-passive tag that depends on its internal battery to work, the enhanced passive tags can function as a regular tag while achieving a much longer read range. More on this can be found in the designs discussed in Chapter 6.

B. Tag Antenna Characteristics

An RFID tag antenna plays a very important role in the overall RFID system performance, as it directly impacts the size, cost, and detection range. Most RFID tags are designed to be affixed on small objects; thus the antenna structures must be as small as possible without unacceptable degradation of the antenna's performance. The maximum reading range is measured in the direction of maximum gain, which is fundamentally determined by the frequency of operation and the tag size.

C. Impedance Match

The other factor in the design of the tag antenna is the RFID chip input impedance, which is highly capacitive. For maximum power transfer between an antenna and its attached load, the impedances of the antenna and the chip must be

conjugate matched. To implement miniaturized low-cost RFIDs tags, it is not feasible to use external matching networks that contain lumped components. Therefore, the matching mechanism has to be integrated within the tag antenna layout. Several feeding techniques are presented in [15, 45, 46]. The most popular techniques are T-matching, single and double-stub tuning, and inductively coupled loop matching. Impedance of the RFID chip should be matched at minimum threshold power levels to maximize the tag range.

D. Tag Detuning

RFID tag antennas are material-sensitive; when RFID tags are placed on metals or high-dielectric materials, they all show impedance mismatch, along with bandwidth and radiation pattern problems which result in decreasing their reading range. Therefore, designing an antenna for an RFID tag that is tolerant of different environments becomes crucial for the successful implementation of an RFID system.

E. Reader Sensitivity

Reader sensitivity, which determines the minimum level of tag signal that a reader can detect, is an important factor in the passive RFID system. The common problem with most RFID readers is the partial leakage of the transmitted energy back into the receiver. In this case, the LNA of the receiver may be saturated, resulting in the decreasing of the dynamic range of the LNA, and increasing the DC offset problem. Consequently, the performance of the RFID system is significantly degraded, including its sensitivity and detection range. Therefore, separating the

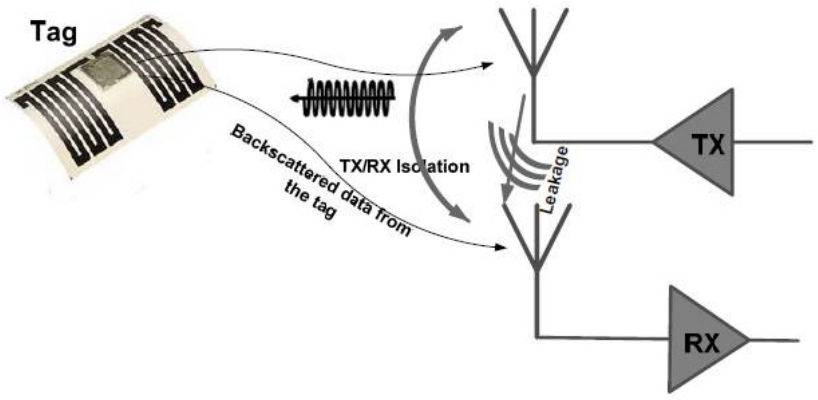

Figure 2–4: An RFID reader implementation using two antennas [47].

weak incoming signal (for example on the order of-70dBm) from the strong transmission signal (e.g., around 30dBm) is crucial in order to achieve high performance in RFID reader systems [47]. The simplest solution is to implement two separate antennas for the TX and RX paths, as shown in Fig. 2–4. However, these two antennas are operating at the same frequency and at the same time. The major concern with this solution is that the closer the antennas are to each other, the greater the coupling and leakage. In [48], simulated and measured results show that two printed antennas on the same PCB cause significant distortion and attenuation to each other. Separating them sufficiently is difficult due to the often limited available space. To diminish the distance between the antennas while improving the isolation between them, an alternative method such as employing an EBG structure is a good candidate for RFID passive systems [48].

2.5 Emerging Applications of Passive RFID Tags

Due to their low cost and long lifetime, passive RFID tags are excellent candidates for the deployment of emerging wireless applications such as sensor networks

and the internet of things (IOT). As stated in Chapter 1, sensor have been successfully incorporated into RFID tags. The integration of RFID sensor technologies gives new perspectives to a broad range of applications, ranging from surveillance and advanced tracing systems, disaster prevention, smart homes to healthcare and tele-medicine.

The characteristic of unlimited lifetime of passive tags can be exploited in applications where neither batteries nor wired connections are feasible because of the relative cost, low power consumption, and complexity. The sensing function can be incorporated within the passive RFID tag design. For example, in a method called On/OFF sensing (or Threshold) the sensed data can be extracted from the tag when it either receives enough power to turn on and respond or not. One risk to the sensor operation in this case is when the material the tag is placed on changes the tag performance detune and might not be detected by the RFID reader [49].

In another method, which can be called "Analog sensing with a tag antenna", a tag antenna or matching circuit's performances can be made sensitive to the changes of sensed parameters, with proper calibration. With the use of a commercial RFID reader sensor data is received. Interpretation of the data relies on the received signal level in the operation frequency band [50]. The final way to combine a sensor with an RFID tag is by having a distinct active sensor block that writes the sensed data into the RFID chip of the tag. It is possible to integrate the active sensor with the RFID chip, but this could increase the cost. Therefore, for an economical solution, the RFID chip's memory is directly accessed via a serial port interface to hold the sensor's data. A tag as a transponder sends this information in response to the reader's query [10].

2.5.1 Requirements for Integrating RFID Technology and Wireless Sensor Networks

The architecture of integrated sensor-tags, an RFID reader and base station is shown in Fig. 2–5. For the efficient integration of RFID systems and wireless sensor networks (WSN), specific requirements should be taken into consideration as described herein [51]:

Accurate and reliable communication: To implement a low-cost WSN, the systems communication protocol should be compliant with the Electronic Product Code (EPC) Gen2 standard. The level of accuracy needed for an integrated RFID-sensor network is dependent on the criticality of the specific application. For example, with a low-cost threshold passive heat sensor that can be placed on a large variety of common packages, a lower degree of resolution is needed, while many other applications require a high resolution and transmission of digital sensor data. Therefore, the method of the integration of sensor and RFID tag can change depending on the accuracy needed.

Energy efficiency: The integrated sensor networks should be energy efficient to transmit of generic sensor data at a low cost. The most preferred integrated RFID tag-sensor networks are self-powered and incorporate RF or solar energy harvesting techniques [10].

Network maintenance survivability: It is the ability to perform remote device configuration and software updates [51]. More information on this topic is found in [51].

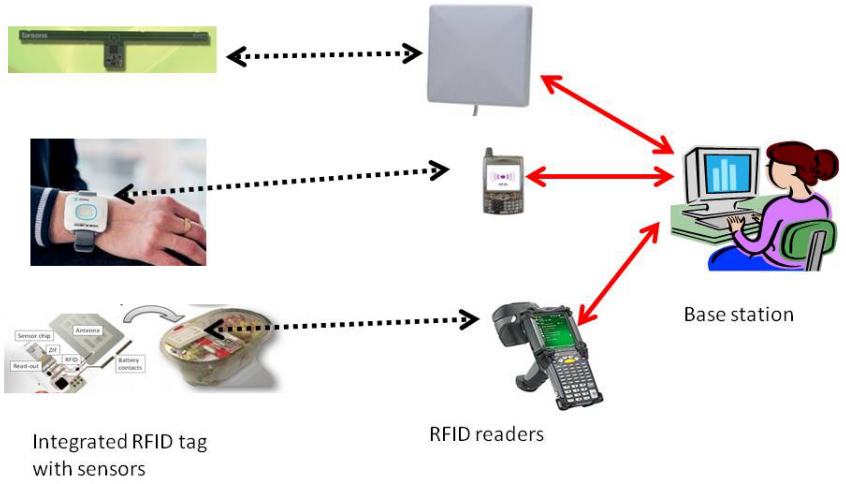

Figure 2–5: Architecture of Integrated sensor-tags, RFID reader and base station [51].

2.6 Summary

In this chapter, an overview of RFID technology is presented. It has been shown how the tag antenna parameters and matching network for connection to the RFID chip can impact the operation of the RFID system. Emerging applications, and the requirements for integrating RFID technology and wireless sensor networks are also presented in this chapter.

Chapter 3

Design and Experimental Evaluation of Miniaturized Monopole UHF RFID Tag Antennas

---

3.1 Introduction

Applications of ultra high frequency band (UHF) RFID services are now reaching beyond supply chain management and tracking to electronic payment and mobile phones [52]. The tag antenna plays an important role in the overall RFID system performance, as it directly impacts the size, cost, and detection range. In RFID applications it is strongly desired to maintain a minimal footprint for the tag. This makes the tag antenna design at the UHF band more critical since the small radiating aperture area could compromise the antenna gain and hence the reading range. Besides the size constraint and gain requirement, the design challenges of RFID tag antennas include matching to the complex impedance of the RFID chip that is discussed in this Chapter as well. Dipole antennas are commonly used in UHF RFID applications, because of their simplicity and omnidirectional radiation characteristics [13]- [53]. However, they are too big at UHF frequencies to be attached to small objects, thus, compact tag antenna designs need to be investigated. To implement

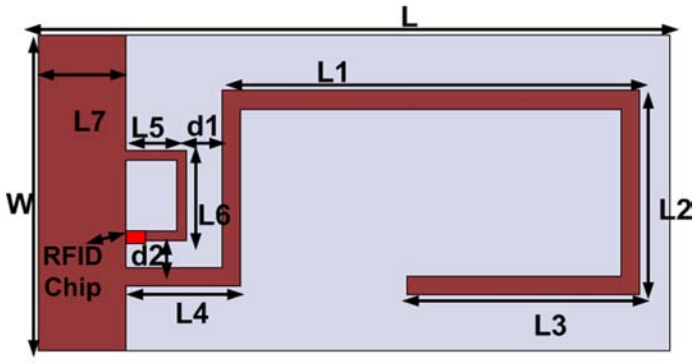

Figure 3–1: Geometry of the proposed printed folded monopole tag antenna, all dimension in mm (L=63, L1=47, L2=21, L3=26.7, L4=9, L5=3.4, L6=7.8, L7=5, W=24, d1=4.6, d2=4.7).

miniaturized low-cost RFID tags, it is not feasible to use external matching networks that contain-lumped components. Therefore, the matching mechanism has to be also integrated in the tag antenna layout. However, the design of the tag antenna and the matching network becomes more challenging when the real part of the chip input impedance is very small.

In this chapter, compact UHF RFID tag antennas are proposed. The design and experimental evaluation of three compact printed monopole antennas for UHF RFID applications are presented. The antennas that include folded, 2D meander and 3D meander monopole designs, are inductively-coupled to RFID chips for conjugate matching. Matching to high as well as low input resistance value can be easily achieved by using this technique just by optimizing the loop area and its coupling to the antenna, i.e., spacing. Moreover, in this chapter the experimental evaluations of the assembled tags, in which the chip is connected to the antenna, is explained. A simple method to measure the radiation pattern of passive RFID tag antennas using a vector network analyzer and by determining a calibrated S_{21} is also proposed.

3.2 Proposed Monopole Tag Antenna Designs

Since, RFID tags are mainly designed to be attached to a variety of consumer packages, they are desired to be as compact and inexpensive as possible. There are three basic factors that affect the pricing and reliability of RFID tags that are: cost of the chip, cost of the tag antenna and cost of the assembly. The cost of RFID tags may be in the range of \$0.12 for tag antennas +\$0.04 for chip +\$0.02 for the processing =\$0.18 for 915 MHz tag antenna size [54]. As also shown in Table 1–3, tag antennas directly impact the size and the cost of smart RFID tags. Therefore, printed monopole designs are attractive candidates for RFID applications

In this work, 3 compact printed monopole tag antennas are designed and fabricated using a 1.524 mm-thick Rogers RO4350B substrate ($\varepsilon_r = 3.66$). The structure and the dimensions of the proposed printed folded monopole antenna are shown in Fig. 3–1. The overall area is $63mm \times 24mm$ which is much smaller compared to the conventional folded dipole presented in [55] as the area is reduced by 64%. For maximum power transfer to the RFID chip an inductively-coupled loop matching mechanism is utilized for the antenna. The input impedance of the RFID chip is $8.2 - j61\Omega$ at 915 MHz. The chip is connected between the ground and the matching loop which inductively couples signal to the antenna. At the near resonance frequency, the real (R_a) and the imaginary (X_a) parts of the input impedance, when looking from the connection terminal of the chip, for conjugate matching are [14, 15, 18, 53]:

$$R_a = \frac{(\omega m)^2}{R_{rb}} + R_{loop} \tag{3.1}$$

$$X_a = \omega L_{loop} \tag{3.2}$$

Where R_{rb} is the radiation resistance of the antenna, m is the mutual inductance between the matching loop and the antenna, and R_{loop} is the resistance of the loop which is very small. Thus, the real part is adjusted by m and R_{rb}. From the inverse relation between the R_a and R_{rb} can be seen why a monopole design is considered for the RFID tag with a high input resistance chip as the dipole topologies exhibit twice the R_{rb} value. At the resonance, the imaginary part of the input impedance (X_a) depends on the self inductance of the loop (L_{loop}). Knowing the imaginary part of the chip, the loop area is adjusted to yield the desired (X_a) value. Also, the distance between the loop and the antenna controls the coupling coefficient and m can be tuned to achieve the required real part of the input impedance.

To reduce the size of the printed monopole antenna even further, meander monopole antennas are developed. Two meander monopole antenna topologies are designed and fabricated. The geometry of the printed 2D meander monopole antenna is shown in Fig. 3–2(a). Like a folded monopole antenna, the radiating body, the feeding loop and the ground are printed on the top layer of the substrate. The overall size of the designed antenna is ($42mm \times 25.7mm$) which is 28% smaller than the folded monopole design shown in Fig. 3–1. In comparison with a pertinent meander dipole design reported in [17] an overall 33% area reduction is achieved. For further size reduction, a 3D meander monopole antenna is also proposed. The 3D meander monopole antenna structure is shown in Fig. 3–2(b), in which conductor traces are implemented on both sides of the substrate and connected using vias each with a radius of 0.381 mm. A matching loop is also used to feed the 3D meander monopole antenna. Like the folded monopole antenna, the dimensions of the matching printed loop and its spacing from the antenna are adjusted by fullwave simulations to yield

the desired impedance values [18]. The overall size of the 3D meander antennas is ($42mm \times 19.7mm$) or equivalently ($0.128\lambda \times 0.06\lambda$). The 3D meander monopole antenna offers the smallest area, which is 45% and 23.4% smaller than the folded and 2D meander monopole antennas, respectively, while offering almost similar performance characteristics as will be seen in the next section. When compared to the dimensions of the compact tags reported in [56]- [57], the proposed 3D meander monopole tag has $39.8\% - 82\%$ less surface area. The designed tag antennas are each integrated with a chip that has an input impedance of $8.2 - j61\Omega$ at the operation frequency of 915 MHz. The simulated results of the antennas input impedance are shown in Fig. 3–3.

At the operation frequency of 915 MHz, the input impedance of the folded, 2D, and 3D meander monopole antennas are $10.7+j62.3\Omega$, $12.3+j62\Omega$ and $10.09+j64.2\Omega$, respectively. Also, At the operation frequency of 915 MHz, the realized gain of the folded, 2D, and 3D meander monopole antennas are 1.7 dB, 0.85 dB and 0.91 dB, respectively. Also, the simulated radiation efficiency of the folded monopole is 94.7%, while 78.4% is observed for the 2D and 78.93% for the 3D meander monopole antennas.

3.3 Experimental Evaluations of the Proposed Tags

To fully evaluate an RFID tag, the radiation pattern, the required minimum power on the tag, the differential radar cross section (RCS) and the reading range should be measured.

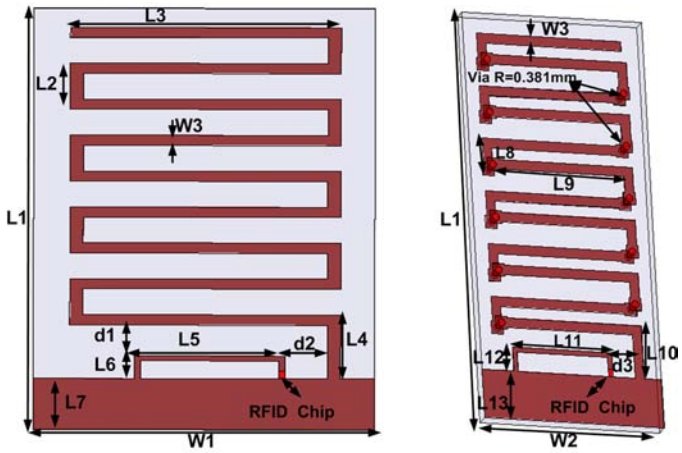

(a) (b)

Figure 3–2: (a) Structure of the proposed printed 2D meander monopole antenna. (b) Structure of the proposed printed 3D meander monopole tag antenna, all dimension in mm (L1=42, L2=4, L3=20.4, L4=9.5, L5=9.9, L6=2.2, L7=5, L8=4, L9=23.6, L10=7.1, L11=8.9, L12=2.5, L13=5, W1= 25.7, W2=19.7, W3=1, d1=6.3, d2=6, d3=3.4).

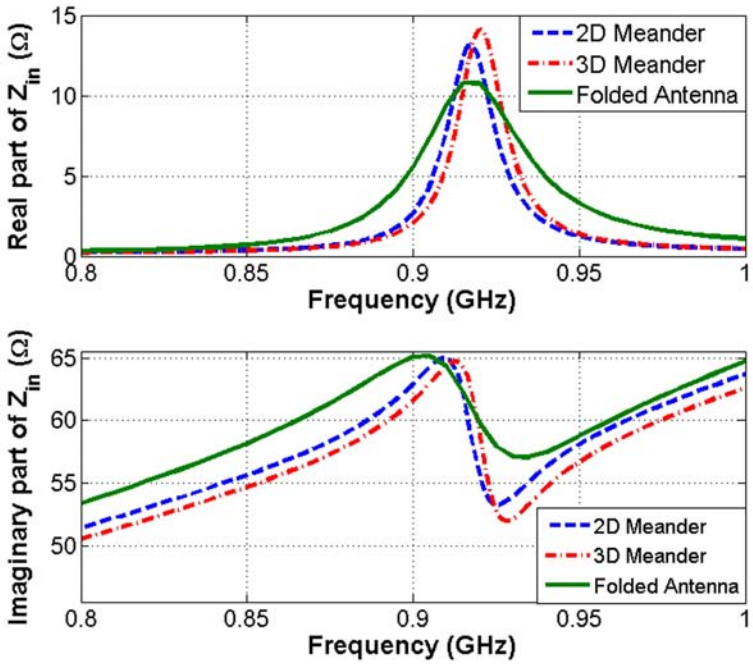

Figure 3–3: Input impedance of the proposed folded, 2D and 3D meander monopole antennas.

A. Radiation Pattern Measurements

Passive UHF RFID tags do not contain an internal power source for their microchip, and generate their needed power from the RF signal received by the tag antenna. Therefore, radiation pattern characterization of the tag antenna is critical in evaluating the performance of an RFID tag since it provides a visualization of the incident power on the tag. To measure the radiation pattern of tag antennas, matching circuits and feeding wires are necessary when a conventional radiation pattern measurement system is used [58]. These additional components, which do not exist when the tag is deployed, influence the radiation pattern. A contactless method in which the feeding wires are removed is introduced in [59] in order to replicate tags operation in practice. In this type of test, two tones are transmitted to the tag and the third-order intermodulation products that are generated by the nonlinear IC of the tag are detected [59]. The amplitude of an intermodulation product is proportional to the nonlinear characteristics of the RFID chip, the amplitudes of the fundamental frequencies and also to the gain of tag antenna. Therefore, the radiation pattern can be obtained by plotting the normalized amplitude of the received intermodulation product. The drawback of this method, in addition to the increased complexity of the test setup, is its dependence on the sensitivity of the receiver. The RFID reader system can be also used to plot the radiation pattern of an assembled tag by sweeping the transmitter power of the reader and measuring the minimum power required to activate the tag at each angle [60]. Like the previous method, the measured pattern is also a function of reader (receiver) sensitivity.

Therefore, in this measurements, a simple method to measure the radiation pattern of passive RFID tag antennas using a vector network analyzer and by determining a calibrated S_{21} is also proposed. The proposed system for radiation pattern measurement of passive UHF RFID tags is shown in Fig. 3–4. This measurement set-up includes a Vector Network Analyzer, two horn antennas and an amplifier. Port 1 of the VNA is connected to the power amplifier to generate 30 dBm and then to the transmitter (TX with gain of 6 dBi) horn antenna. The transmitter antenna is placed close to the RFID tag under test (at 0.69 m distance which is in the far field region of the antenna) to activate the RFID chip. Accounting for propagation losses the power received by the RFID antenna is 8 dBm which is higher than the minimum power required (-13 dBm). Both the RFID holder and the transmitter (TX) are mounted on the turntable of the anechoic chamber to ensure a continuous illumination field for the tag under test. The receiver (RX) antenna is connected to Port 2 of the VNA to measure S_{21}. The tag is placed on a foam substrate as shown in Fig. 3–4 and the distance between the RX antenna and the RFID tag is 1.84 m. Radiation pattern of the fabricated $3D$ meander monopole antenna with the microchip was measured using this set-up in an anechoic chamber. The first step in this measurement is calibration in order to account for the reflections inside the chamber such as those reflected from the chamber walls or from the holder to which the tag is attached. This is done by measuring S_{21} across the selected frequency band when no RFID tag is present. This test is repeated at each angle of the turntable from 0^0 to 360^0 stepped by 5^0. The measured value of S_{21} at each angle includes the internal reflection inside the anechoic chamber, which is used as a calibrating reference. Next, the S_{21} is measured again at each angle in the presence of the RFID

tag. The reference S_{21} values are subtracted from these new measured values to find the received (a.k.a. return) signal from the RFID tag. The radiation pattern of the RFID tag can then be obtained simply by plotting the normalized measured return signals at each frequency point in the selected bandwidth. Fig. 3–5 presents the simulated and measured radiation patterns at the operation frequency of 915 MHz for 3D meander monopole prototype. The measured half power beam width is 80^0. The radiation patterns are omnidirectional and similar to those of dipole antennas. The radiation pattern characteristics of the two other designed antennas are very close to those of the 3D meander monopole. Hence these radiation plots are not presented here for brevity.

B.Power Sensitivity

The proposed folded, 2D, and 3D meander RFID tags were measured in an anechoic cabinet designed for evaluating the performance of UHF RFID tags at Voyantic Ltd. laboratory [61]. The transmitter and receiver antennas in this measurement system are linearly polarized providing a flat 8 dBi gain response at the frequency range of 800 to 1000 MHz. The measurement system also includes a wideband circulator for monostatic radar measurements with over 20 dB port isolation throughout the 800-1000 MHz range as shown in Fig.3–6. The circulator is connected to an RFID tester that generates query commands with selected modulation, data rate, and encoding formats for UHF tags operating under ISO 18000-6c (EPC Class 1 Gen2) protocol. The power sensitivity of the RFID tag is measured by sweeping the transmit power across the selected frequency band to detect the minimum power required to obtain a correct tag response at each frequency point. The transmit power starts from a value to which the tag does not respond and then it is increased by

0.1 dB steps until a correct response is obtained. The maximum power generated by the transmitter system is 27 dBm. Fig. 3–7 presents the results of the required minimum transmit (also referred to as threshold) power on the tag in the forward link. In calculation of these values, the gain of the transmitter antenna, which is 8 dB, and the calculated free-space path loss of 23 dB are considered to obtain the power on the tag. These results demonstrate that the tags respond correctly across the entire frequency band of 800 to 1000 MHz when at most 3.28 W of effective isotropic radiated power (EIRP) is incident on the tags.

C. Radar Cross Section

The minimum power needed for identifying the tag in radar terminology translates into the strength of the backscattered signal at the reader. Therefore, the differential radar cross section (RCS), which determines the ratio of the backscattered power from the tag to the incoming power sent by the transmitter, is also obtained from the following formula for the monostatic radar measurement configuration [41]:

$$\Delta RCS = \frac{P_{received}(4\pi)^3 d^4}{P_t G_t^2 \lambda^2} \tag{3.3}$$

where the power of the received modulated signal from the tag is denoted as $P_{received}$. P_t is the power transmitted by the reader and d is the distance between the tag and the transmit/receive antenna with the gain of G_t.

The tag is vertically positioned on the z-axis and faced the TX/RX antenna with the angle $\varphi = 0^0$ and at the distance of 0.45 m. The results of RCS as a function of frequency of the proposed tags are presented in Fig. 3–8. The peak measured RCS of the folded monopole and the 2D, and 3D meander monopole RFID tags are (-21.9 dBsqm) and (-30.66 dBsqm) and (-30.32 dBsqm), respectively. A tag with a strong

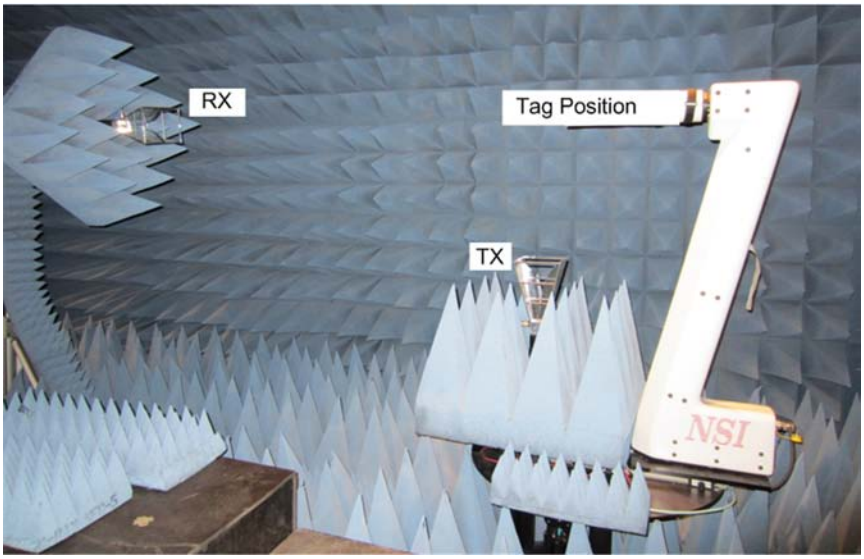

Figure 3–4: Proposed measurements setup.

response can be easily detected by a reader and as expected, the folded monopole tag with the largest physical area creates the strongest response of the three designed antennas.

D.Reading Range

The most common and probably the most important indicator in evaluating an RFID tag is its reading range. From the measured results of the required minimum (threshold) power for creating a correct tag response at each frequency point in the selected bandwidth, the reading range of the tag can be found using the following formula [17].

$$r_{max} = d\sqrt{\frac{P_{EIRP}}{P_{min}G_tL_c}} \tag{3.4}$$

where d is the distance between the tag under test and the transmitter antenna of the measurement system. P_{min} is the minimum transmit power obtained from the measurement system for generating a correct tag response, G_t is the gain of TX

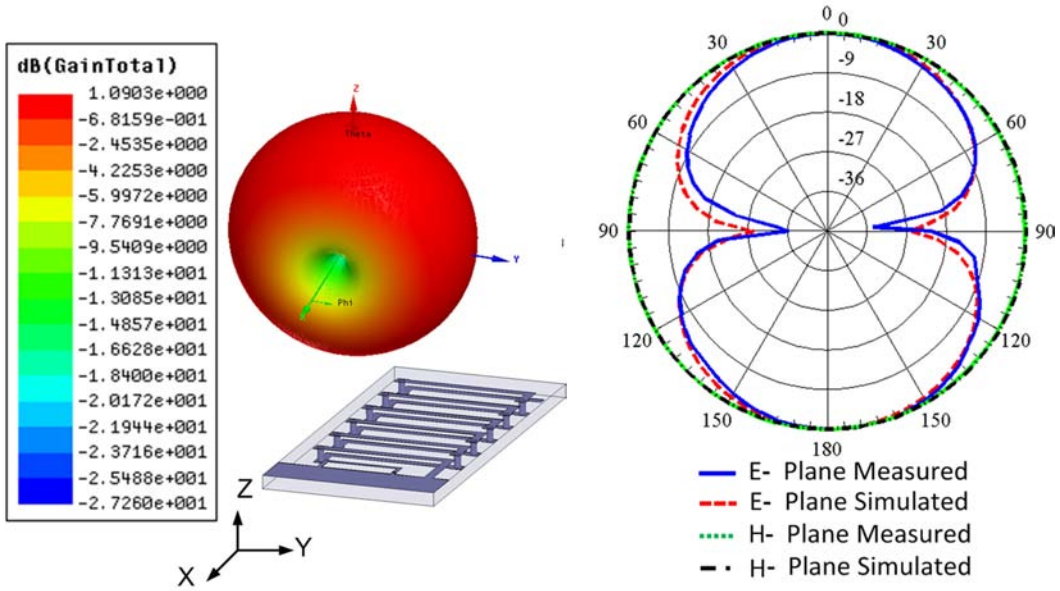

(a) (b)

Figure 3–5: Radiation pattern at 915 MHz of the 3D meander tag: (a) simulated 3D radiation pattern, (b) Measured and simulated 2D radiation pattern.

antenna, L_c is the loss in the connection cable and P_{EIRP} is the allowed maximum transmit power which is determined by the effective isotropic radiated power ($EIRP$) of $3.28W$, ($ERP = 2W$) that is recommended by the European Telecommunications Standards Institute (ETSI) [17]. For other countries that allow $4W$ of $EIRP$, a 10.43 % should be added to the reading range results. The maximum reading range for each of the proposed RFID tags versus the frequency over the 800-1000 MHz band is presented in Fig. 3–9. It can be observed that the proposed RFID tags are functional across the entire UHF frequency band of 860 to 960 MHz. The maximum readable ranges of the folded, 2D and 3D meander monopole tags are 6.38 m, 5.39 m and 5.24 m, respectively, with an EIRP of 3.28 W, which are superior to the maximum reading of comparable antenna topologies such as the meander dipole tag antenna presented in [17] with the reading range of 5 m.

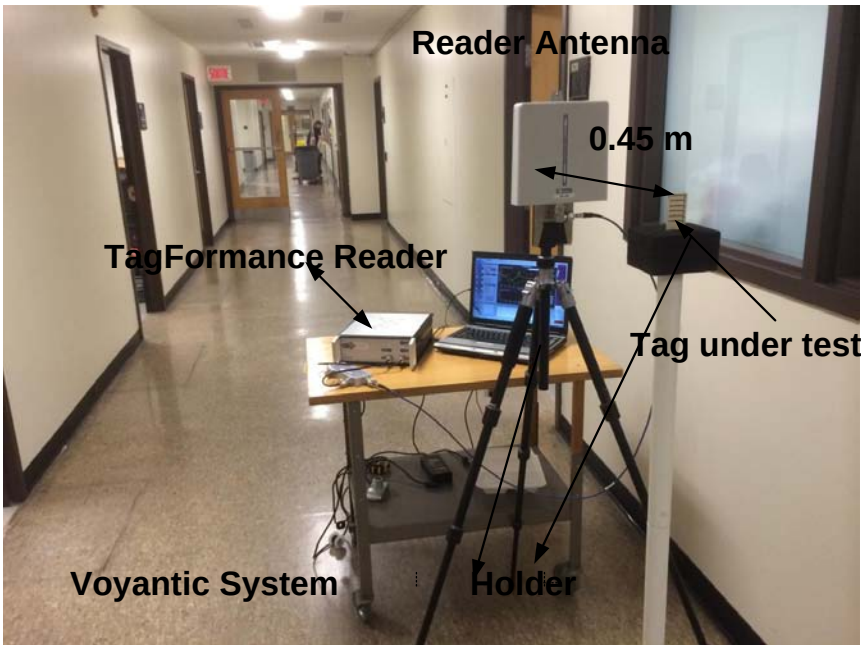

Figure 3–6: TagFormance (Voyantic syestm) measurements setup.

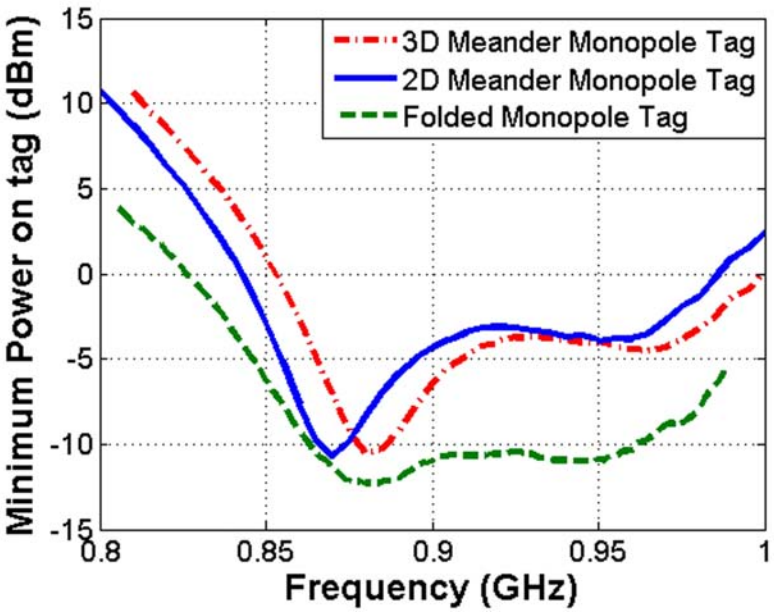

Figure 3–7: Minimum required transmit power on the tag for generating the correct tag response.

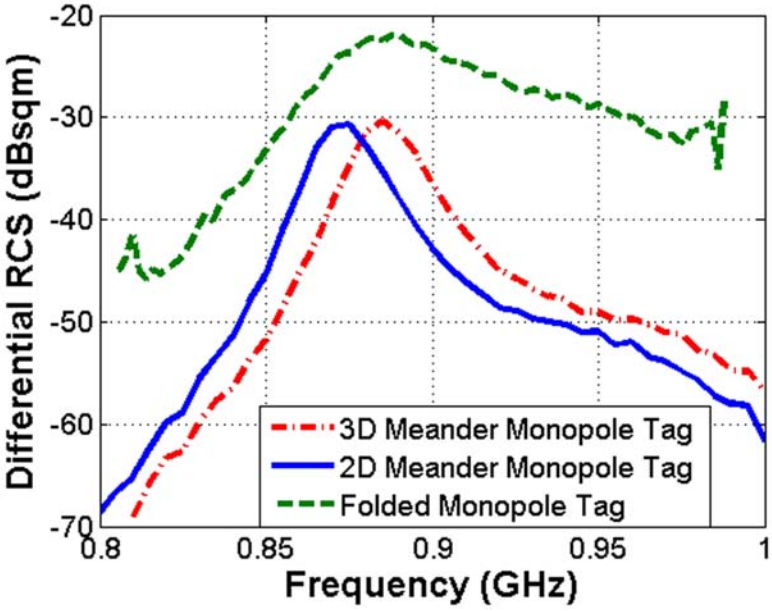

Figure 3–8: Differential radar cross section (RCS) of the proposed tags.

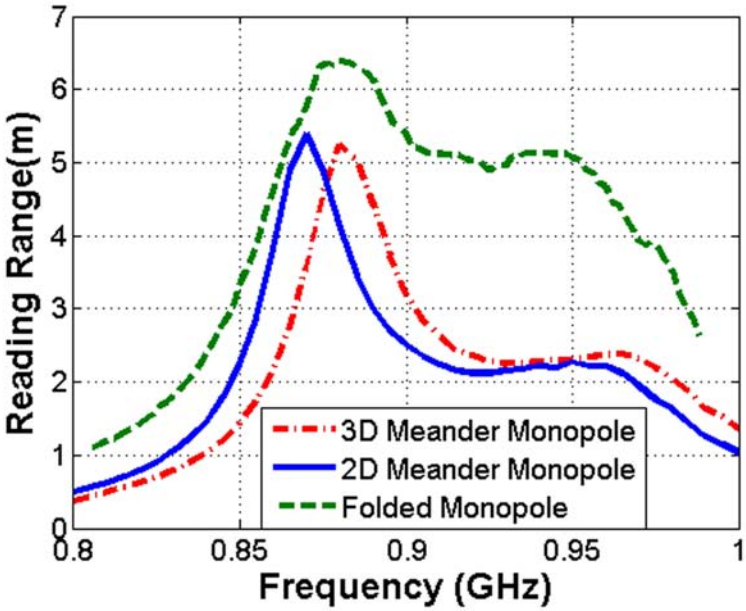

Figure 3–9: Reading ranges of the proposed tags as a function of frequency.

3.4 Summary

Three compact printed monopole antennas are fabricated for use in UHF RFID tags that contain a chip with an input impedance of $8.2 - j61\Omega$. A method for measuring the radiation pattern of the passive RFID tag was presented using a network analyzer and by determining a calibrated S_{21}. Using the proposed method the radiation pattern of an assembled tag antenna including the chip can be measured without any probes or cables directly connected to the antenna. This is important as it represents how the tag is used in practice. The radiation pattern of the prototyped $3D$ meander monopole tag was measured showing an ominidirectional shape similar to that of a conventional dipole antenna. The power sensitivity of the designed RFID tags was also measured by sweeping the power source and determining the minimum power level needed for generating a correct response to a command. The experimental results also demonstrated that the maximum readable range of the proposed folded, 2D and 3D meander monopole tags are 6.38 m, 5.39 m and 5.24 m, respectively, with an $EIRP$ of 3.28 W. The proposed RFID tags (especially the folded monopole) are functional across the worldwide UHF band, thus offering a compact, inexpensive and efficient solution for passive UHF RFID tags that can be marketed globally. However, efficient tags for the global market can be developed by using a tunable design that are discussed in the next chapter.

Chapter 4

Compact Tunable Passive UHF RFID Tag Prototype for Global Operation

---

4.1 Introduction

As indicated earlier in this thesis, the RFID systems are subject to different regional regulations in terms of the output power and frequency allocations. For example, in China the UHF RFID systems are required to operate at 840-845 MHz and 920-925 MHz bands, while in Europe, North America and Japan 866-869 MHz band, 902-928 MHz band, and 950-956 MHz band are designated for UHF RFID operation, respectively [7,62,63]. In order to place a UHF RFID product in the global market, it is needed to design an RFID system that is tunable or wideband enough to cover the entire UHF RFID band. This adds new requirements to the existing challenges in designing UHF RFID tags that include maintaining a minimal footprint for the tag, and matching to the RFID chip. Several miniaturized UHF RFID tag antennas have been proposed in literature [18, 64–68]. However, it is very difficult to achieve maximum reading range at different frequency bands simultaneously and a tunable design is more desirable [69]. Another advantage of a tunable RFID tag

is compensation for the loading of the environment and variations of RFID chip impedance due to the parasitic effects, process variations and packaging [17].

In this Chapter, the design and implementation of a compact tag which covers the whole UHF RFID bands with acceptable and comparable performance is proposed. A miniature tunable passive RFID tag is developed based on the earlier developed designs of compact printed monopole tags reported in Chapter 3. In this Chapter, the proposed tag antenna incorporates a tunable inductor to achieve tuning capability while providing the added benefit of miniaturization of a printed folded monopole. The preliminary design of folded monopole tag in Chapter 3 is optimized in this chapter for implementation using a Rogers laminate and an RFID chip whose operating frequency covers from 840MHz to 960 MHz. The fabricated prototype is evaluated through a set of rigorous laboratory and commercial field tests proving that the proposed tag works with a minimal on-tag transmit power across the global UHF RFID bands making it suitable for different regions and countries.

In order to obtain the antenna mode frequency response of the tunable tag, a simple measurement method is proposed [21]. Using a wide band horn antenna and Vector Network Analyzer (VNA), the frequency response of the tunable tag can be obtained by determining a calibrated (S_{11}) as will be shown in the following sections.

4.2 Overview of Tunable RFID Tags

Bending the arms of a printed dipole and monopole antenna creates an electrically longer antenna in a smaller area [18]. However, reducing the tag's area degrades the reading range and the operational bandwidth. Often, miniature tag

designs cover narrower bands and do not achieve comparable levels of performance at different UHF RFID frequency bands. Several techniques have been proposed to design miniature UHF RFID tags [18, 65–68]. Table 4–1, presents the previously developed compact RFID tag antennas. Clearly it can be noted that the miniature tags cover a narrow bandwidth with a shorter reading range compared to an RFID tag that occupies a large area. As well, it was shown in Chapter 3 Fig. 3–9 that the achieved maximum reading range of 5.3 m at 888 MHz band dropped to 2.3 m at Japan's UHF RFID band, and to 1.03 m at 840 MHz, the UHF RFID band of China. To address this problem, a dual-band meander dipole loaded with spiral resonators, and a planer inverted F antenna (PIFA) are proposed for UHF RFID tags in [62] and [70]. The disadvantage of these designs is that they operate only at the two UHF RFID bands of Europe and US and still they are subject to detuning and losing their optimum in-band performance due to loading effects and tolerances of the RFID chip impedance (resulting because of parasitic effects, process variations and packaging) [17]. In [17] the impact of loading effects and tolerances of the RFID chip impedance is experimentally investigated showing tag's resonant frequency shifting significantly from the expected value. The measurement results of variations of RFID tag range versus frequency for different samples shows 20 MHz difference between the sample with the lowest shift and the one with highest shift in the peak reading range due to ASIC packaging and process variations.

In [17], [71] and [72], a type of adjustable RFID tag is reported for operation at different bands in 840 MHz to 960 MHz range. However, the common drawback of the tunable tags of [17], [71] and [72] is that the operational frequency bands are

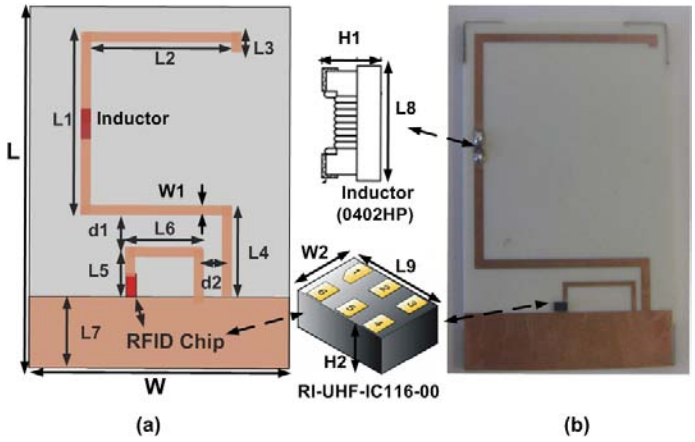

Figure 4–1: (a) Layout of the proposed tag antenna; All dimension are in mm (L=40, L1=27, L2=21, L3=2.5.7, L4=6, L5=3.4, L6=8.35, L7=6.5, L8=1, L9=1.45, L10=3 mm, L11=7 mm, W=24, W1=1, W2=1, d1=1.6, d2=0.65, H1=0.61, H2=0.55). (b) Photograph of the fabricated tunable tag.

controlled by physically changing the layout of the antenna via removing or attaching copper strips. Thus, simple compact tunable tags need to be realized.

4.3 Proposed Miniaturized Tunable RFID Tag Antenna Design

The compact tunable printed monopole antenna introduced in Chapter 3 is redesigned to incorporate a chip inductor, i.e. $0402HP$ provided by Coilcraft [73]. The RFID tag substrate is a 1.524-mm-thick Rogers RO4350B laminate with the relative permittivity of ($\varepsilon_r = 3.66$). The antenna and its printed loop feed system are optimized via fullwave simulations to be integrated with an RFID chip (RI-UHF-IC116-00, provided by Texas Instruments [74]), whose operating frequency is from 840 MHz to 960 MHz. The input impedance of the chip is $10.5 - j78\Omega$, $9.8 - j73\Omega$, $8.2 - j61\Omega$ and $7.2 - j53\Omega$ at the operation frequencies of 842.5 MHz, 866.5 MHz, 915 MHz and 953 MHz, respectively. These are the frequencies of operation of the RFID chip in North America, Europe, China and Japan as indicated by the manufacturer

[74]. The printed loop feed is designed to achieve conjugate matching and maximum power transfer between the highly capacitive RFID chip and the antenna. The tag structure and all the physical dimensions are shown in Fig. 4–1. It can be observed that the overall area of the tag is $40 \times 24mm^2$, while the non-tunable folded monopole tag antenna in Chapter 3 and shown in Fig. 3–1 is $63 \times 24mm^2$. The integrated chip inductor is modeled as a complex impedance (i.e. a series resistor and inductor) in the HFSS simulation as well be seen in this section. The series resistance at the desired simulation frequencies can be calculated from the measured S-parameters (reported in the data sheet) or by the equivalent lumped element circuit provided by Coilcraft [73]. Fig. 4–2 shows the equivalent lumped element model for the chip inductor. The resistance R_{VAR}varies with frequency according to ($R_{VAR} = K \times \sqrt{f}$). While the other parameters (R_1, R_2, C, L, K) are provided by the manufacturer. The calculated equivalent resistance and inductance are presented in Fig. 4–3. The equivalent resistance of the chip inductor ($0402HP-36nH$) versus frequency shows a resistance change between 3.8Ω to 4.8Ω from 800 MHz to 1000 MHz (The equivalent series resistance at 953MHz is 3.5Ω). To tune the tag, three other chip inductors, $0402HP-40nH$, $0402HP-43nH$, and $0402HP-47nH$ are also considered. Typical values for the equivalent resistance of these chip inductors ($0402HP-40nH$, $0402HP-43nH$ and $0402HP-47nH$) are $R = 3.8\Omega$ at 915 MHz, $R = 4\Omega$ at 866 MHz and $R = 4.8\Omega$ at 843 MHz, respectively. These parameters are included in HFSS simulation. Also, Note that in the simulations the RFID chip is modeled by its equivalent input impedance values given in the component data sheet. The simulated results of the antenna input impedance for different inductor values are presented in Fig. 4–4 showing tuning of the resonance frequency to a desired operation frequency across the

entire regulated UHF RFID band. For example, to operate the tag at the frequency band suitable for Japan (950-956 MHz), the 36 nH inductor is used. At the center frequency of 953 MHz, the antenna input impedance is $6.9 + j58.1\Omega$ which provides a close conjugate match to the RFID chip impedance of $7.2 - j53\Omega$. To tune the tag antenna to the North American band (902-928 MHz) the inductance is increased to $38.5nH$ and the input impedance of the antenna at the center frequency of 915 MHz yields a $13.4 + j57\Omega$ value to conjugate match the $8.2 - j61\Omega$ input impedance of the RFID chip. By increasing the inductor value to $43nH$, the antenna can operate at the European band (865-868 MHz) with the antenna input impedance of $10.4 + j68\Omega$ (at 866.5 MHz RFID chip impedance is $9.8 - j73\Omega$). To operate the tag in China, the $46nH$ inductance is chosen resulting in the input impedance of $13.5 + j64\Omega$ at 842.5 MHz (RFID chip impedance is $10.5 - j78\Omega$). The reflection coefficient of the antenna is calculated using 4.1 [75] for different values of the tunable inductor and the results are plotted in Fig.4–5. It can be seen that the widest 3 dB bandwidth is obtained when L=40 nH.

$$\Gamma = \frac{Z_a - Z_c^*}{Z_a + Z_c} \tag{4.1}$$

Where $Z_c = R_c + jX_c$, is the RFID chip impedance, which can be either obtained from the supplier or measured by the designer. $Z_a = R_a + jX_a$, is the simulated or measured impedance of the implemented RFID tag antenna. To realize a perfect conjugate match for an assembled RFID tag $Z_a = Z_c^*$.

Considering these values, further simulations are conducted to observe, directivity and efficiency. It is found that the gain of the antenna for all four bands is around 2.2 dB. The efficiency is 54% at 953 MHz, and 52%, 48% and 46% at 915 MHz, 866 MHz and 843 MHz, respectively.

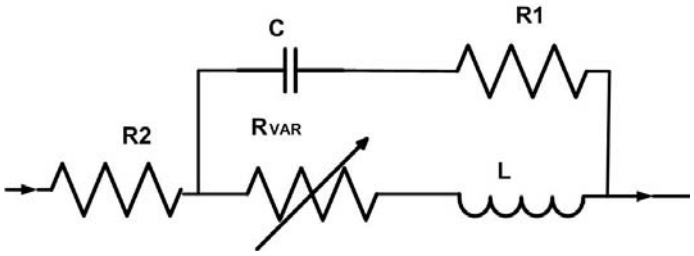

Figure 4–2: Equivalent circuit structure of the chip inductor (0402HP)[73].

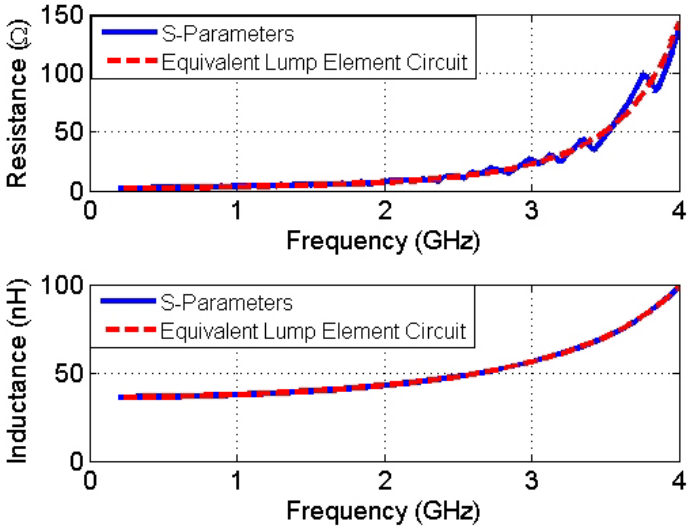

Figure 4–3: Calculated inductance and internal resistance of the chip inductor (0402HP).

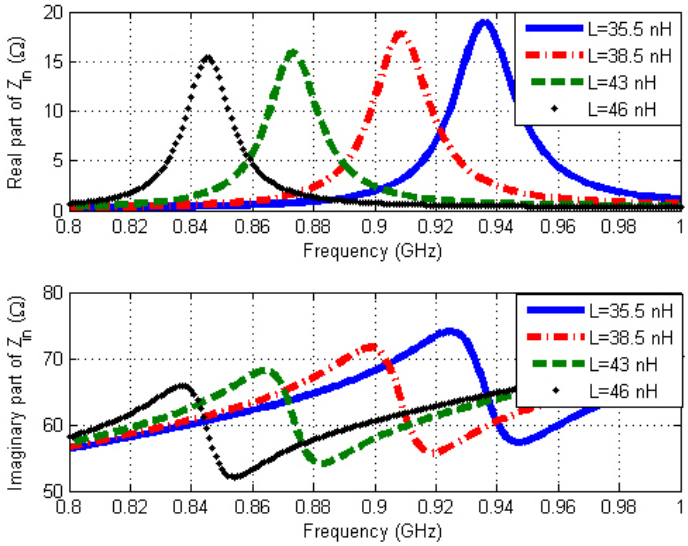

Figure 4–4: Input impedance of the tag antenna with different inductor values.

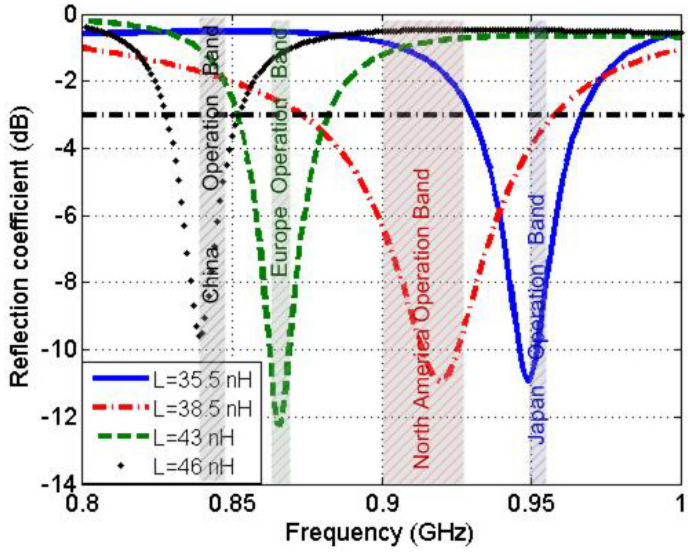

Figure 4–5: Magnitude of S11 of the proposed tunable RFID tag antenna.

Table 4–1: Compact UHF RFID Tags In Literatures

Published literature	Tag'size Proposed/ literature	Read range	Operational band
[65]	$83.6 \times 51.4mm^2$	$6.8\&4.4m$	$885MHz\&925MHz$
[18]	$63 \times 24mm^2$	$6m$	$866MHzto952MHz$
[18]	$40 \times 19.7mm^2$	$5.2m$	$888MHz$
[66]	$55.5 \times 11.9mm^2$	$5.4m$	$920MHz$
[67]	$47.1 \times 14.8mm^2$	$4.87m$	$915MHz$
[68]	$36.2 \times 8.2mm^2$	$4.1m$	$915MHz$

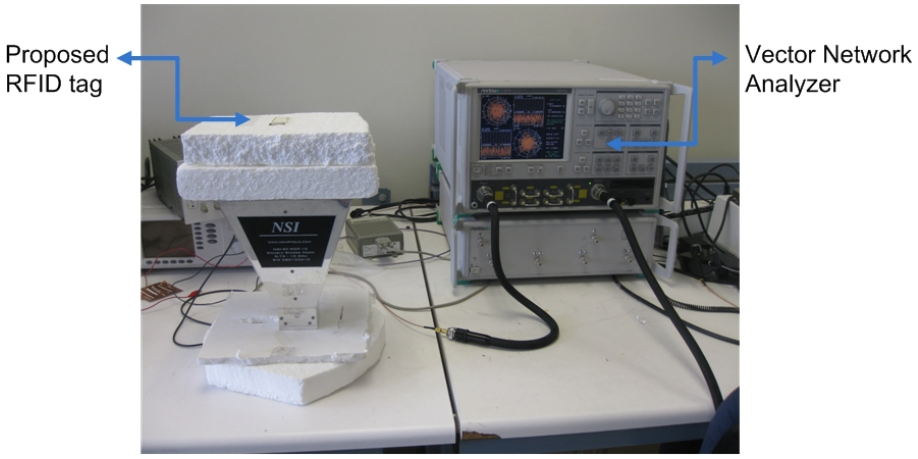

Figure 4–6: The test setup for measuring frequency response of the RFID tag.

4.3.1 Experimrntal Evaluation of the Proposed Tunable RFID Tag

A. Observing Tuning in the Frequency Response Measurement

To confirm tuning the tag with the proper choice of inductance, the frequency response was evaluated in the lab using the following proposed method by determining a calibrated S_{11} [21]. The tag was held 20 cm away from the aperture of a wideband horn antenna along its central axis as shown in Fig.4–6. For each value of inductor, the reflection coefficient was measured for the OFF and ON states. For the first case (OFF), the reflection coefficient was measured when the VNA supplied power was around -20 dBm (Note that the propagation path loss at 800 MHz is 16.53 dB and at 1000 MHz is 18.47 dB and the transmitter antenna gain is 6 dBi). Since

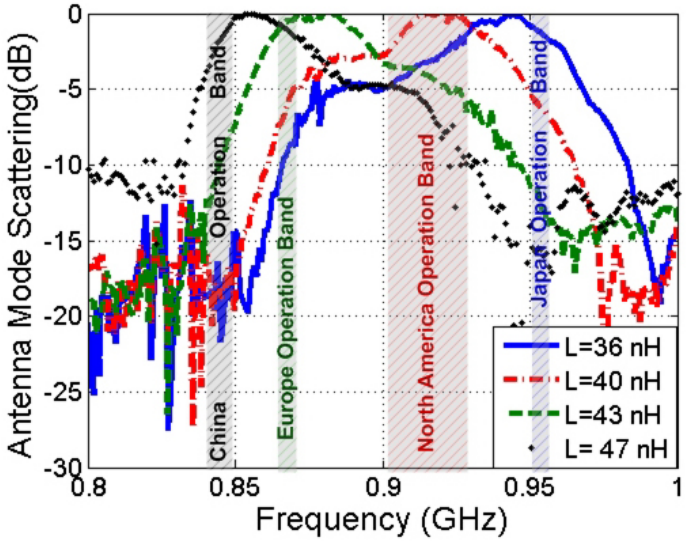

Figure 4–7: Measured frequency response with different values inductor.

the nominal threshold power of the RFID chip is -13 dBm, this input for illumination power assures that the RFID chip is OFF. The second case (ON) was measured after increasing the power to 15 dBm to turn the RFID chip on. To remove the effects of the tags structural mode as well as the scattering from the surrounding objects, and to obtain its normalized frequency response (a.k.a. antenna mode scattering [21]), the OFF state result is subtracted from the ON state result. The normalized measured results for different inductor values ($36, 40, 43$ and $47nH$) are presented in Fig. 4–7. The peaks in the measured reflection coefficient demonstrate tuning the resonance frequency of the tag to any operation bands allocated for the UHF RFID applications.

B. Power Sensitivity and Differential Radar Cross Section

In the next step, instead of a laboratory set-up, a commercial RFID tag measurement system [61] was used to evaluate the power sensitivity of the tag at Voyantic

Laboratory. The transmit power was incremented by 0.1 dB steps (starting from 0 dBm), at each test frequency across the 800 MHz to 1000 MHz band, to detect the minimum power required to obtain a correct tag response. The distance between the reader and the tag in this commercial test system is 0.45 m.The measured results are presented in Fig. 4–8 demonstrating that the tag can be activated across the global UHF RFID bands with a minimum on tag power as low as -11.55 dBm by switching between 4 inductance values. Considering the 23.57dB (at 800 MHz) to 25.51 dB (at 1000 MHz) propagation loss, this means the minimum on-tag transmit power can be between -9.53 dBm to -11.55 dBm. With this measured level of power sensitivity, it can be concluded that this passive tunable tag can be detected with a variety of commercial readers sold globally. The differential radar cross section (ΔRCS) was also measured by means of the same monostatic test configuration at Voyantic Laboratory. By recording the received back scattered power from the tag in response to the threshold transmitted power by the reader, the differential radar cross section (ΔRCS) was obtained using the Equation 3.3 presented in Chapter 3. The ΔRCS plots as a function of frequency for the prototyped tag with the selected inductors are shown in Fig. 4–9. The peak measured ΔRCS of the tag with $L = 36nH$ is $-25.1dBsqm$ (at 953 MHz, Japanese band). With $L = 40nH$, it is $-24dBsqm$ (at 915 MHz, North American band), and $-28dBsqm$(at 866 MHz, European band) for $L = 43nH$, while it is $-27.7dBsqm$ (at 843 MHz) for the Chinese band with an inductor value of $L = 47nH$.

C. Reading Range

The reading range of the tag versus operation frequency can be obtained from the formula given in Equation 3.4. In these measurements the minimum transmit power

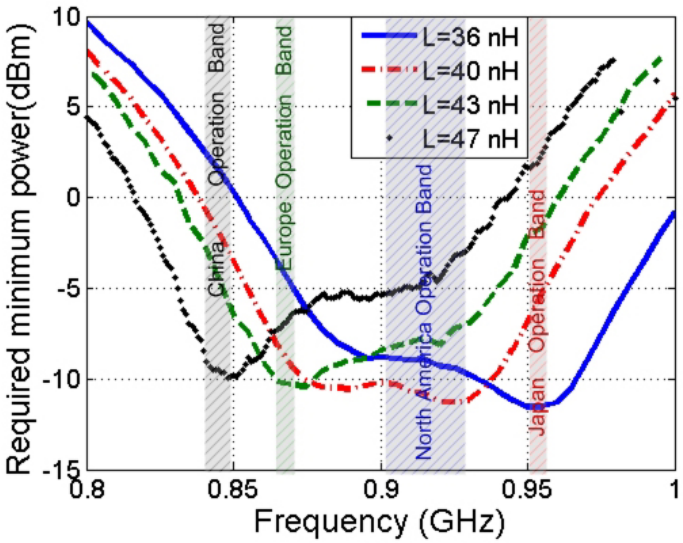

Figure 4–8: Minimum required transmit power on the tag for generating the correct tag response by switching between 4 inductance values ($L = 36nH, 40nH, 43nH$ and $47nH$).

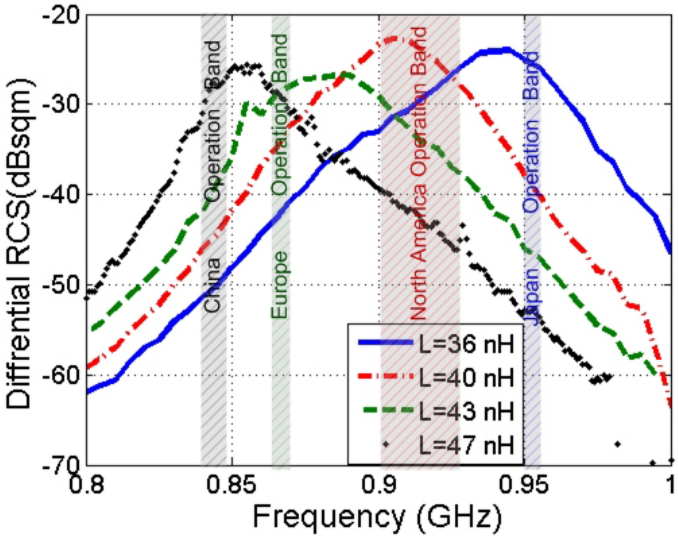

Figure 4–9: Differential radar cross section (RCS) of the proposed tags by switching between 4 inductance values ($L = 36nH, 40nH, 43nH$ and $47nH$).

required from the reader to activate the tag at each frequency (found in the earlier test) was applied across 800 to 1000 MHz. The maximum $EIRP$ used in reading range calculations was $3.28W$, ($ERP = 2W$) as recommended by the European Telecommunications Standards Institute ($ETSI$) [17]. For countries or regions that use $EIRP$ of 4W, e.g., North America, 10.43% should be added to the reading range results. The reading range versus frequency with different inductor values is plotted in Fig. 4–10. It can be observed when the inductor is $L = 36nH$ the maximum reading range is 5.4 m at 953 MHz which is the center frequency at the Japanese band, while the reading range at the North American, European and Chinese bands are 4.3 m, 2.4 m and 1.2 m, respectively. In order to operate the same tag in North America, Europe, and China the inductance of the embedded inductor chip should be increased to $40nH$, $43nH$ and $47nH$, respectively. With these inductors, the maximum reading ranges of 5.44 m, 5.16 m and 4.84 m at the North American, European and Chinese bands are achieved, respectively. Note that with applying 4 W $EIRP$ the reading range increase to 6.01 m in the North American band.

D. Radiation Pattern

The other important measurement in characterization of tag functioning is the radiation pattern of the tag antenna. Similar to a conventional radiation pattern measurement, it gives information about the main directions of spatial pattern of distribution of radiated power/field by the tag antenna. Unlike conventional antenna designs that are matched to 50Ω, RFID tag antennas are loaded with the complex impedance of the RFID chip which is not a standard setting in the pattern measurement. Therefore, it is important to investigate the radiation pattern of the

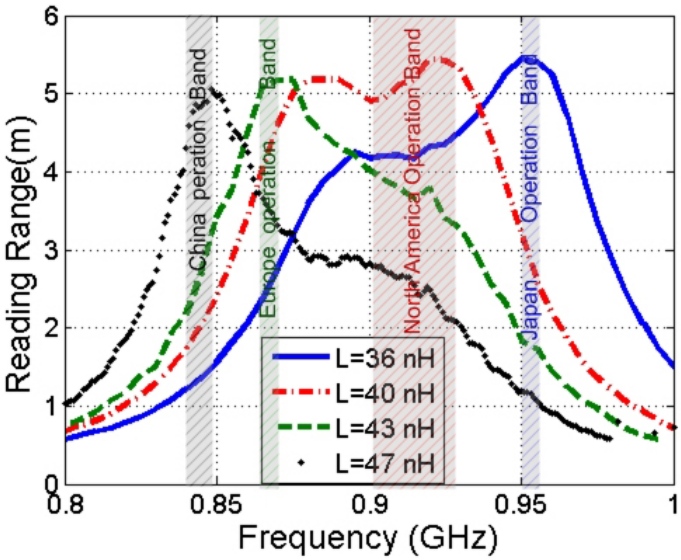

Figure 4–10: Reading ranges of the proposed tags as a function of frequency with $L = 36nH, 40nH, 43$ and $47nH$.

RFID tag with an assembled and activated chip to observe any pattern deterioration that can happen in actual tag operation. If metallic cables are used to switch the RFID chip on, the radiation pattern of the tag antenna will be impacted. To eliminate this effect, the Tagformance test system at Voyantic laboratory was used to extract the radiation pattern from power sensitivity measurements without any physical feed connection [60]. In this measurement, the power sensitivity extracted at measured θ, ϕ angles is normalized to the measured minimum threshold power and plotted as a function of angle. The measured radiation patterns with inductance values $40nH$ and $36nH$ at the operation frequency of 915 MHz, 953 MHz, respectively, are presented in Fig. 4–11 and 4–12 as samples of this test. Fig. 4–12 also shows the 3D simulated pattern for better visualization. There are very minimal differences between the radiation patterns of the assembled tag at other RFID operation bands. The measured half-power beam width in all cases is around 86^0 and as can be seen from the shown x-y, y-z and x-z plane cuts the radiation patterns are omnidirectional

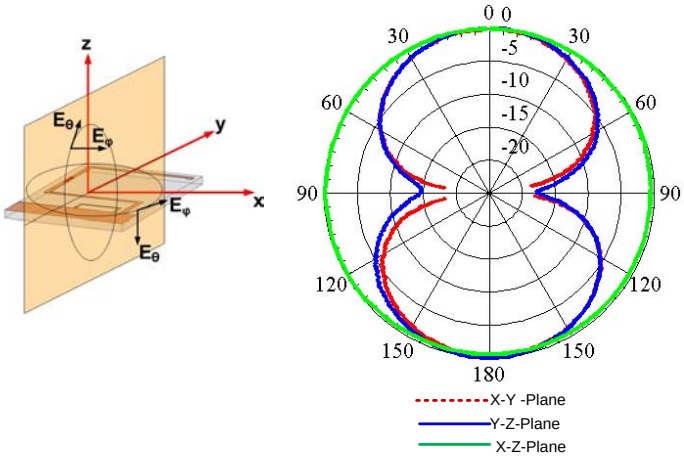

Figure 4–11: Measured radiation pattern of the RFID tag at 915 MHz with inductance value of 40 nH.

and similar to those of dipole antennas. The efficiency and gain of the antennas can be found using a reference antenna with known gain and connected to the same chip as presented in [76].

4.4 Proposed Tag Integrated With a Tunable Inductor

In the previous measurements, the proposed tunable tag is incorporated with chip inductors. By switching between four inductance values, the tag can be tuned to operate efficiently at different frequencies bands. However, the tag can be simply tuned using a tunable inductor (i.e. 164-01A06L, $26nH$ to $34nH$), provided by Coil craft) as shown in Fig. 4–13. The tuning method is done by means of an aluminum core that is integrated inside the inductor [73]. By changing the aluminum core, the tag can be tuned from 840 MHz to 960 MHz as shown in Fig. 4–14. Currently, there is no equivalent circuit model for the integrated tunable inductor. Thus, from the experimental measurement the tunable inductor (model number $164-01A06L$, ranging from $26nH$ to $34nH$) was selected to tune the RFID tag across the global

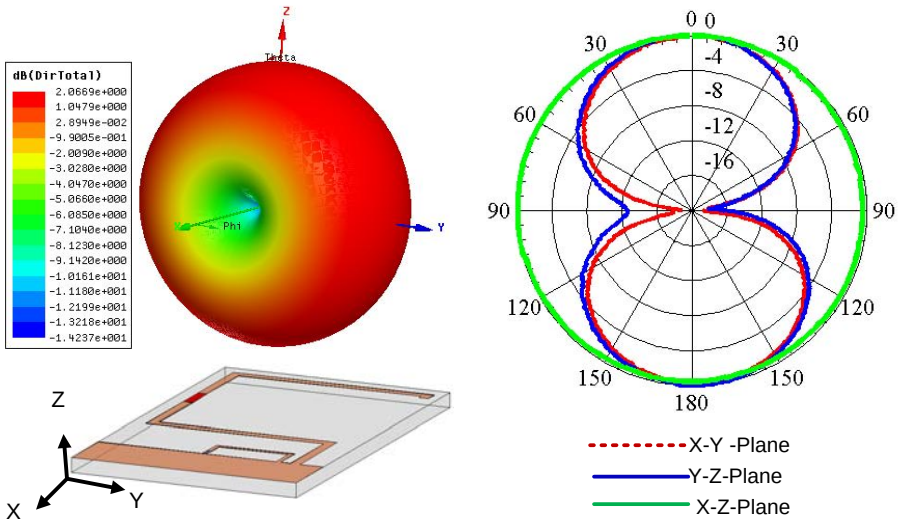

(a) (b)

Figure 4–12: Radiation pattern at 953 MHz of the tunable tag: (a) simulated 3D radiation pattern, (b) Measured 2D radiation pattern.

frequency operation. The maximum reading range of the tunable RFID tag across the global operational frequency bands is presented in Fig. 4–14. With the tunable inductor, the maximum reading ranges of 5.94 m, 5.9 m , 6 m and 6.1 m at the Japanese, North American, European and Chinese bands are achieved, respectively.

4.5 Summary

In this Chapter an overview of tunable RFID tags is presented. This is followed by describing the novel tunable UHF RFID tag antenna design developed in this research work. First, a tunable compact printed folded monopole tag antenna is presented. The proposed tag antenna is integrated with an RFID chip whose operational frequency covers the global regulated UHF RFID bands. For size reduction and tuning, a tunable inductor is incorporated in the tag antenna. This results in

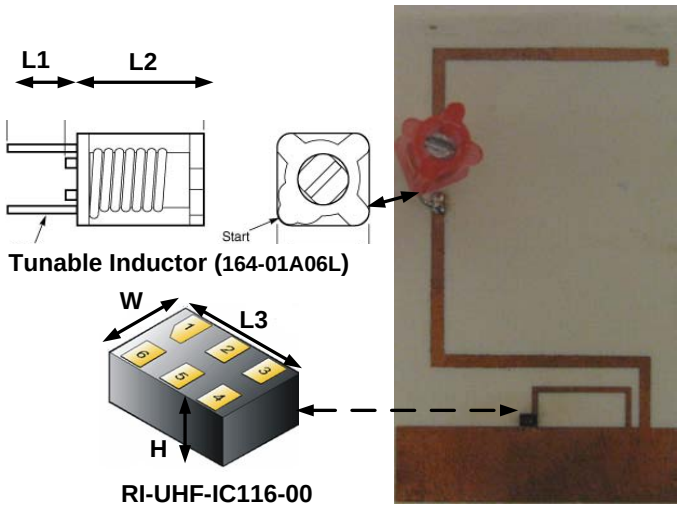

Figure 4–13: Photograph of the fabricated tunable RFID tag antenna incorporated with a tunable inductor (164-01A06L).(L3=1.45, L1=3 mm, L2=7 mm, W=1mm, and H=0.55 mm).

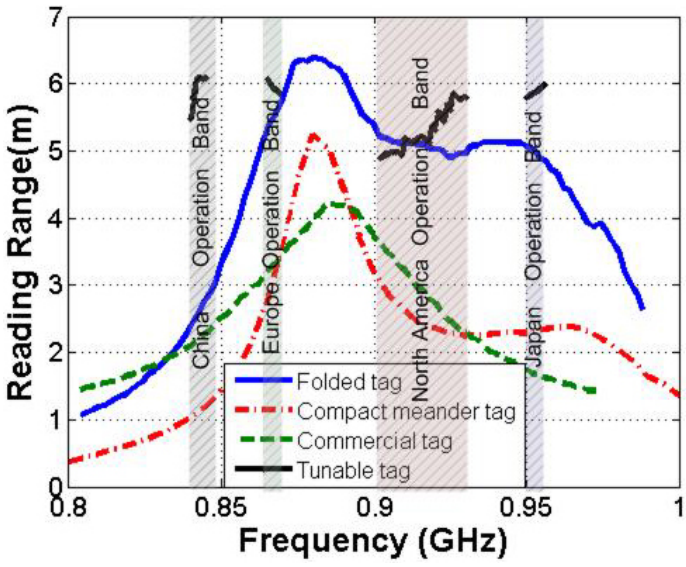

Figure 4–14: Reading ranges of the proposed tags as a function of frequency with a tunable inductor (164-01A06L, $26nH$ to $34nH$) .

an area reduction of 36.5% comparing with a conventional folded monopole tag antenna. The tag is fabricated and experimentally evaluated; the frequency response is measured with a simple method using a network analyzer, and by determining a calibrated S_{11}. Other parameters, such as power sensitivity, differential radar cross section and reading range also were evaluated via a commercial RFID measurement system. Prototypes with switching chip inductors and using one packaged tunable inductor are developed and evaluated. All the measured results demonstrate that the tag can be tuned using the tunable inductor to operate efficiently at any desired UHF RFID bands. With a maximum effective isotropic radiated power of 3.28 W from the reader, the tag can be correctly identified in approximately 6 m distance in any region in the world (5.9 in Japan and North America, 6 m in Europe and 6.1 m in China). The developed compact passive tag proves to be a viable solution that can be marketed globally for a variety of UHF RFID applications.

Chapter 5

Miniaturized Passive UHF RFID Tag Antennas for Identification of Metallic Objects

---

5.1 Introduction

When implementing an RFID system, it is often desired to have a compact tag with minimal detuning of its performance due to the loading of identification objects, and to extend the reading range without increasing reader's power. These objectives impose contradictory constraints on designing tag antennas, meaning that the tag antenna should be high gain to support a long reading range, while being small which translates into increased back radiation and interaction with the object it is mounted on. Conventional RFID tags, usually meander [18] or folded [77] dipole and monopole-type tag antennas, are influenced by the characteristics of the identification object due to their omnidirectional radiation. Their resonance frequency, input impedance, radiation pattern and efficiency degrade, especially when they are mounted on metallic surfaces or placed in close proximity to the human body. To reduce tag-material sensitivity, RFID tag antennas are typically required to have unidirectional radiation patterns. The most commonly adopted undirectional tag

antenna geometries are microstrip patch antennas [24, 78–80]. Patch antennas are popular not only because of their unidirectional radiation pattern (high front-to-back-lobe ratios) but also because of their high gain and ease of fabrication. However, their main drawbacks are their relatively larger footprint in comparison with the meander and folded dipole type candidates, and the limited bandwidth resulting from the half-wave length design requirements. Thus, several techniques have been proposed to implement compact patch antennas which include adding parasitic patches [24], reactive loading with T-shaped microstrip lines [78], etching thin multi-slots on the patch [79], and using a pair of U-slots [80]. These techniques also degrade the gain [24], [78], which is an essential parameter for increasing the reading range. Another method uses electromagnetic bandgap (EBG) substrate and harnessing the slow-wave propagation to reduce the patch footprint, which is shown to minimally impact the radiation characteristics [80]. When EBG structures are designed to operate as artificial magnetic conductors (AMCs), they can dramatically decrease back radiation thus reducing antenna interaction with the identification object.

In order to reduce the material sensitivity of the proposed compact printed monopole tag antennas presented in Chapter 3, a shielding structure such as an AMC can be incorporated in the tag antenna profile [81]. Using an AMC as the ground plane of printed dipoles and monopoles, prevents degradation of the tag's performance due to short-circuiting of the antenna by a metallic identification object and also improves antenna directivity.

In this chapter, first, a miniaturized UHF tag antenna consisting of a microstrip patch backed by an EBG structure is designed and implemented. The antenna's input impedance is conjugate matched to the RFID chip by an inset feed on the patch [21].

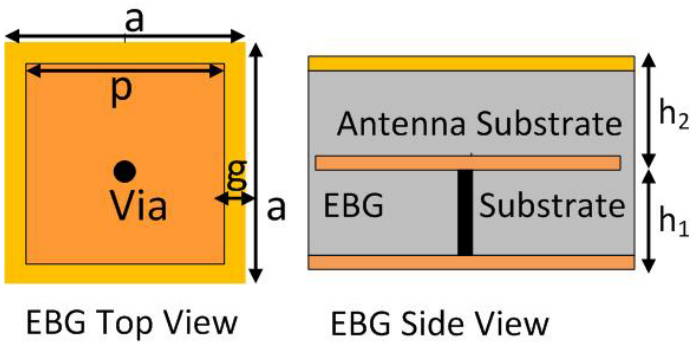

Figure 5–1: Schematic of the unit cell of the shielded mushroom-EBG structure used for miniaturization. All dimensions are in mm :$a = 18.5, p = 18, g = 0.25, h_1 = h_2 = 1.524$.

Full-wave simulations are conducted to evaluate the antenna performance. This is followed by testing a fabricated prototype to obtain its antenna mode frequency response, radiation pattern and reading range in the two cases of stand alone tag and the tag mounted on a metallic sheet.

Second, a printed meander monopole tag antenna [14, 18] is designed to include an artificial magnetic conductor (AMC) structure as its reflector. The antenna is integrated with an RFID chip having an input impedance of $8.2 - j61\Omega$ at the operation frequency of 915 MHz. For maximum power transfer, the tag antenna's input impedance is conjugate matched to the RFID chip by implementing a T-matching technique in the antenna layout [81]. Full-wave HFSS simulations are conducted to evaluate the performance of the antenna backed by a 4 cell $\times$ 4 cells AMC surface. To demonstrate the efficiency of this approach, the reading range of the fabricated prototype tag is measured using a commercial RFID reader (GAO 216010) in a typical deployment environment.

5.2 Design of a Miniaturized Patch Antenna Using Electromagnetic Bandgap Structures

Due to unidirectional radiation patterns with small front-to-back (F/B) lobe ratio characteristic, microstrip patch antennas are suitable candidates for the realization of tag antennas for the identification of metallic objects. As the size of the patch antenna is proportional to half of the operating wavelength, a conventional patch antenna operating at UHF bands can be of considerable size in space-limited environments. The most common techniques used for patch antenna miniaturization are employing a higher-permittivity material for the antenna substrate and incorporating slot patterns on a patch [23] [24], each having their own drawbacks. The size reduction that is achieved using a high-permittivity substrate is proportional to the square root of its relative permittivity. Often, a high dielectric loss is associated with high-permittivity materials. Meanwhile, incorporating slot patterns on a patch only achieves approximately a $10\% - 20\%$ size reduction, while gain, bandwidth, and efficiency are compromised [25].

An EBG structure supports slow-wave propagation modes whose wavelengths are smaller compared with those in free space and dielectric. Thus, the size of a patch antenna can be significantly miniaturized by simply integrating it above an EBG structure, such as the mushroom-type EBG substrate presented in [82]. The EBG structure is designed using a Rogers 4350B substrate with the relative permittivity and loss tangent of $\varepsilon_r = 3.66$ and $\tan \sigma = 0.004$ such that the first mode exhibits slow-wave behaviour at the UHF frequency band of interest. The thickness of the substrate is 1.524 mm. The unit cell as represented in Fig. 5–1 is a square dielectric slab ($a \times a$) topped with a grounded patch ($p \times p$), where $p = a - 2g$ and is equal

to 18.5 mm. The diameter of the via and the gap between the two adjacent EBG patches are 0.8 mm and 0.5 mm, respectively. A Finite Element high frequency Eigen value solver (i.e., Ansoft-HFSS) is used to extract the dispersion diagram shown in Fig. 5–2. It can be seen that the first mode supports slow waves. At the frequency of 940 MHz, λ_{slow} is nearly 95.05 mm. Fig. 5–3 illustrates the schematic of the proposed rectangular patch antenna composing of an inset feed and a mushroomtype EBG structure underneath. The patch antenna is initially designed using standard formulas with this wavelength value and then optimized using HFSS, yielding L_{patch} and W_{patch} equal to 54 mm and 51 mm, respectively. An array of 16 EBG unit cells backs the patch with the overall area of $76mm \times 76mm$. Compared to conventional patch antennas, i.e., without an EBG structure, the overall antenna area, including the EBG surface underneath, is reduced by 29.11%. Indeed, a size reduction of almost 70% to $59mm \times 79mm$ is expected for the next version of the proposed antenna that is backed by a 4 cells $\times$ 3 cells EBG surface instead. The tag antenna is designed to be integrated with an RFID chip (RI-UHF-IC116-00) provided by Texas Instruments, whose input impedance characteristic versus frequency is shown in Fig. 5–4. The input impedance of the RFID chip is capacitive. Therefore, to achieve maximum power transfer between the tag antenna, with the input impedance shown in Fig. 5–4, and the chip, conjugate impedance match should be realized. This is achieved by an inset feed line as shown in Fig. 5–4. The chip leads are connected to the bottom ground by using a via (other than the EBG cells vias) and to the inset line feed. The real part of the input impedance of the antenna can be controlled by varying the location of the inset feed along the y-axis away from the patch center [21]. Once the desired real part is achieved, the imaginary part of the input impedance is tuned

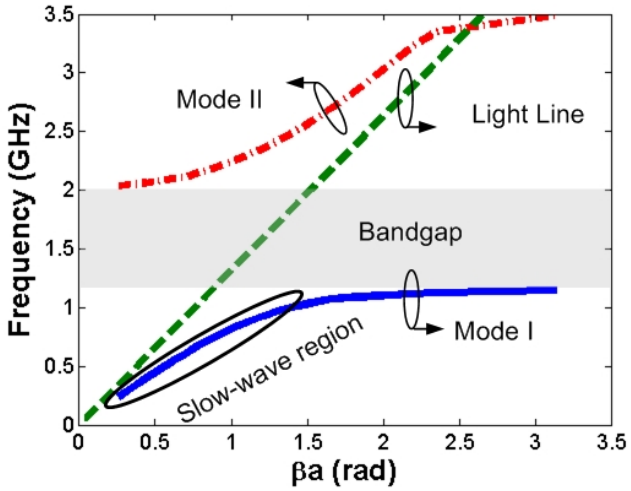

Figure 5–2: Dispersion diagram of the EBG unit cell.

by controlling the length of the inset feed line. Fig. 5–4 demonstrates the simulated results of the real and imaginary parts of the antenna input impedance. At the operation frequency of 940 MHz, the antenna input impedance is $20.35 + j62.14\Omega$ and the radiation efficiency and directivity are 70%, 6.44 dB, respectively.

5.3 Tag Characterizations

Once the RFID tag is fabricated, it is essential to characterize the assembled tag for its frequency response, radiation pattern and maximum reading range.

5.3.1 Frequency Response Measurements

In order to obtain the frequency response of the tag, first, it is simulated in Ansoft-HFSS under illumination by a planewave with the power of 1 Watt as shown in Fig. 5–5. In this simulation, the chip is represented by an equivalent series RC network with $R_{chip} = 8.2\Omega$ and $C_{chip} = 2.85pF$ (input impedance in active mode, i.e., ON state). By sweeping the illumination frequency and observing the

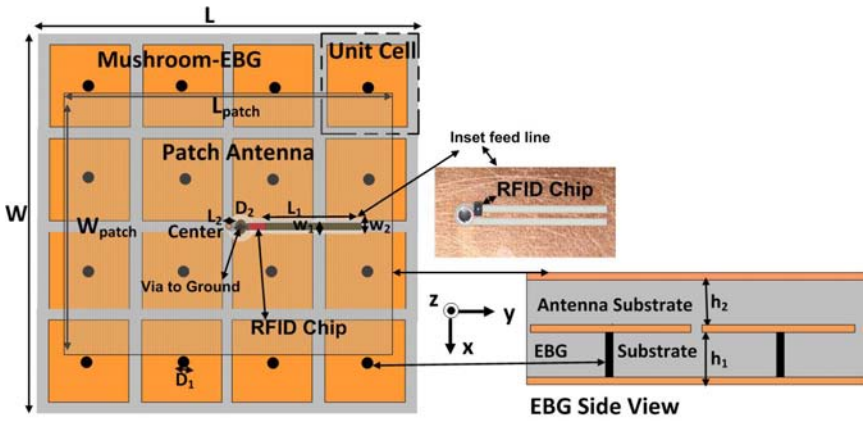

Figure 5–3: Miniaturized patch antenna on a mushroom EBG substrate; The physical dimensions of the antenna are as follows (all dimensions are in mm): $L = 76, W = 76, L_{patch} = 50, W_{patch} = 67.2, L_1 = 17, L2 = 4, D_1 = 0.8, D_2 = 0.762, a = 18.5, p = 18, g = 0.25, h_1 = h_2 = 1.524, W_1 = 0.6$ and $W_2 = 2.3$.

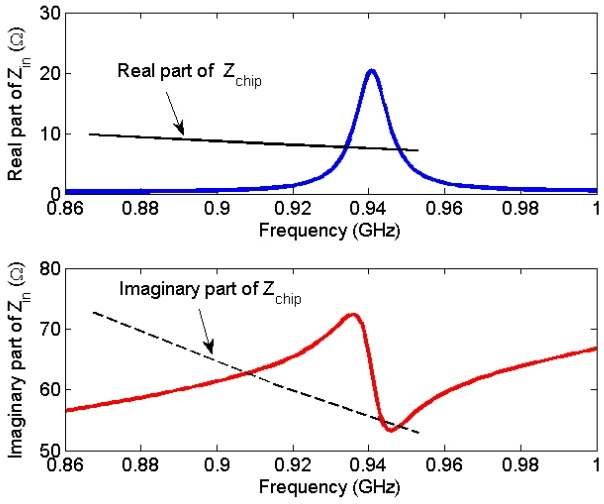

Figure 5–4: Simulated input impedance of the proposed tag antenna and the input impedance of the chip.

scattered electric field (i.e., E_{scat}) at a distance of 20 cm away from the patch surface along z-axis, the total scattered field is obtained (see Fig. 5–5(a)). The scattered field includes, the tags antenna mode and structural mode [21]. The former is the component of interest and represents the performance of the assembled tag antenna with the chip. The latter mode is due to the scattered wave by the physical structure which should be subtracted from the total scattered field. In simulations the chip is modeled by an open circuit when the incident power is below the threshold and the chip is OFF. By performing two simulations, when the chip is ON (conjugate match impedance) and OFF (open-circuit) and subtracting the latter E_{scat}, from the former fields, the antenna mode scattering is obtained. The simulated result is shown in Fig. 5–5(b), demonstrating that the tags operating frequency occurs at 940 MHz. For comparison purposes, the magnitude of normalized radar cross section (RCS) of the tag in monostatic case (transmitter and receiver are collocated) is plotted in Fig. 5–5. The frequency response of the tag obtained from the two tests follow a similar trend in predicating the peak frequency except for a slight shift.

The frequency response of the tag was also obtained experimentally; a wide band horn antenna was connected to a calibrated Vector Network Analyzer (VNA) and the reflection coefficient was recorded for the two cases of ON and OFF states. The tag was held 20 cm away from the aperture of the horn along its central axis and the reflection coefficient was measured when the VNA supplied power is around -20 dBm. This illumination power guarantees that the chip is OFF since $P_{threshold} = -13$ dBm. After increasing the power to +5 dBm to turn on the chip, the reflection coefficient was recorded and the OFF state result is subtracted from it to remove the effect of tags structural mode and also the scattering from the surrounding objects.

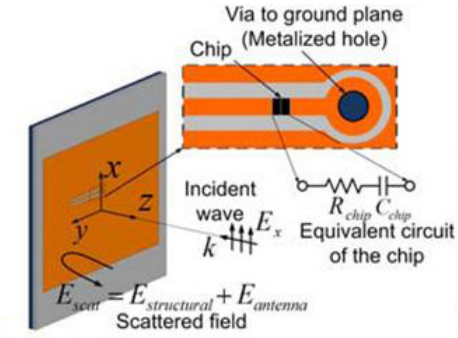

(a)

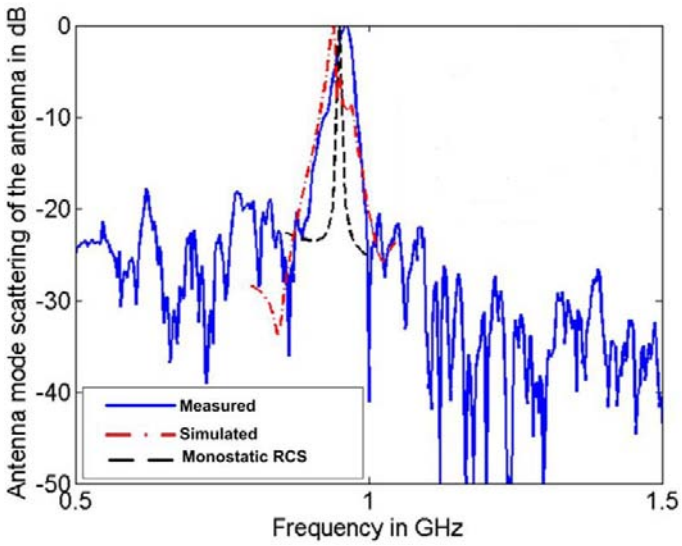

(b)

Figure 5–5: (a) The schematic of the simulated patch in Ansoft-HFSS. (b) Frequency response of the proposed tag, measured and simulated.

The normalized value of the measurement results are also demonstrated in Fig. 5–5 indicating a peak power at 960 MHz which is slightly different from simulation results due to fabrication and test errors.

5.3.2 Radiation Pattern Measurement

For pattern measurement in an anechoic chamber, since the input impedance of the antenna is not 50Ω, a matching circuit is integrated in the antenna layout using

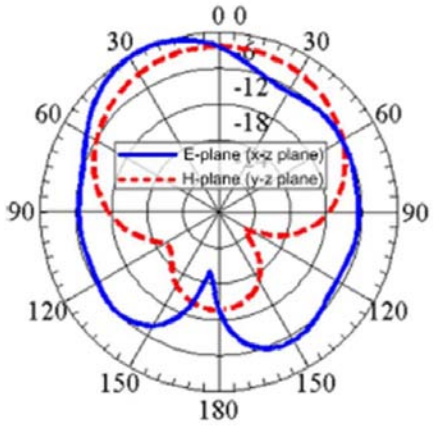

Figure 5–6: Radiation pattern of the tag antenna measured at the resonance frequency (i.e., 960 MHz) of the tag obtained from frequency response measurement.

a lumped element π-network composed of two parallel capacitors ($3pF$) and a series inductor ($10nH$). These values were obtained through an optimization process using a High Frequency Circuit Simulator, i.e., ADS software. The patterns are found at 960 MHz where the antenna mode resonance is seen as described in the previous section. The radiation pattern was measured in a compact range anechoic chamber and the E- and H-plane cuts (i.e., x-z and y-z plane), normalized to the maximum value, are shown in Fig. 5–6. It can be seen that the back radiation is not as low as expected, especially in the E-plane, which is due to the relatively smaller size of the tag, but still considerable since it is close to 5.2 dB front to back ratio.

5.3.3 Maximum Reading Range Measurement

Fig. 5–7 shows the setup used for estimating the maximum reading range. In this measurement, a commercial RFID reader (GAO 216010), was available and it was mounted on a base at the height of H_1=1.3 m above the ground. The tag, as Fig. 5–7 demonstrates, was placed on a mast with the height of H_2=1.3 m.

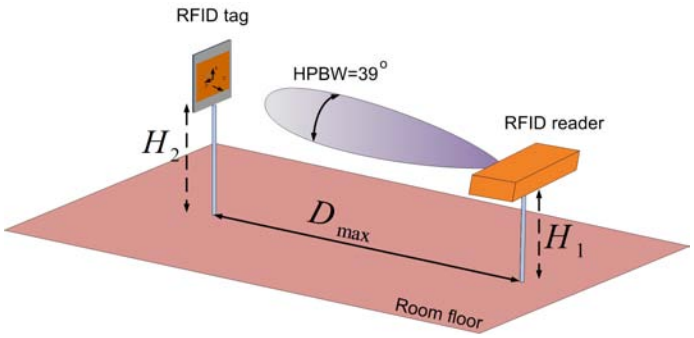

Figure 5–7: Schematic of the setup used for measuring tag's maximum reading range.

By increasing the distance of tag from the reader while collecting the tag signal, the maximum reading range of 11 m was obtained. Beyond this distance tag was not detectable. To evaluate the performance of the tag when placed on an object, a rectangular metallic (Copper) sheet with the area of $200mm \times 300mm$ was considered as the identification object. Since the radiation pattern results show a smaller back radiation as opposed to front radiation, it is expected that the performance to be minimally impacted by the object it is mounted on. The tag was attached at the center of the metallic sheet and the maximum reading range of approximately 11 m was measured.

5.4 Passive UHF RFID Printed Monopole Tag Antenna for Identification of Metallic Objects

As indicated earlier, compact RFID tags based on printed monopole antennas presented in Chapter 3 do not operate efficiently in proximity to high permittivity materials and metallic surfaces. To reduce tag sensitivity to the identification object, a shielding structure such as an artificial magnetic conductor (AMC) is incorporated in the antenna profile [81, 83]. AMC is a good candidate to replace the ground plane of low-profile antennas. There are two important advantages when AMC is used

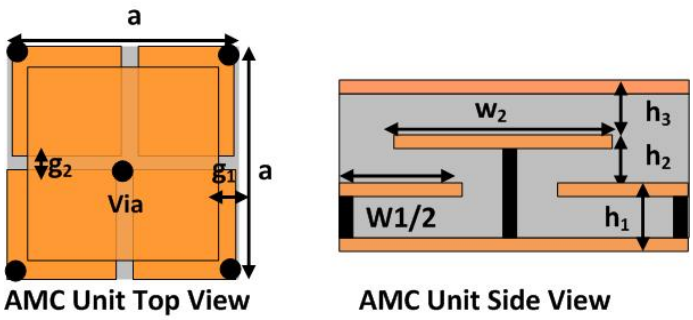

Figure 5–8: Schematic of AMC unit cell. All dimensions are in mm (W1=25.675, W2=26.675, h1=1.524, h2=0.508, h3=0.508, a=27.175, Radius of vias=0.762, g1=0.25, g2=1.5)

instead of a ground plane; first, it prevents degradation of the antenna performance due to short-circuiting by the metallic identification object. Second, the antenna directivity can also be increased [81,84]. The challenges in employing AMC structures in the UHF tag design are miniaturization of the unit cell, and ensuring reduced back radiation (or equivalently reduced sensitivity to the identification object) without significantly impacting the reading range of the RFID system. In this work, the printed meander monopole tag antenna presented in Chapter 3 is redesigned to include an artificial magnetic conductor (AMC) structure as its reflector.

5.4.1 Mushroom-Type AMC and Antenna Design

A three-conductor-layer mushroom-type structure is considered for implementing the AMC. This particular configuration is chosen due to its more compact footprint in comparison with its two-metal layer counterpart. Through fullwave simulations and by conducting reflection phase test [85], the AMC is designed to create an almost in-phase reflection of an incident wave across the North American UHF RFID band. The unit cell of the designed AMC is shown in Fig. 5–8 along with its dimensions. A Rogers RO4350B substrate with the relative permittivity and loss

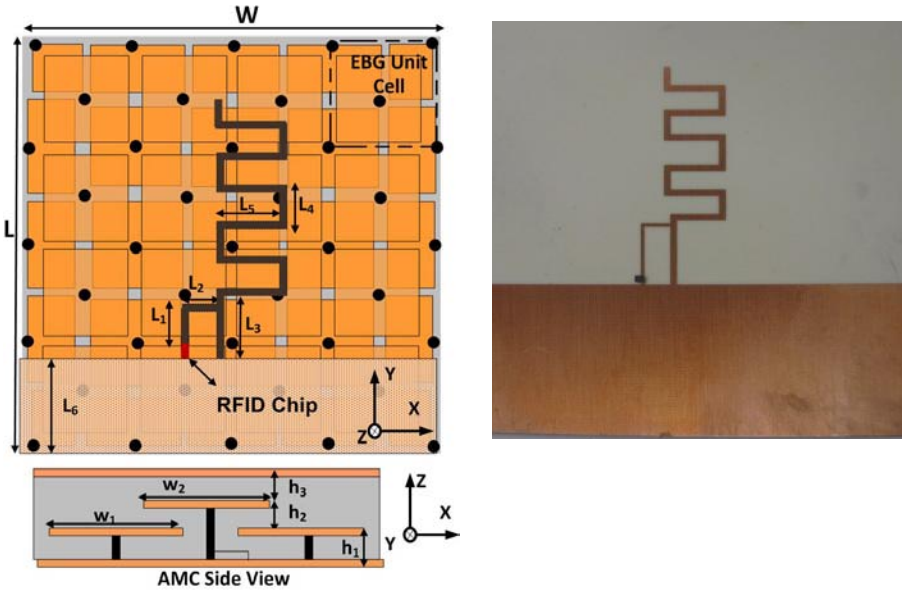

Figure 5–9: (a)Schematic of the proposed tag antenna. All dimensions are in mm (L=W=83.625, L1=9, L2=4.8, L3=10, L4=5, L5=8.9, L6=25, W1=25.675, W2=26.675, h1=1.524, h2=0.508, h3=0.508, a=27.175, Radius of vias=0.762, g1=0.25, g2=1.5). (b) Photograph of the fabricated AMC tag antenna.

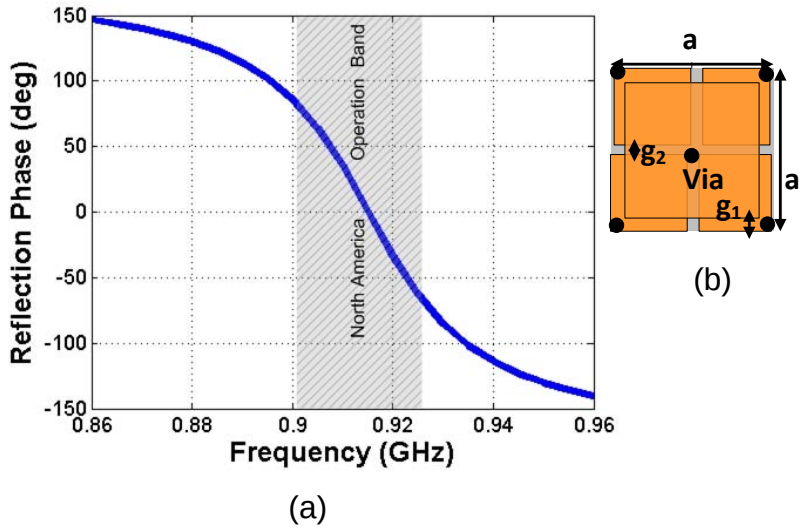

Figure 5–10: (a) The reflection phase response of the AMC substrate (b) Schematic of AMC unit cell. All dimensions are in mm (a=27.175, g1=0.25, g2=1.5and Radius of vias=0.762).

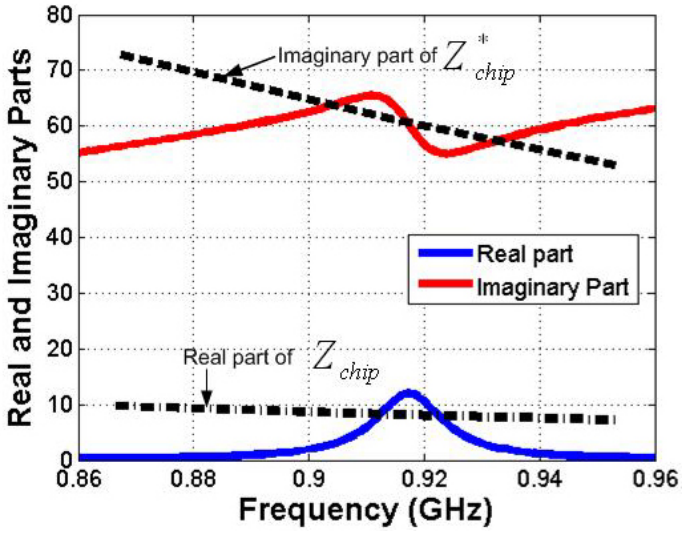

Figure 5–11: Simulated input impedance of the proposed tag antenna and the input impedance of the chip.

tangent of $\varepsilon_r = 3.66$ and tan $\sigma = 0.004$ is used for fabrication. The reflection phase response of the AMC substrate is plotted in Fig. 5–10. The reflection phase crosses zero at around 915 MHz. The overall dimension of the proposed antenna mounted on a 4 cells $\times$ 4 cells AMC surface is $83.625mm \times 83.625mm \times 2.54mm$. The printed monopole antenna is integrated with an RFID chip with an input impedance of $8.2 - j61\Omega$ at the operation frequency of 915 MHz. For conjugate matching between the chip and the antenna, the T-matching technique is incorporated in the antenna layout as shown in Fig. 5–9. The dimension of L_1 and L_2 of the matching networks are optimized using HFSS to maximize the power transfer between the chip and the antenna.

5.4.2 Simulation and Measurements of the Proposed Tag

The simulated input impedance of the proposed antenna is shown in Fig. 5–11. At the operation frequency of 915 MHz the input impedance of the antenna is $10.8 + j63.4\Omega$. Referring to these results the reflection coefficient of the antenna

is calculated using Equation 4.1 and plotted in Fig. 5–12. The bandwidth of the antenna as defined by the S_{11} of less than -3dB is 40 MHz (896 to 936 MHz) which covers the UHF North American band. Compared to the printed monopole antenna without the AMC surface (results not shown for brevity) the bandwidth is reduced by 40 MHz. At the operation frequency of 915 MHz, the simulated radiation efficiency is 76% for the proposed antenna and 98% for the monopole antenna without the AMC. The directivity of the antenna with and without AMC is 3.9 dB, and 1.92 dB, respectively. The simulated $3D$ and $2D$ radiation pattern of the proposed antenna are shown in Fig. 5–13. The front to back ratio of the proposed antenna is 3.9 dB. Next, the fabricated assembled tag is experimentally evaluated. The most important parameters in evaluating the assembled RFID tag are its power sensitivity, differential radar cross section (ΔRCS), and maximum reading range. The measured minimum required transmit power on the tag for generating the correct tag response is presented in 5–14. The minimum power to activate the tag is -14.35 dBm obtained at operation frequency of 942 MHz, while it is -12.9 dBm at operation frequency of 947 MHz when the tag directly attached to a copper sheet ($200 \times 300mm^2$). Also, the ΔRCS with and without a copper sheet ($200 \times 300mm^2$) is -21.1dBsqm, and -24 dBsqm, respectively. A commercial RFID reader (GAO 216010), with maximum EIRP (4 W) is used to measure the maximum reading range of the tag. The tag is detected by the reader when initially placed close to the reader. Then, it is gradually moved away until it becomes undetectable by the reader. The maximum reading range is thus determined to be 10 m and 8.3 m when the tag is in a free standing condition and when backed by a Copper sheet ($200 \times 300mm^2$), respectively. The

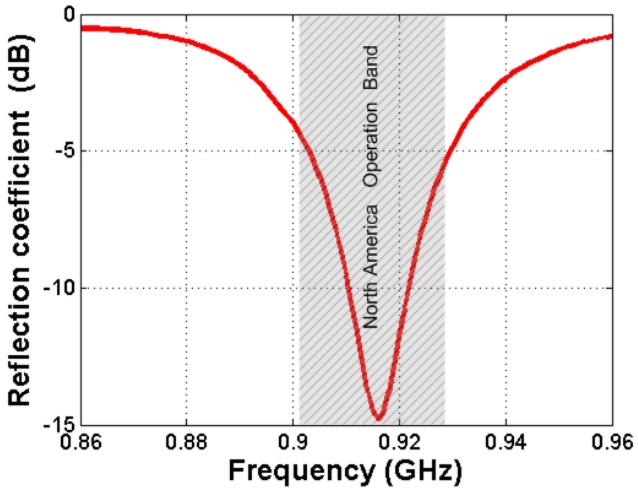

Figure 5–12: Magnitude of S11 of the proposed antennas.

achieved maximum reading range is superior to the values reported for dipole antennas in free space and on metallic objects (9 m and 7 m, respectively) in [84]. The design described in [84] contains 5 cells × 3 cells and occupies a volume of $(124mm \times 76mm \times 4.8mm)$ which is 25.8% larger compared with the present design.

5.5 Summary

A miniaturized patch antenna using embedded electromagnetic band gap structures is presented in this chapter. Compared to a conventional microstrip patch antenna the size of the proposed antenna is reduced by 29.11%. The antenna is fabricated for use in UHF RFID tags that contain a chip with an input impedance of $8.2 - j61\Omega$. For conjugate matching, the embedded inset feed is employed. Experimental results demonstrate that the proposed tag works efficiently in free space and

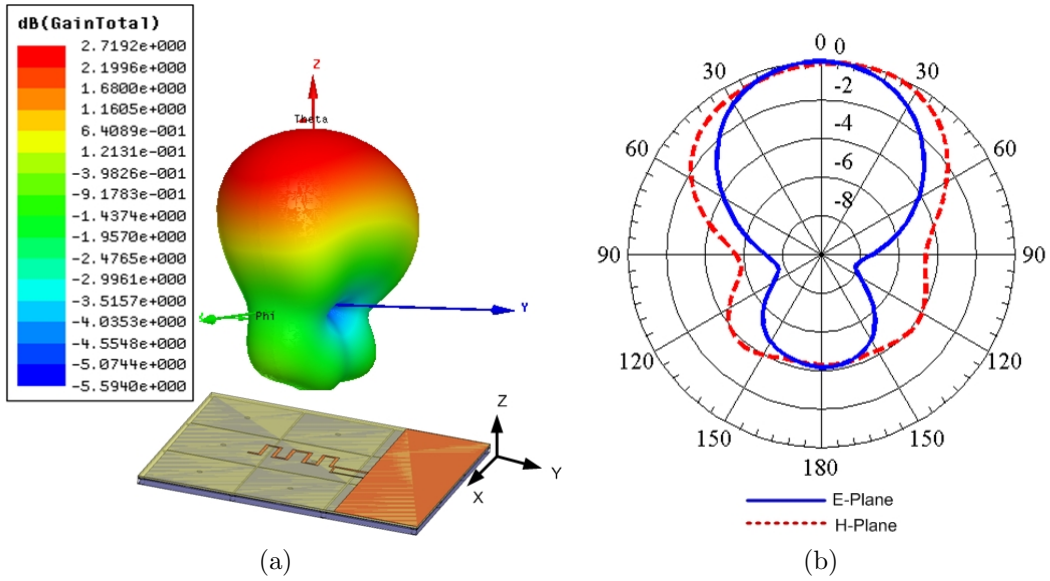

(a) (b)

Figure 5–13: 3 Simulated radiation pattern of the proposed antenna at 915 MHz. (a) 3D pattern, (b) 2D pattern.

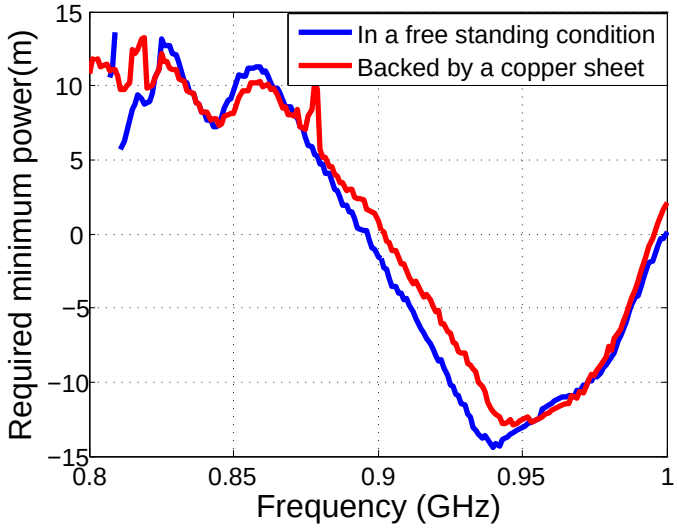

Figure 5–14: Minimum required transmit power on the tag for generating the correct tag response.

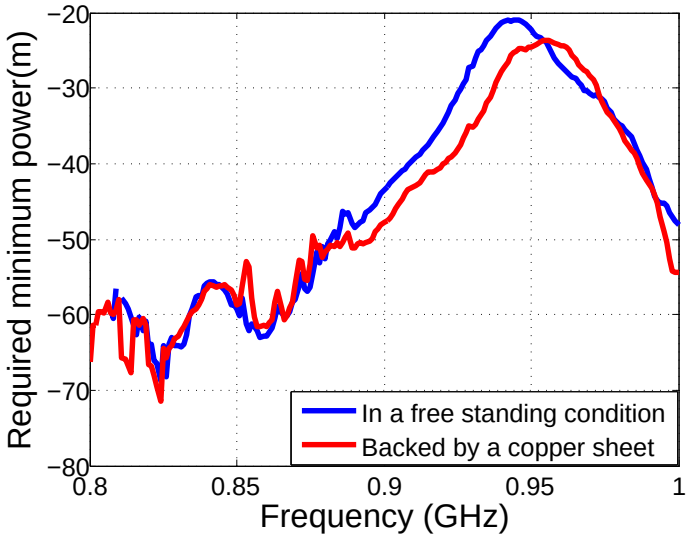

Figure 5–15: Differential radar cross section (RCS) of the proposed tag.

even when the tag is placed on a metal plate. In both cases, a maximum readable range of almost 11 m is achieved.

Also, a printed meander monopole tag antenna incorporating a 4 cells × 4 cells AMC surface for UHF RFID applications is proposed. The designed tag antenna is integrated with an RFID chip with an input impedance of $8.2 - j61\Omega$. The T-matching technique is utilized in the antenna layout for conjugate matching. The tag antenna is fabricated and the assembled tag is experimentally evaluated using a commercial RFID reader. Experimental results demonstrate that the proposed tag works efficiently in free space and when placed on a metal (Copper) plate. The achieved maximum reading ranges in free space and when it is directly attached to a metal sheet are 10 m, and 8.3m, respectively.

Chapter 6

Design and Characterization of RFID Tag Antennas for Enhanced Power Sensitivity

---

6.1 Introduction

As discussed in the previous chapters, the appropriate choice of RFID tag antenna configuration, a tag location with respect to the reader, and the material characteristics of identification objects, and tag and reader sensitivities are the key factors in successful implementation of an RFID system. Based on the link budget analysis presented in [86] and [87], the power sensitivity of the RFID IC is the central factor that determines the reading range when all other important parameters i.e. antenna gain and reader's power, are selected for the best performance. One way to improve the power sensitivity and thus the reading range, under optimum antenna and system operation condition, is by implementing efficient RF to DC conversion circuits in the RFID chip. Although there has been some progress in this direction, as well as in reducing the tag-IC's power consumption, the limited range problem has not been completely solved using this method [27, 29, 88]. Another way to enhance the reading range of passive tags is to increase the received power of a passive tag.

Increasing a reader's transmission power seems like a simple solution of boosting the power harvested by a passive tag. In reality, however, this is impractical due to health considerations and regulation constraints. Therefore, a new design of an enhanced RFID tag that has an additional means of supplying power, especially from a renewable energy source needs to be investigated to achieve a longer reading range.

In this chapter, the design and implementation of enhanced passive tag by using a free energy source (solar), which provides the tag IC with a portion of operating power to extend the reading range, is proposed. A patch antenna integrated with a new generation of an RFID chip that has an additional pin for connection to an external energy source is proposed. Since the enhanced passive tag requires less power from an incident radio wave, the reading range is much longer than that of a conventional tag with the same reader transmission power. The enhanced passive tag can function as an ordinary tag without an external power source as well. Consequently, the life span of the proposed enhanced passive tag can be as long as that of an ordinary passive RFID tag. Another technique for extending the reading range uses a multiple-port RFID chip with multi-antennas to receive more than one copy of the reader's signal [42–44]. In this chapter, compact planar dual meander monopole antennas are proposed for integration with a multiple-port UHF RFID chip with an input port impedance of $11 - j143\Omega$. For maximum power transfer between the antennas and the chip, inductive-coupling mechanism is utilized. The tag antenna is fabricated and the the power required for tag activation as well as the detection range are measured. Also, the results are compared to those of a commercial tag with a single-port RFID chip that has gone through the same measurements as those of the designed tag antenna.

6.2 Overview of Methods for Enhancing the Power Sensitivity of the Passive RFID Tags

The operation principle of an EPC global Gen2 RFID system is that the reader transmits continuous waves (CW) to provide energy for the backscatter carrier signal of the tags [89]. In addition, the reader also sends the pulse-interval encoding (PIE) reader-to-tag (R-T) commands to tags and receives the tag-to-reader (T-R) responses [89]. As shown in Fig. 6–1 the continuous waves emitted from the reader is used to generate the required power to activate the tag. In accordance with the Friis equation, the available power at the tag P_{tag} can be presented as follows:

$$P_{tag} = P_{CW}(\frac{\lambda}{4\pi d})^2 G_{reader} G_{tag} \tag{6.1}$$

where λ is the wave length at the operation frequency, while G_{reader} and G_{tag} are the antenna gain of the reader and the tag, respectively. P_{CW} is the power emitted from the reader.

When the RFID IC is activated, it listens to the R-T commands and then the tag sends its modulated backscatter (MBS) signal to the reader by adjusting its impedance match between the IC and antenna appropriately to generate MBS T-R signals. The available power of the MBS signal at the reader can be presented by:

$$P_{reader} = P_{tag}(\frac{\lambda}{4\pi d})^2 G_{reader} G_{tag} \tag{6.2}$$

Therefore, the maximum reading range of the passive RFID tag is mainly determined by the power of the MBS received at the reader, P_{reader}, and by the amount of power that is available for the tag IC, P_{tag} . The amount of power that it backscatters to the reader depends on the signal quality of the MBS, which can usually be improved by

using a high sensitivity reader. Thus, the available power at the tag P_{tag} is the main factor that determines the maximum reading range of a passive tag as mentioned earlier. Due to restriction of local regulations for the Effective Isotropic Radiated Power (EIRP), increasing the reader transmission power is not a practical solution to improve the available power at the tag P_{tag}.

Therefore, several approaches have been proposed to improve the available power at the tag of the passive RFID system and increasing the reading range [31, 89]. As shown in Fig. 6–1, the available power on the tag can be enhanced by utilizing multiple unmodulated (CWs) from different frequencies to illuminate a passive tag simultaneously [89]. The additional continuous wave emitters (CWEs) are deployed close to the tag to radiate extra unmodulated CW power [89]. By using this method the tags are less dependent on the reader power. Nonetheless, it is deemed inefficient due to the need for supporting additional operating frequencies (besides the reader's signal) by the tag and the extra CWE transmitters that increase the complicity and cost. Another method proposed for creating enhanced passive RFID tags is presented in [31, 32]. In this technique the additional continuous wave emitters (CWEs) are integrated with the RFID tag as shown in Fig. 6–2. Two different power sources, a battery or solar cells, can be used to power up an oscillator that generates a single tone unmodulated CW that is fed to the RFID chip via a coupler. This method is also inefficient because of integration of additional circuits on the tag. As well, the coupling network should be carefully designed to minimize loading of the oscillator on the tag at RFID operation band and maximize power transfer to the tag from the oscillator at a different frequency. In [90], a new design to improve the reading range of a passive RFID tag using a wireless identification sensing platform (WISP)

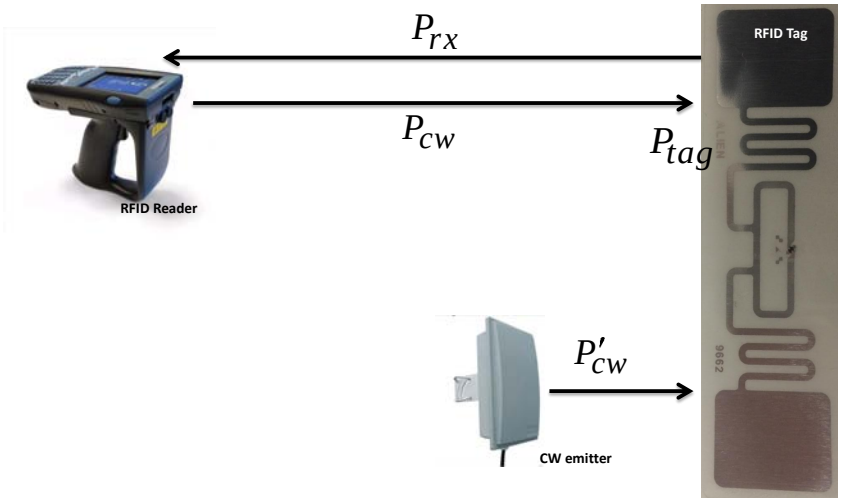

Figure 6–1: Enhanced passive RFID tag using multiple unmodulated (CWs) [89].

is presented. WISP is a passive printed circuit board (PCB) RFID tag that has an additional pin for direct connection to a power supply source. Although WISP has many attributes similar to a conventional RFID tag circuit, it is not a direct stand-in for a commercial IC. Notably, the reading range that is obtained by WISP is less than half of a commercial RFID tag, and the input impedance of WISP is very different from that of an RFID IC, thus, requires a different antenna design [90]. In the process of this research work, when still multi-port RFID chips were not available, WISP boards were investigated. Since, an extra pin was made available for power, it was considered to include a secondary antenna or a renewable energy source to supply power via this pin. Utilizing two antennas system [43] occupies a relatively large area. A superior design to address the area problem are presented in section 6.5 of this chapter.

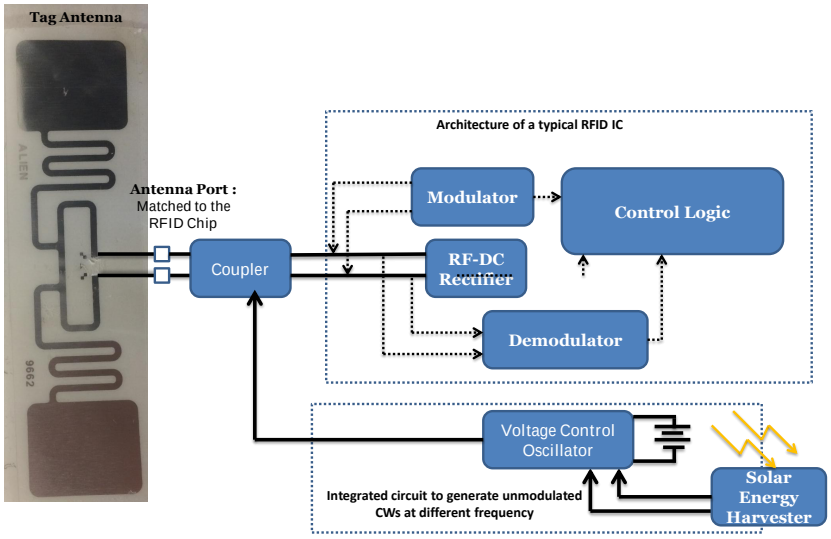

Figure 6–2: Architecture of an enhanced passive RFID tag using multiple unmodulated (CWs) [32].

6.3 Enhanced RFID Tag Antenna with a Thin Film Solar Cell Overlay

With use of the new generation of RFID IC (Monza X) [33] which has an additional pin for a power supply source, a patch antenna tag is designed. It should be mentioned that the nice feature of this RFID chip is that it also can be connected to second antenna to improve the available power to the tag or to reduce its polarization sensitivity. The power sensitivity of the RFID IC Monza X with single and dual port configurations, and also with a Battery in the read mode is shown in Fig. 6–3. The power sensitivity of the IC with a single port connection is -17 dBm, and it is -19.5 dBm in a two-antenna realization, while it is -24 dBm when a battery power supply is connected the single antenna configuration. In the design proposed in this thesis, a patch antenna is connected to the RFID IC whose input impedance is $18.6 - j171\Omega$ at the operation frequency of 915 MHz. The tag antenna is designed to operate at the

North American operation bandwidth (902 MHz to 928 MHz). A Rogers RO4350B substrate ($\varepsilon_r = 3.66$ and 1.524 thickness) was considered for implementing the tag antenna. At 915 MHz, the length and the width of the radiating patch is optimized by using HFSS simulator yielding L=83 mm and W= 82.8 mm. The geometry of the patch antenna is depicted in Fig. 6–4. For maximum power transfer between the RFID IC and the tag antenna an inductive loop matching technique is used as shown in Fig. 6–4. The dimensions of the inductive loop is optimized for conjugate matching, thus yielding $L_1 = 18.8mm, L_2 = 7.9mm$, and $d = 0.6mm$. For the solar-cell overlay, the (a-Si:H) solar cells developed by the POWERFILM INC. [91] were selected. The multilayered (Si:H solar cell) consists of a flexible polyimide carrier, an aluminum layer and a p-i-nsilicon layer that is located between two transparent conductive zinc oxide (ZnO) layers. These solar panels (SP3-37) appear as thin, light, flexible films that can be cut to fit the radiating patch. The overall size of the solar panel is ($L \times W \times T = 64 \times 37 \times 0.2mm$). The solar panel with this size produces a maximum current of 22 mA at the operating voltage of 3 V in full sun illumination intensity. The solar cell strips are glued onto the top of the antenna, and connected to the DC lines of the RFID IC with small wires as shown in Fig. 6–4. Since the fringing electric fields at these radiating edges are responsible for antenna radiation, the solar cell strip are also positioned in such a manner that the edges of the patch antenna are not covered.

6.4 Simulation and Measurements of the Proposed Solar Powered Tag

The simulated results of the input impedance of the tag antenna and the input impedance of RFID chip are presented in Fig. 6–5. At the operating frequency of 915 MHz the input impedance of the chip ($18.6-j171\Omega$) is conjugate matched to the input impedance of the tag antenna $33.9 + j168.2\Omega$. Also, the power sensitivity and the reading range of the proposed enhanced tag were measured using the TagFormance set up [61]. The power sensitivity measurement results are presented in Fig. 6–6. The proposed tag is experimentally evaluated in an indoor lighting condition. The measured required minimum power when the tag operating similar to a regular RFID tag (without energy harvester) is -18.5 dBm at the operating frequency of 934 MHz. When the external power source are used the power sensitivity of the tag is enhanced. The measured required minimum power to activate the tag is -26.2 dBm (at 934 MHz) with the battery assisted operation mode, while it is -25.4 dBm (at 940 MHz) with the solar energy harvesting. Due to loading effects of the solar panel, a small shift in the resonance frequency (6 MHz), from 934 MHz to 940 MHz is observed in the power sensitivity measurements. The reading range measurement results are also presented in Fig. 6–7. When there is no extra energy source the maximum reading range is 12.45 m, while the reading range achieved with the battery and solar energy harvesting (indoor environment; office light) are 30 m and 27.2 m, respectively. In full sun illumination (out door), the proposed tag also achieves a maximum reading range similar to a battery range (30 m).

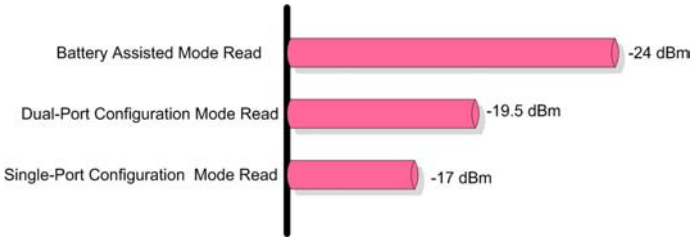

Figure 6–3: Power sensitivity of the new generation Monza X [33]

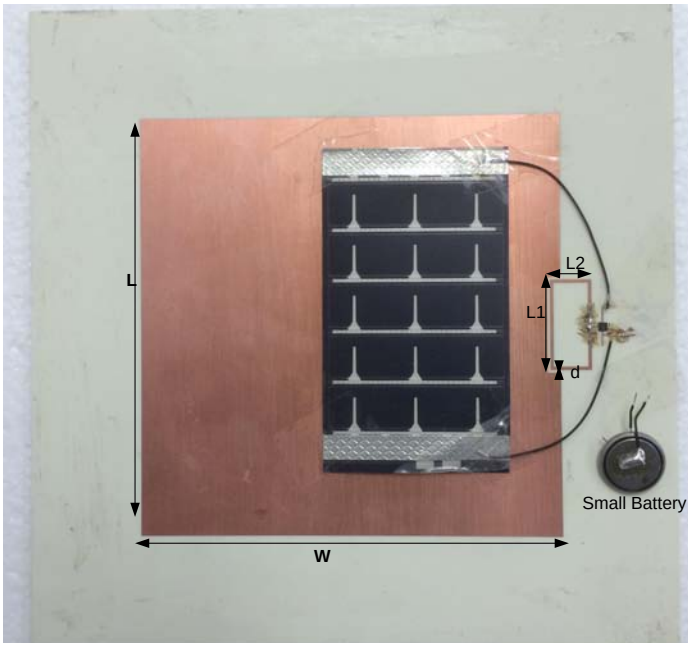

Figure 6–4: Proposed enhanced passive RFID tag using solar energy.

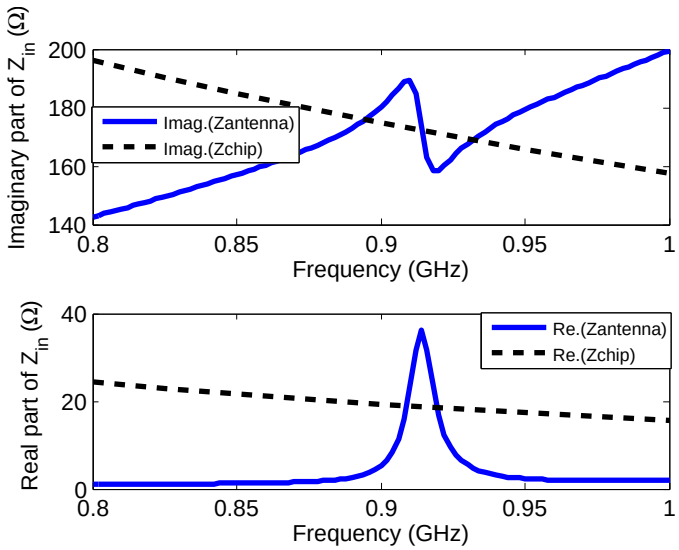

Figure 6–5: Simulated input impedance of the tag antenna and RFID chip.

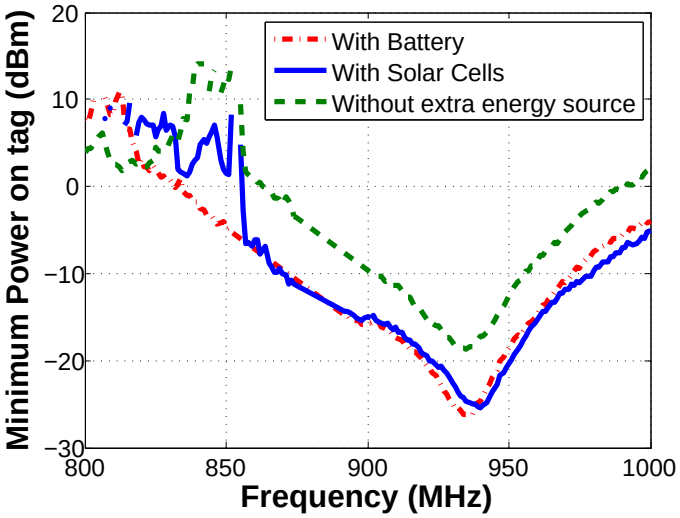

Figure 6–6: Measurement results of the power sensitivity of the proposed RFID tag with battery, solar energy harvesting, and without any extra energy source other than the reader's RF signal.

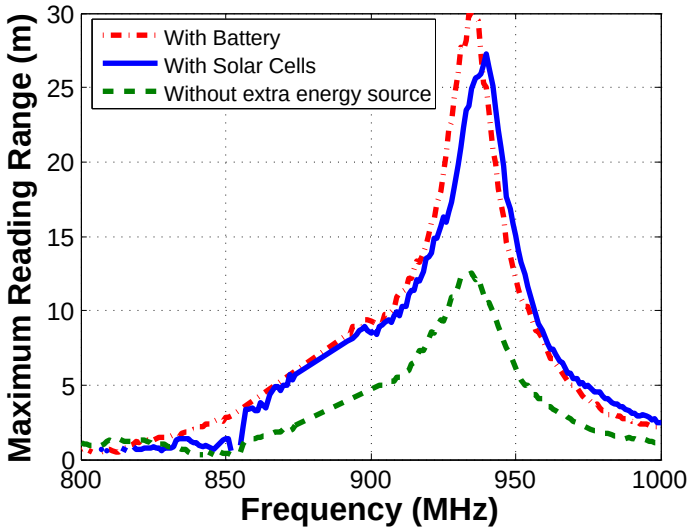

Figure 6–7: Measured results of maximum reading range of the proposed RFID with battery, solar energy harvesting and without any extra energy source other than the reader's RF signal.

6.5 Design and Characterization of a Compact Dual Printed Meander Monopole Tag Antenna

Although, the solar energy harvesting has shown promising results and enhanced reading range from 12.4 m (without an energy harvester) up to 27.2 m (with an energy harvester), size and cost remain to be tag implementation bottleneck. Therefore, another technique for increased operating range with a minimum cost and complexity is introduced by utilizing a multi-port RFID chip with multi-antennas to receive more than one copy of signal from the reader [42–44]. In addition to the reading range, the orientation sensitivity of the tag with respect to the reader can be enhanced by utilizing a multiple tag antennas [42–44]. Still, the main design challenges are maintaining a minimum foot print and implementing matching circuits between the multi-port chip and multiple antennas to cover the entire UHF RFID band (860 to 960 MHz). The compact meander monopole antennas introduced in Chapter 3 [18, 42], are used to create new tags in this chapter. For maximum power transfer

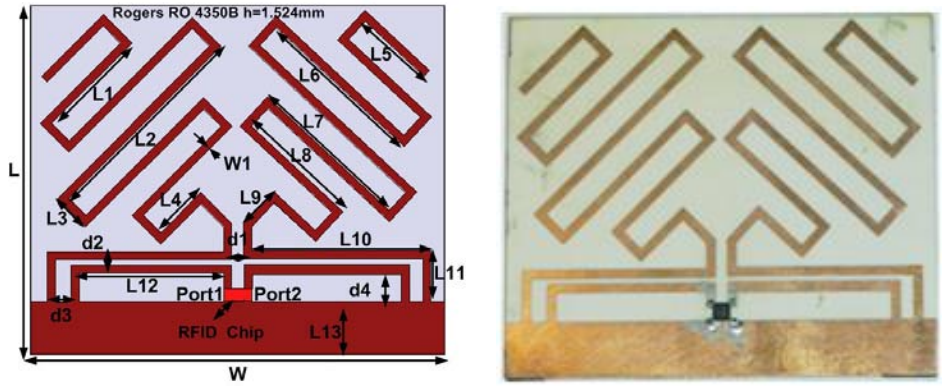

(a) (b)

Figure 6–8: a) Geometry of the proposed printed meander monopole tag antenna, all dimension in mm (L=51, L1=14, L2=26.5, L3=5, L4=7, L5=9.9, L6=21.5, L7=20.5, L8=18.5, L9=5.4,L10=22.1, L11=6.3, L12= 18.4, L13=6.5, W=43, W1=1, d1=1.5, d2=0.65, d3=1.6, d4=3.5). b) photographic of the proposed tag.

between the dual monopole antennas and multi-port RFID chip that has the input impedance of $11 - 143\Omega$ at each port, an inductive coupling matching method is used.

6.5.1 Proposed Tag Antennas Design

The layout and the design parameters of the proposed dual meander monopole antenna is shown in Fig. 6–8. For miniaturization and conjugate matching between the 2-port chip and dual antennas, two inductive printed loops are implemented. At near resonance frequency, the imaginary and real parts of antenna input impedance with the feeding loops can be adjusted independently using formulas presented in Chapter 3. When both meander monopole antennas are included, the final dimensions of the matching loops are optimized using HFSS simulations. The proposed dual tag antenna is fabricated on Rogers substrate with thickness of 1.524 mm and dielectric constant of 3.66. The dimensions of the meander antennas and the matching loops are shown in Fig. 6–8. The overall area is $43mm \times 51mm$ which is relatively

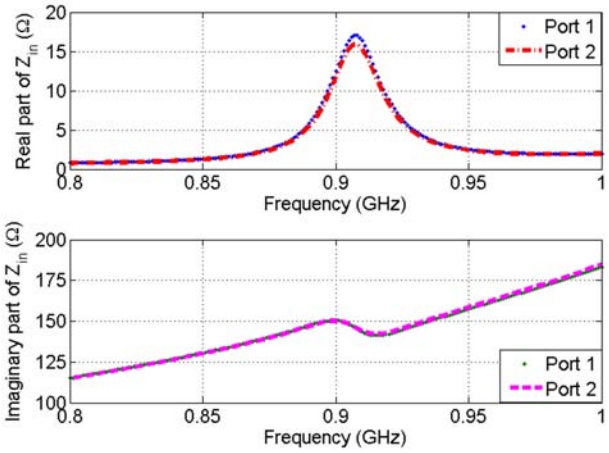

Figure 6–9: The real and imaginary part of the input impedance of the dual meander monopole antenna.

smaller compared to the area of a conventional crossed dipole antennas presented in [43], i.e. $150mm \times 150mm$.

6.5.2 Simulation and Experimental Evaluations of The Proposed Tag

The simulated results of the antenna input impedance are shown in Fig. 6–9. At the operation frequency of 915 MHz the input impedance of the proposed dual meander monopole antenna, is $(15.87 + 142.21\Omega$; at port 1), and $(16.64 + j142.14\Omega$; at port 2). The simulated radiation efficiency is 80 %, while the gain is 1.13 dB.

The performance of the fabricated prototype antennas were also tested at Voyantic Ltds laboratory [61]. The power sensitivity of the RFID tag is measured by sweeping the transmit power across the selected frequency band to detect the minimum power required to obtain a correct tag response at each frequency point.The measured results are presented in Fig. 6–10. The minimum power required for tag activation is lower than the required power to turn on a commercial single RFID tag antenna [19]. The required minimum power of the proposed tag is -15 dBm at the

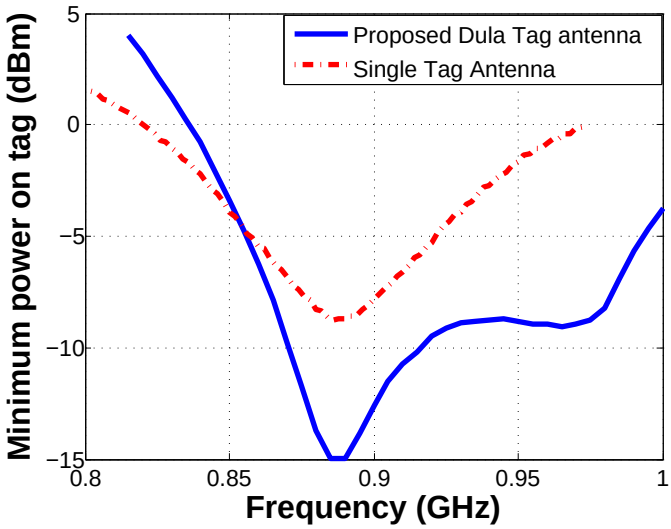

Figure 6–10: Minimum required transmit power on the tag for generating the correct tag response.

operation frequency of 890 MHz, while is -8.7 dBm at 890 MHz for a single tag antenna in [19]. The maximum reading range versus the operation frequency is shown in Fig. 6–11, which is 8.65 m, while it is 4.21 m for a single tag antenna in [19]. This shows that the proposed tag functions better than the tag with a single-port RFID chip. Note that other tag designs reported in [92], [11], that use high gain antennas, and in [43], which contains a dual dipole design, yield comparable maximum reading ranges to what was achieved by our proposed design, i.e. 7.61 m, 10.4 m and 8.2 m, respectively. However, the area of our design is considerably smaller ($51mm \times 43mm$) than the areas stated in [92], [11] and [43], i.e. ($140mm \times 80mm, 76.8mm \times 76.8mm$, and $150mm \times 150mm$).

6.6 Summary

As shown in this Chapter, enhance passive RFID tags (EPT) demonstrate significant performance improvement in terms of read range extension. Compared with

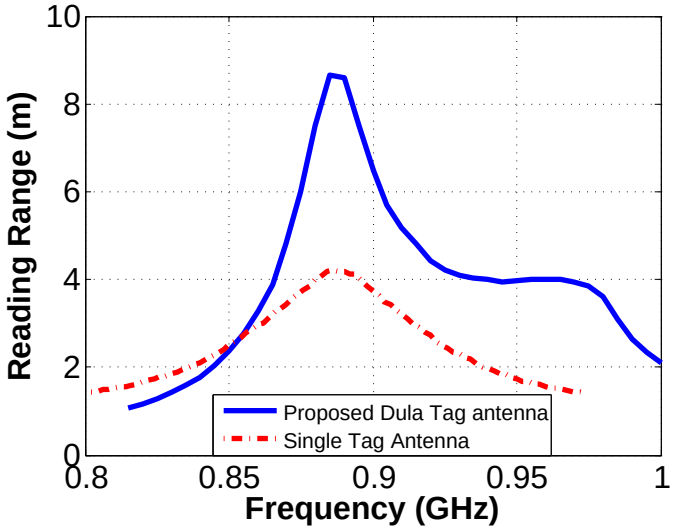

Figure 6–11: Reading range of the proposed dual tag antenna and single tag antenna tags as a function of frequency.

a regular tag in the same access range, an EPT requires less reader power. Thus, this advantage can be very attractive in the applications using low-power mobile readers. A patch tag antenna incorporating solar cell has been proposed to achieve an improved reading range for a passive RFID tag. This design yields 27.2 m.

Moreover, compact dual printed monopole antennas are proposed. To operate with multi-port RFID chips. The challenges in the proposed design configuration is conjugate matching of the antennas to the multi-port chip while achieving a small layout area. Inductive coupling via a printed loop is employed to eliminate the need for a matching circuit with lumped components. The prototyped tag antennas which is considerably small, requires a lower power to correctly respond to a reader in comparison with a single RFID tag antenna. The maximum readable range of this proposed tag is 8.65 m, offering a promising solution for compact passive UHF RFID tag applications.

Chapter 7

RFID Tag-Based Sensor

7.1 Introduction

RFID technology has been recently employed in sensor applications that require low-cost low-power wireless nodes with radio identification and sensing capabilities [9] [93]. As previously discussed in Chapter 2, RFID-enabled sensors can be implemented by different techniques. Among these, analog sensing with tag antenna (based on measuring a minimum power needed to activate the tag or measured received signal level) [94], and using tag-enabled sensor for the transmission of generic sensor data (tag's user data is supplied by a specific sensor) [9, 95–98] are the most attractive techniques.

To make an RFID tag sensitive to physical parameters, in the analog sensing techniques, either the antenna's or the matching circuit's electrical/electromagnetic performance is made sensitive to the changes of an environmental parameter such as humidity, temperature, etc. [50, 93, 94, 99–101]. A common RFID reader can be used for detection of the threshold power needed to activate the tag or measure the received signal level for several frequency points selected in the operation frequency

bands [50, 93, 94, 99–101]. In these designs, the main downside is their compromised short reading range, need for calibration and the fact that they can only be used for a set of a specific applications.

In this chapter, single and dual band patch antennas for implementation of UHF RFID tag-based-sensors are proposed. First, a prototype example using a passive resistive sensor is presented. Then, to improve the reading range of the proposed sensor, solar energy harvesting is included in the design. The proposed patch antenna incorporates multiple RFID chips (RI-UHF-IC116-00) provided by Texas Instruments, with power sensitivity of -13 dBm and input impedances of $8.2 - j61\Omega$ at the operation frequencies of 915 MHz. For maximum power transfer between the RFID chips and the antennas, inductively-coupled loop and inset coupled feeds are integrated in each antenna layout. One port in each antenna is dedicated for attaching a resistive sensor as a load in parallel with the RFID chip. Few normal resistors are used as an alternate way to represent the resistive sensor in simulations and measurements. The proposed tags are fabricated and experimentally evaluated using a commercial RFID test system.

7.2 Single and Dual Band Patch Antennas for UHF RFID Tag-Based Sensor Applications

Examples of low-cost RFID tag-based sensors that use off-the-shelf RFID chips and readers have been introduced in [50, 94, 99–106]. In [50, 94, 99–102], a pair of RFID tag antennas is employed for identification and sensing; one of the tags serves as a reference signal, while the other is used as a sensor node. The reference node

has a common RFID tag configuration, while different approaches are adopted to implement the sensor node in [50, 94, 99–102].

The sensed physical quantity is determined from the ratio of the minimum transmit power required from the reader to activate the reference and sensor nodes, or the power ratio of the received signals from reference and sensor nodes and comparing it to benchmark laboratory experiments with the same tags, RFID chips and similar sensors [50, 94, 99–103]. In the designs of [50, 94, 99–103] the tag antennas are often of a dipole topology. Due to the omnidirectional radiation, these types of antennas are influenced by the characteristics of the identification object as discussed in Chapter 5 [103]. These changes in the tag antenna characteristics affect the reference and sensor nodes's signals, thus reducing the sensing accuracy [101] and [103]. To overcome this problem, in [103], patch antennas are also used for RFID sensors but still in a multiple tag arrangement. To reduce the cost, and the overall size of the developed sensor architecture, the sensor and the reference ports must be integrated in one ordinary RFID tag, as is done in this thesis. Including both nodes in one antenna, exposes both sensor and reference nodes to similar environmental condition, e.g. temperature. In addition, this also ensures similar power levels for switching on the RFID chips, as a large separation between the sensor and sensor nodes will raise the risk of dissimilarity of the received powers due to propagation path variations. Therefore, a multiport RFID patch antenna is proposed for UHF RFID tag-based sensor applications. Single band antennas, operating at the 902-928 MHz (North American frequencies) and dual band antennas covering both the 865-868 MHz, (European frequency band) and 902-928 MHz frequency bands are presented in the following sections.

7.2.1 Principle of the Multi-Port RFID Tag-Based Sensor Design

Consider the Friis Formula relation reported in Chapter 6 Equation 6.1 to determine the power received by the tag. This Equation can be updated (for this context) as follows to determine the power transferred to the chip, P_C, by the tag antenna as [102]:

$$P_C = \left(\frac{\lambda_0}{4\pi d}\right)^2 G_R(\theta,\varphi,\psi)\, G_T(\theta,\varphi,\psi)\, \tau P_t \eta_p \tag{7.1}$$

where λ_0 is the free space wavelength, d denotes the distance between the reader and the tag. G_T, G_R represent the tag, and the reader antenna's gain ψ is the environmental parameter that could affect antenna gain (i.e. material [107], humidity [108, 109], and temperature [110]) and τ is the power transmission coefficient of the tag, defined as:

$$\tau = \frac{4R_{Chip}R_{Antenna}(\psi)}{|Z_{Chip} + Z_{Antenna}(\psi)|^2} \tag{7.2}$$

The other parameters in Equation 7.1 are P_t, the power transmitted by the RFID reader, and η_p , the polarization mismatch between the reader and the tag antenna.

The power received by the reader can be expressed by a radar equation as [102]:

$$P_R = \left(\frac{\lambda_0}{4\pi d}\right)^4 G_R^2(\theta,\varphi,\psi)\, G_T^2(\theta,\varphi,\psi)\, \tau P_t \eta_p \rho(\psi) \tag{7.3}$$

where $\rho(\psi)$ is the modulation efficiency of the tag, which is a function of the antenna and chip impedances [111]. It is also related to the tag's radar cross section as identified in [111]. The power received by the tag to activate the microchip or to be scattered by the tag is a function of the physical characteristics of the target where the tag is attached. Thus, any change in the target parameters causes a change in the power received by the tag, as well as in the scattered power that is received by

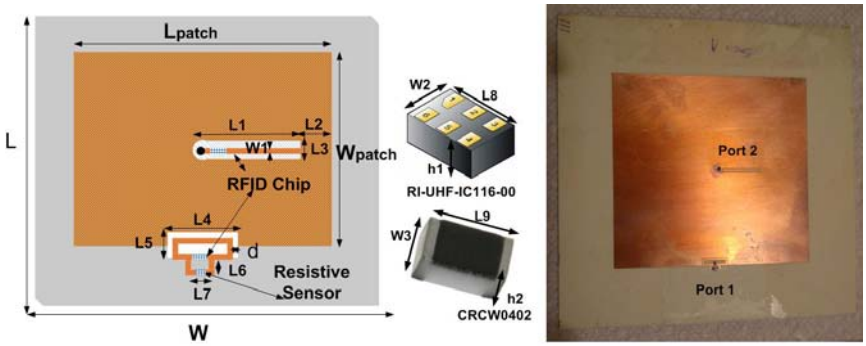

Figure 7–1: Geometry of the proposed single band patch antenna. All dimensions in millimeters (L_{Patch}= 83, W_{Patch}=79.6 , L=126 , W=126, L1=18.6 , L2=21, L3= 1.7, L4=11 , L5= 3.1, L6=1.5 , L7= 4.6, L8=1, L9=1 , W=79.6, W1=0.6, W2=0.5, W3=0.5, h1=0.55, h2=0.35, d=0.2.

the reader. By detecting these changes, the target's properties can be monitored in real time. However, preliminary laboratory experiments are needed to generate a calibrated reading of the backscattered signal from the sensor tag or the minimum power required from the reader to activate the tag. In our studied case, multiport RFID tags are proposed. The sensor port is integrated with a resistive moisture or resistive temperature sensor [94] and [50], while the other port (the reference port) is perfectly matched to the tag antenna. Any change in the resistance of the sensor due to humidity or temperature variation introduces a mismatch between the antenna and the sensor port. As a result, the reader should transmit higher power to activate the sensor port in comparison with the reference port. Since the threshold power of the chips ($P_{threshold}$) is almost the same for the same type of chips and the reference and sensor port are integrated in the same tag, the parameter of reader-to-tag distance can be dropped by calculating the ratio of the required minimum transmit power ($P_{t_{min}}$) to activate the two chips ($P_C \geq P_{threshold}$) (sensor and reference ports) using Equation 7.1. The calibration power-up curve at any arbitrary distance from the

reader can be obtained as follows:

$$P_{t_{min}}^{relative} = \frac{P_{t_{sensor}}}{P_{t_{reference}}} = \frac{\tau_{referencePort}}{\tau_{sensorPort}} \tag{7.4}$$

By measuring this power ratio, it is possible to map it to sensor data and thus to determine humidity or temperature at the tag's location.

7.2.2 UHF RFID Sensor Tag Design

A. Single Band UHF Patch Antenna Design

The tag antenna shown in Fig. 7–1 is designed and fabricated using a single layer substrate, a Rogers RO4350B ($\varepsilon_r = 3.66$) with h= 1.524 mm to operate at the North American UHF RFID band (902-928 MHz). The length of the patch antenna is approximately one-half of a wavelength at the operating frequency of 915 MHz, yielding L_{patch}=83mm and a width of W_{patch}=79.6mm. The overall dimensions of the tag are 126 mm x 126mm, including the ground plane. To further reduce the footprint, the patch antenna is backed by an EBG structure as described in [21] and then redesigned with multiple feeds. In this manner, a size reduction of almost 70% to 59mm x 79 mm is obtained for the multiport patch tag antenna. Multiple RFID chips (RI-UHF-IC116-00 [74]) provided by Texas Instruments are used. The power sensitivity of the chip is -13 dBm and the input impedance is $8.2 - j61\Omega$ at 915 MHz and $9.8 - j73\Omega$ at 866.5 MHz. The inductive loop and inset feeds provide the conjugate match between the chips and the antenna ports. The port with an inset feed is chosen as the reference node. By changing the length of the inset feed (L1), the imaginary part of the input impedance is adjusted to yield the desired input impedance value. The real part is optimized by controlling the position of the via

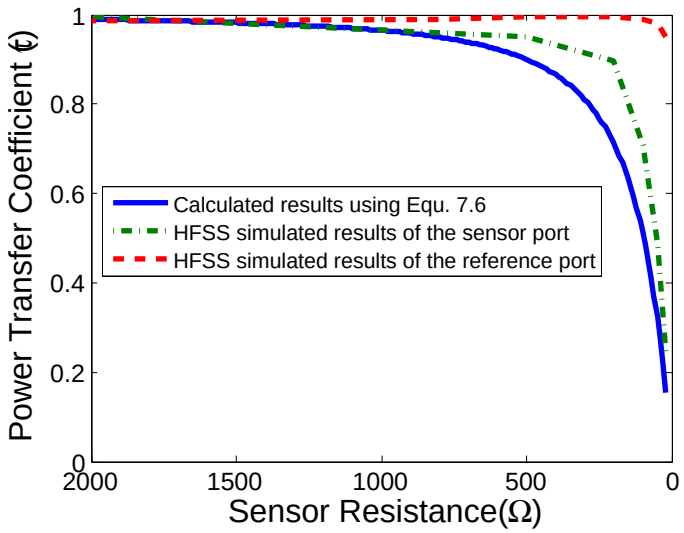

Figure 7–2: Power transfer coefficient at the port of a single-band patch antenna with different resistors.

inside the patch antenna [21]. The second chip is connected to the antenna via an inductive loop, the design of which is described in Chapter 6. The final dimensions of the inset feed and of the loop as shown in Fig.1 are optimized using the HFSS simulator. The sensor can be directly connected to the tag antenna (in series or parallel arrangements) [94] or inductively coupled to the tag [50]. In this prototype the sensor is directly connected to the matching loop in parallel with the RFID chip (See Fig. 7–1). The reflection coefficient, Γ of this port as seen by the RFID chip is [94]:

$$\Gamma = \frac{(Z_{Antenna} \parallel Z_{Sensor}) - Z^*_{Chip}}{(Z_{Antenna} \parallel Z_{Sensor}) + Z_{Chip}} \tag{7.5}$$

If the tag antenna is designed to be conjugate matched to the chip impedance ($Z_{Antenna} = Z^*_{Chip}$), the reflection coefficient (Γ) becomes:

$$\Gamma = \frac{-\left(Z^*_{Chip}\right)^2}{2Z_{Sensor}Re\left(Z_{Chip}\right) + |Z_{Chip}|^2} \tag{7.6}$$

Adding the resistive sensor in parallel with the sensor port, introduces a mismatch

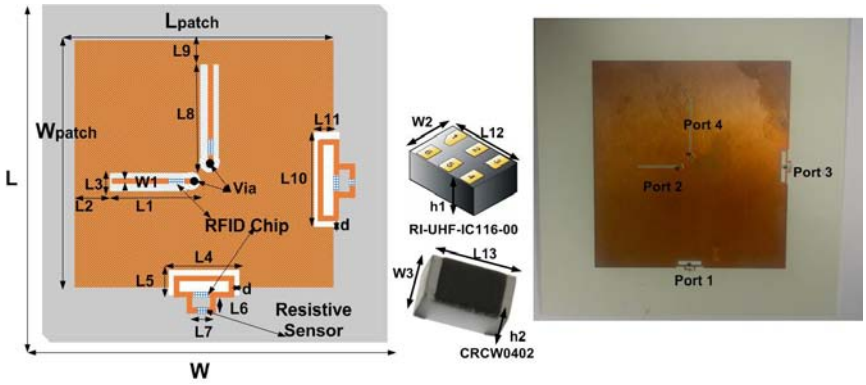

Figure 7–3: Geometry of the proposed dual band patch antenna. All dimensions in millimetres (L_{Patch} = $80, W_{Patch}$ = 85 , L=126 , W=126, L1= 17.3, L2=18, L3= 1, L4=11 , L5=3 , L6= 1.5, L7=4.6 , L8=22.8 , L9= 14, L10=14.1, L11=,3.4 L12=1, L13= 1, W=79, W1=0.3, W2=0.5, W3=0.5, h1=0.55, h2=0.35, d= 0.2.

($|\Gamma|$ becomes larger than zero) between the antenna and the RFID chip. Thus, the harvested power from the RFID reader signals will not be completely transferred to the chip circuitry, as a part will be reflected (power transfer coefficient $\tau = 1 - |\Gamma|^2$). Compared to the reference port that is perfectly conjugate matched to the tag antenna, the reader requires to transmit higher power to activate the sensor port. Accordingly to Equation (7.6), the reader will not be able to activate the sensor port when ($|\Gamma| = 1, Z_{Sensor} = 0$), while the best case to activate the sensor port (perfectly conjugate matched) is when ($\Gamma = 0, Z_{Sensor} = \infty$). The proposed tag is simulated using HFSS simulator where normal resistors (Thick film chip resistors CRCW0402) with different resistance values ($2k\Omega$, $1k\Omega$, 500Ω, 200Ω, 100Ω, 50Ω, and 20Ω) are connected one at a time in the inductive loop as an alternative way to represent a resistive sensor (e.g. a Write Once Read Many WORM [94] or thermistor NTCLE100E3681JB0 [112]). The calculated power transmission coefficient results using Equation (7.6) and the simulated results of the reflection coefficient of the tag with these resistors are presented in Fig. 7–2. In both calculation using 7.6 and HFSS simulator, the chip impedance is set to be $8.2 - j61\Omega$ (provided from data sheet [74])

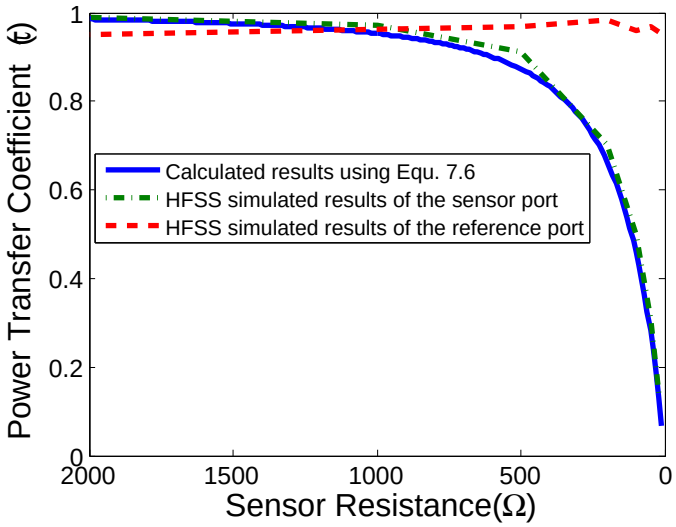

Figure 7–4: The power transfer coefficient port of the dual-band patch antenna with different resistors.

and the results are calculated at the center frequency of the North America band (915 MHz). As expected, when the resistor values that are connected in parallel with the chip change, a mismatch between the chip and the antenna is introduced. The mismatch increases when the value of the resistor is decreased. There is a small variation in the power transmission coefficient at the reference port, but it is higher than 94 % across the entire North American band. Thus, the reference port's chip is expected to be activated with a minimum transmit power from the reader and changing resistance values at the sensor port does not have any impact on it as will be seen from the power measurement in the next section. The simulated efficiency and directivity at the center of the North American frequency band, 915 MHz, with a well-matched sensor port with $R = 2K\Omega$ is 55 % and 6.4 dB, respectively. Also, the simulated front to back ratio is 11.4 dB at 915 MHz. Thus, the proposed tag is more immune to the loading effect of background material than the traditional sensors reported in [50, 94, 99–102].

B. Dual-Band UHF Patch Antenna Design

Although patch antennas are less sensitive to background material than the dipole-based designs, they also suffer from inherent narrow bandwidth and do not cover the whole regulated UHF RFID operation bands (860-960 MHz). Therefore, a dual-band patch antenna is proposed to operate at two regulated operational frequency bands (902-928 MHz, North America) and (865-868 MHz, Europe). The dual-band patch antenna is implemented by extending the design presented in previous section through introducing of two orthogonal inset feeds and two inductive loops, as shown in Fig. 7–3. The resonance frequency of each band is optimized by tuning W_{patch} (to be resonant at the European band) or L_{patch} (to be resonant at the North American band). The final dimensions are shown in Fig. 7–3. Like the single-band design, the RFID chips and sensors are connected in the inductive loop and inset feeds, as shown in Fig. 7–3. The feeds are optimized using an HFSS simulator to match the input impedance of the chip ($8.2 - j61\Omega$ at 915 MHz and $7.9 - j73\Omega$ at 866 MHz) to the antenna. However, in this multi-band design, the two RFID chips that are connected to the inset feed matching networks can only be replaced by one multiport RFID chip [15], where different port of the chip can be connected to the inset feed matching for operation at different bands. The sensor is only connected to the loop-fed ports, and the dual-band tag antenna is simulated with different values of resistors (i.e., $2k\Omega$, $1k\Omega$, 500Ω, 200Ω, 100Ω, 50Ω, and 20Ω) attached in parallel to the RFID chip one at a time. The simulated and calculated results using Equation 7.6 of the power transmission coefficient only at the European band are presented in Figs. 7–4. The results for the North American band are very close to those shown for the single band tag sensor in Fig. 7–2. The simulated results demonstrate that

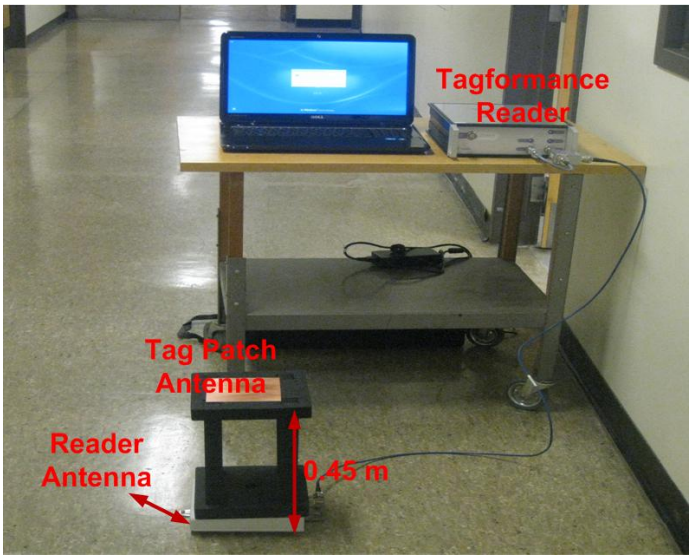

Figure 7–5: Tagformance measurement set-up.

the introduced sensor disturbs the conjugate matching condition at its port connection as expected. The power transmission coefficient of the reference ports at both bands are higher than 94%; thus, the reference chips can be activated with minimum transmit power from the reader, as will be seen in the next section. The simulated efficiency and directivity at the center of the European frequency band, 866 MHz, with a well-matched sensor port with $R = 2K\Omega$ are 41% and 6.2 dB, respectively, while, the simulated front to back ratio is 9.6 dB at (866 MHz).

7.2.3 RFID Tag-Based Sensor Evaluation

A. Power Sensitivity Measurements

Since sensor operation is based on measuring the relative activation power of the sensor and reference port's chips, the power sensitivity measurement needs to be conducted to generate the calibration curve of the power-up levels. In addition, measuring the power sensitivity of the assembled tag provides information about the

optimum operation frequency. Thus, any shift in the resonance frequency due to antenna fabrication tolerances or the tolerances of RFID chip impedance because of parasitic effects, process variations and packaging can be observed. In this test, a commercial RFID measurement system (Tagformance) was used [61]. The measurement system is shown in Fig. 7–5, where the reader is connected to a computer to control the operation frequency band, the sweeping frequency step, and the maximum output power. The measurement system also includes a wide band circulator for monostatic radar measurements with over 20 dB port isolation throughout the 800-1000 MHz range. Tagformance was selected to perform the power sensitivity measurements, because it cover wide operation frequency bands compared to a commercial RFID reader, e.g. GAO 216010 reader [20] that only operates in narrow bands 865 to 868 MHz, European band, and 902 to 928 MHz, North America band. With this commercial reader, the optimum operation frequency cannot be predicted if it is shifted out of the reader's operational bands. The tag was placed on top of the foam holder at a 0.45 m distance from the reader as shown in Fig. 7–5. The power sensitivity for the integrated RFID chips was then measured with different thick film chip resistors (CRCW0402), i.e., $2k\Omega$, $1k\Omega$, 500Ω, 200Ω, 100Ω, 50Ω, and 20Ω, soldered one at a time for each port and each test to represent the resistive sensors. This allows the power sensitivity of the sensor to be measured without the need to use a climate room. First, the single band patch antenna is measured across the 800-1000 MHz frequency band. The system starts by transmitting low power (-5 dBm) and then increases the output power by 0.1 dBm until the reader detects the tag's response. The required minimum transmit power needed to activate the sensor port is recorded for different resistance values and plotted in Fig. 7–6. It

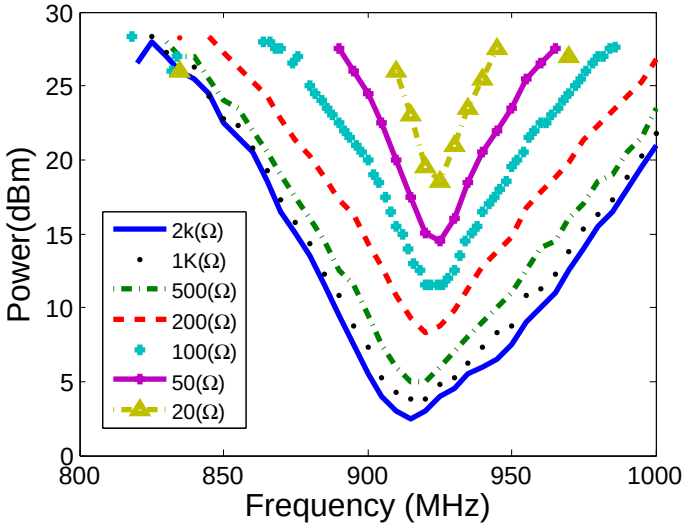

Figure 7–6: Measured minimum transmit power required to activate RFID chip at the sensor port of the single band RFID sensor of Fig. 7–1 with different resistance values.

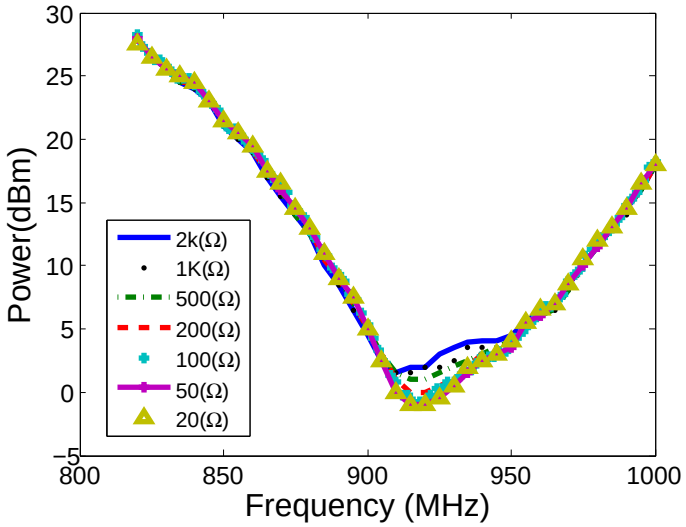

Figure 7–7: Measured minimum transmit power required to activate RFID chip at the reference port of the single band RFID sensor of Fig. 7–1 with different resistance values.

can be observed that the required minimum power from the reader (P_t) to activate the sensor port is inversely proportional to the sensor's resistance. The sensor port is activated with a transmit minimum power of 2.5 dBm when the sensor resistance is high ($2k\Omega$), while it needs higher power (18.5 dBm) when the sensor resistance is

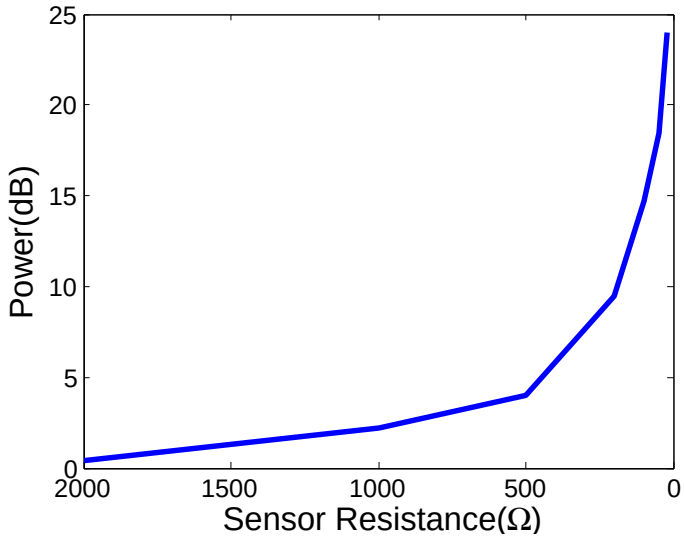

Figure 7–8: Measured transmit power difference between sensor port and reference port at 915 MHz for single band sensor.

very low (20Ω). The required transmit power of the reference port is also measured for different resistance values that are connected at the sensor port. The measured results are presented in Fig. 7–7. The changes in the resistance values at the sensor port cause small changes in the required transmit power (e.g., 1.5 dBm at 915 MHz when $R = 2k\Omega$, and -0.98 when $R = 20\Omega$) of the reference port due to the coupling effect between the two ports. It can be clearly seen that the optimum operation frequency of the proposed tag occurs at the center frequency of the North America band, 915 MHz. At this operation frequency, the tag can be activated with a minimum transmit power of -0.98 dBm to activate the RFID chip at the reference port. Thus, the differential power-up curve is calculated using Equation 7.4 at the operation frequency of (915 MHz) and presented in Fig. 7–8.

The proposed dual band sensor tag was also evaluated and the power sensitivity for two operation bands (North American and European) were measured. The power sensitivity of the sensor Port 1 and reference port 2 that operate at the North

American frequency band are very similar to the measured results of the single-band sensor, as shown in Figs. 7–9 and 7–10. Like the previous design, the required transmit power is increased when the sensor resistance decreases. The required transmit power at the sensor and at the reference ports for the European band is presented in Fig. 7–11 and 7–12, respectively. The optimum operation frequency of the sensor is at 915 MHz for the North American band, where the the required minimum power is -1 dB to activate the chip at the reference port, while for the European band the optimum operation frequency is 885 MHz, and the required minimum power needed for activation of reference port's chip (port 3) is -1.4 dBm. It can be observed here that due to fabrication tolerances the center frequency considered for operation at the European band is shifted out of the 865 MHz to 868 MHz. The sensor still operates at the European band but not with the minimum possible power transmit. The curves of differential power-up levels at the operation frequency of 915 MHz (North American band) and for the European band at the operation frequency of 866 MHz are calculated and presented in Fig. 7–13. Due to the frequency shift described earlier at the European band, a slightly higher differential power-up level is needed compared to that of the North American band.

B. Radiation Pattern Measurements

RFID tag antennas are loaded with the complex impedance of RFID chips, which is highly cpacitive. This is not the standard setting (50Ω) in the conventional pattern measurements as explained in Chapter 3 section 3.3. Therefore, it is important to investigate the radiation pattern of the RFID tag with an assembled and activated chip to observe any pattern deterioration. The Tagformance test system was used in an anechoic chamber to extract the radiation pattern from the power sensitivity

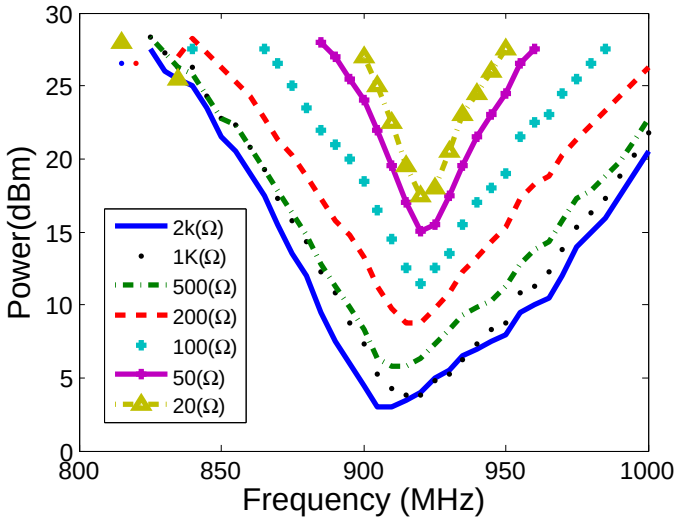

Figure 7–9: Measured minimum transmit power required to activate RFID chip at the sensor port (port 1) of the dual band RFID sensor of Fig. 7–3 with different resistance values.

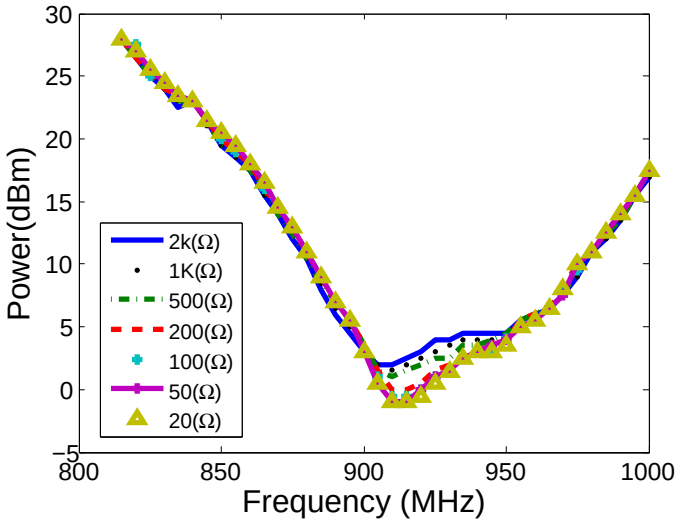

Figure 7–10: Measured minimum transmit power required to activate RFID chip at the reference port (port 2) of the dual band RFID sensor of Fig. 7–3 with different resistance values.

measurements without any physical feed connection [61]. The radiation pattern of the single-band tag antenna at the operation frequency of 915 MHz is measured when both the sensor and reference chips are connected and also without the resistive sensor connected at the sensor port. The measured results are presented in Fig. 7–14. Also,

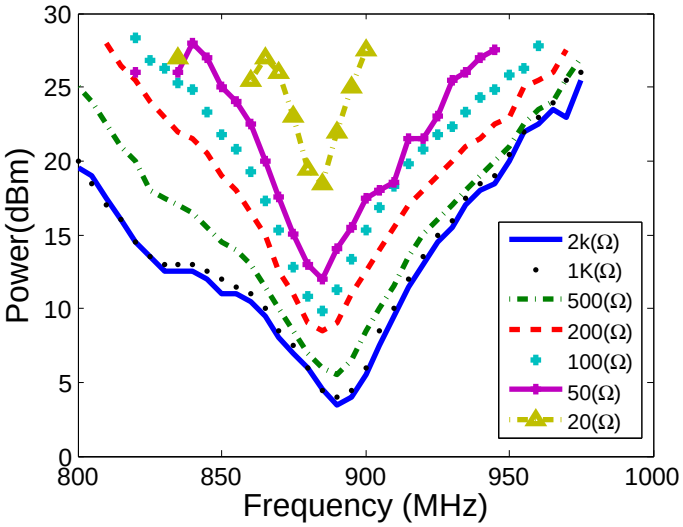

Figure 7–11: Measured minimum transmit power required to activate RFID chip at the sensor port (port 4) of the dual band RFID sensor of Fig. 7–3 with different resistance values.

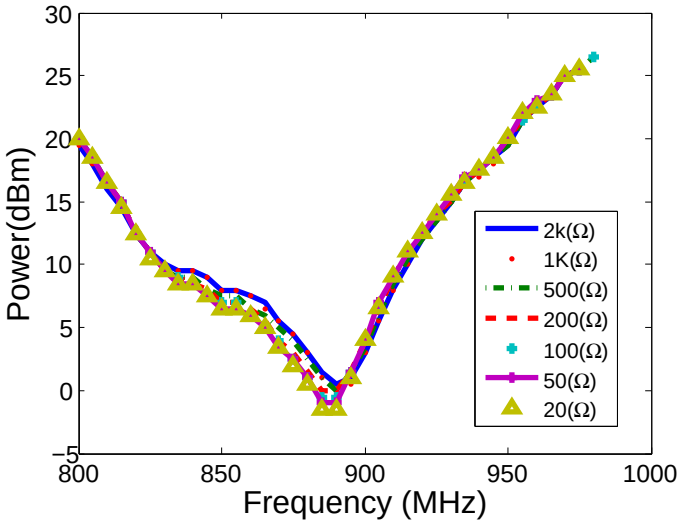

Figure 7–12: Measured minimum transmit power required to activate RFID chip at the reference port (port 3) of the dual band RFID sensor of Fig. 7–3 with different resistance values.

the radiation pattern of the dual-band tag at the operation frequency of 866 MHz is presented in Fig. 7–15. The measured front to back ratio is 9.8 dB at 915 MHz for the single-band design, while it is 8.4 for the dual-band tag antenna at 866 MHz. The realized antenna gain, $\tilde{G}(\theta, \phi)$, can be determined by using the power method

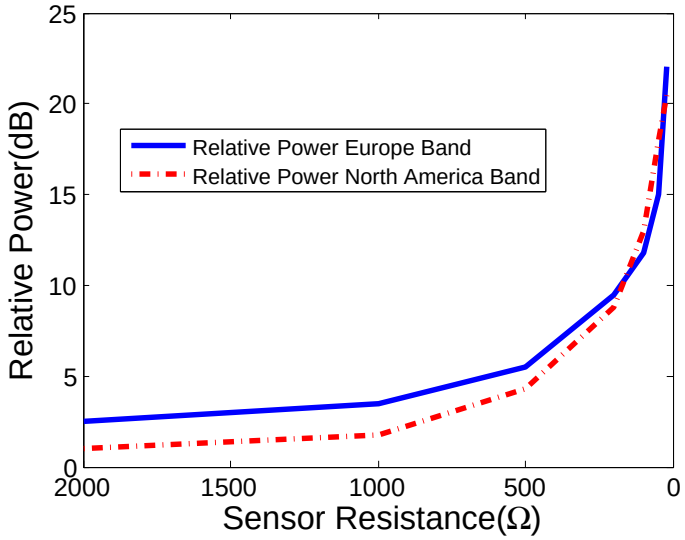

Figure 7–13: Measured transmit power differences between sensor ports and reference ports, at 866 MHz, (European Band) and at 915 MHz (North American band) for dual-band sensor.

presented in [113, 114] using the fallowing equation:

$$\tilde{G}(\theta,\phi) = \frac{P_{Threshold}}{P^t_{min} G_t} \left(\frac{\lambda}{4\pi d}\right)^{-2} \tag{7.7}$$

where $P_{Threshold}$ is the threshold power of the RFID chip, P^t_{min} is the minimum power to activate the chip, G_t is the reader antenna gain and d is the distance between the tag under test and the reader antenna. The realized gain of the both single and dual band sensors versus frequency are shown in Fig. 7–16. The realized gain of the single-band tag antenna is 4.8 dB at 915 MHz, while it is 4.9 dB for the dual-band antenna at an operation frequency of 885 MHz.

7.2.4 Temperature Sensor Measurement Results

In the previous section it was shown the proposed tags could successfully operate with a resistive sensor with a range of $2K\Omega$ to 20Ω. Currently, there are many passive, compact and low-cost sensor which similar resistance variations available

and suitable for direct integration with the proposed tag antennas. An example of a printed low-cost humidity or temperature sensor is a 1-bit write-once-read-many (WORM) presented in [50, 93, 94]. in our measurement, the proposed tag was integrated with another sensor available in our lab (Thermistors - NTC NTC) [112] that has a similar resistance variation range to those described in Section 7.2.3, i.e., $1.9K\Omega$ at 0^0C to 196Ω at 60^0C. These types of sensors are not equipped with discrete electronic components that would increase the price of the whole sensor unit. Therefore, it is feasible to install such sensor units on a variety of consumer products in the proposed RFID tag sensor's designs described earlier. Some of the physical characteristics of Thermistors - NTCLE100E3681JB0 and NTCLE100E3221JB0 are summarized in Table 7–1 . From Table 7–1 it can be seen that the two available sensors have different resistor values at room temperature. Since there was no climate room available during the time of these measurements, these two temperature sensors were only used to extract the power sensitivity of the proposed single band sensor and to demonstrate the sensing principle of the RFID tag-based sensor operation and not for the actual temperature measurements. The power sensitivities of the RFID chip at the sensor port, Port 1, and reference port, Port 2, are presented in Fig. 7–17. It can be seen that the sensor port requires higher power than the reference port, and that the ratio of the power transmitted to the sensor port to that transmitted to the reference port can be, can be extracted to determine temperature if a calibration table or a climate room were available.

7.2.5 Power Sensitivity Measurements on Consumer Products

To demonstrate the use of this type of sensor tag, measurements were conducted using some consumer products and boxes. The Tagformance RFID measurement

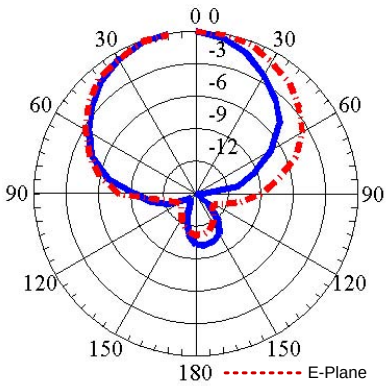

Figure 7–14: Measured radiation pattern of the single-band design at 915 MHz.

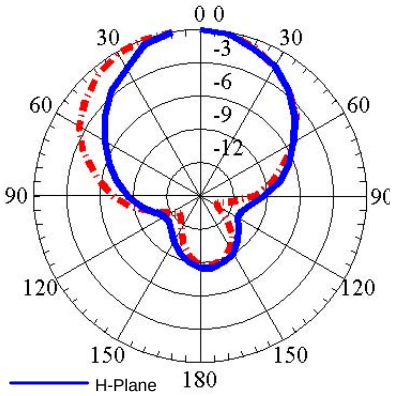

Figure 7–15: Measured radiation pattern of the dual-band design at 866MHz.

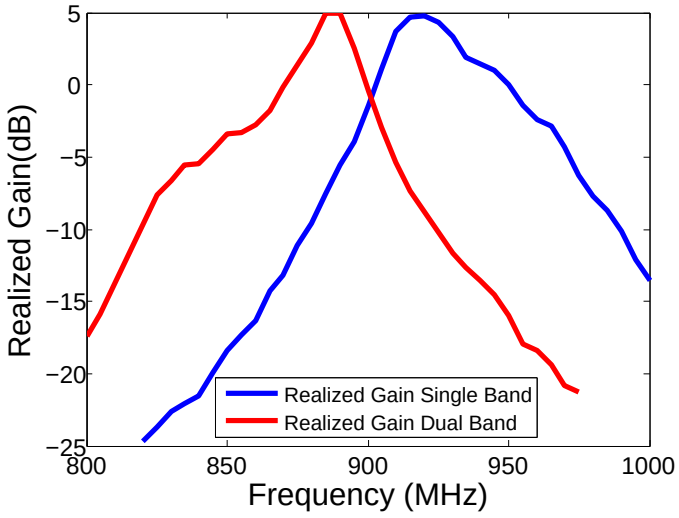

Figure 7–16: Measured realized gain for single and dual-band sensor.

system was used in this evaluation. In these measurements, the tag antenna was attached to the exterior of the packages, with the z-axis of the tag facing the reader antenna, as shown in Fig.7–18. The performance of the RFID temperature sensor tag is analysed when placed on two different types of packages. First, the RFID temperature sensor tag is attached to a box that is filled up with plastic items, and then the RFID tag is attached to a box containing metallic cans. Since the

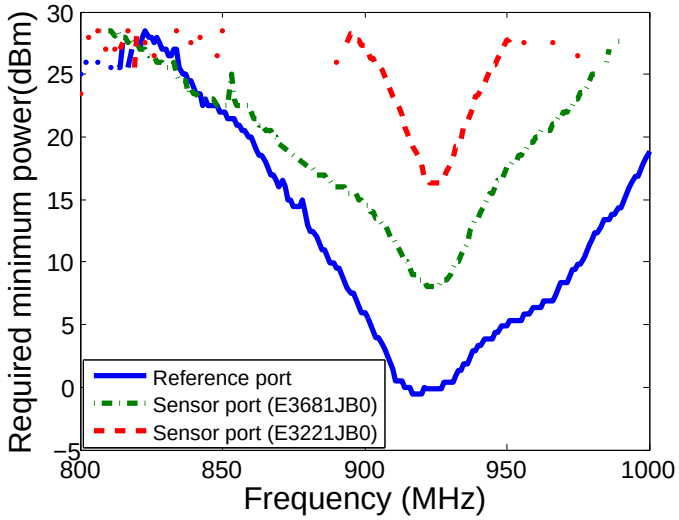

Figure 7–17: Measured minimum transmit power required to activate RFID chip at the sensor port of the single band RFID sensor of Fig. 7–1 with Thermistor - NTC NTC sensors.

Table 7–1: physical characteristics of Thermistors - NTCLE100E3681JB0 and NTCLE100E3221JB0

Thermistors-NTCLE100E3681JB0											
Temp.(^{0}C)	0	5	10	15	20	25	30	35	40	45	50
RT Ω	1941	1554	1253	1016	828.8	680.0	561.0	465.2	387.8	324.8	273.3
Thermistors-NTCLE100E3221JB0											
Temp.(^{0}C)	-25	-20	-15	-10	-5	0	5	10	15	20	25
RT Ω	2117	1636	1274	999.1	789.4	628.0	502.9	405.3	328.7	268.2	220.0

principle method of sensing depends on the power sensitivity measurements, the tag is therefore first measured in free space and then attached to the two different packages. The measured results of the required minimum power for both ports in these two tests are presented in Figs.7–19 and 7–20. When the proposed sensor is attached to the top of a box containing plastic items, the minimum power needed to activate the RFID chips at the reference and sensor ports are very close to those of pertinent ports in free standing tag measurements. Thus, the loading effects of these types of items are negligible. However, when the proposed sensor is attached to the packages containing metallic objects, a small change in minimum power for RFID

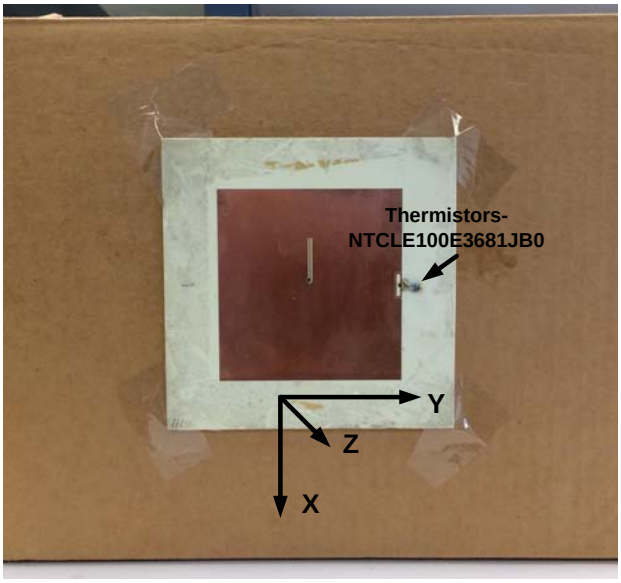

Figure 7–18: Measured packages with Thermistors- NTCLE100E3681JB0.

chip activation is seen compared to the measurements of free standing tags. For example, the required minimum power at 920 MHz for a sensor port is 8.4 dBm in a free standing tag, while it is 7 dBm when placed on the box of metallic cans. Fig.7–21 presents the loading effect of the two different packages on a sample monopole RFID tag described in Chapter 3. The loading effects of a box containing plastic items causes a large shift in the resonance frequency and increases the required minimum power compared to the RFID tag sensor of Fig. 7–1. The monopole antenna tag dramatically loss its performance when placed on the box containing metallic cans. Therefore, it can be observed that the proposed tag sensor described in this section is more immune to the loading effects of consumer products compared to RFID tags that use wire antennas for sensor implementation [50, 94, 99–103].

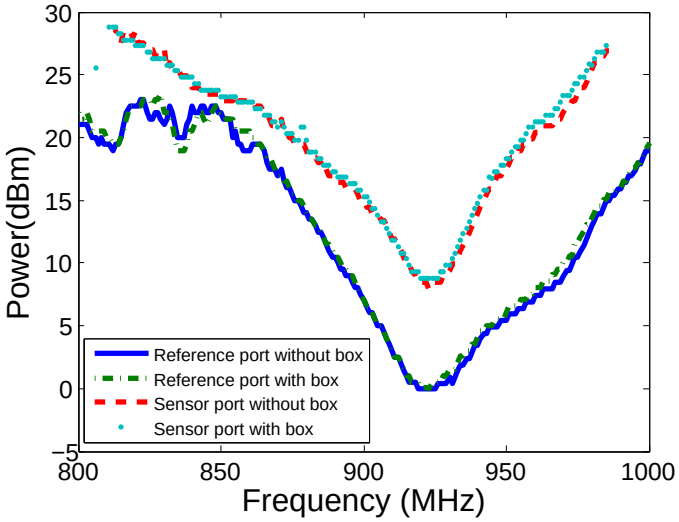

Figure 7–19: Measured required minimum power for the reference and sensor ports of the tag in Fig. 7–18 attached to a box containing plastic items.

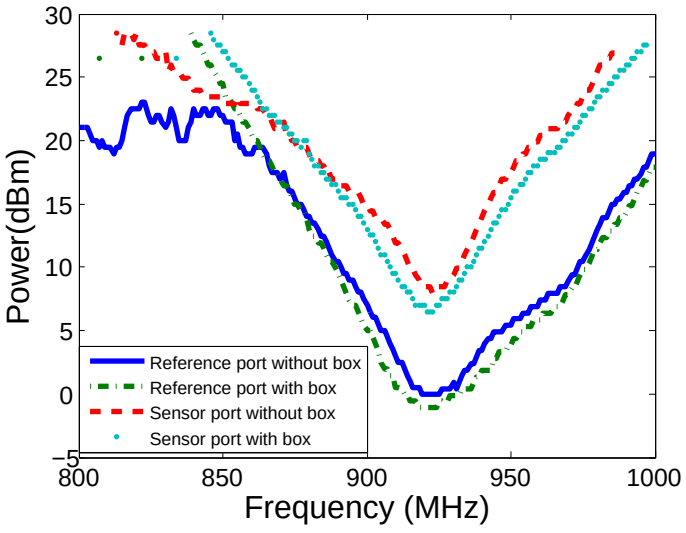

Figure 7–20: Measured required minimum power for the reference and sensor ports of the tag in Fig. 7–18 attached to a box containing metallic items.

7.3 Solar Powered RFID Tag-Based Sensor

As mentioned in the previous section, sensor data is extracted from the power ratio described in Equation 7.4. It was also concluded from power sensitivity measurements that the introduced mismatch due to the resistive sensor reduced the power sensitivity of the sensor port. Thus, the reading range of the sensor port will be reduced. In fact these types of sensors suitable for use in short range applications, e.g., 1 m [94]. Nonetheless, the reading range of the proposed sensors can be extended by improving the power sensitivity of both the reference and the sensor ports. Therefore, an improved design was developed herein. In this prototype, the power sensitivity of the IC is increased by including an additional energy source. A Monza X RFID chip that has two pins for DC connection is used in the tag, which is designed to operate at the North American bandwidth (902 MHz to 928 MHz). A Rogers RO4350B substrate (ε_r = 3.66 and 1.524 thickness) is considered for implementing the tag antenna. At 915 MHz, the length and the width of the radiating patch is optimized by using HFSS simulator, yielding L=83 mm and W= 82.8 mm. The inductive loop matching technique is used to feed the RFID chip. The dimensions of the inductive loop are optimized for conjugate matching, resulting in L1=18.8 mm, L2=8.5mm, d=0.6 mm. Also, a thin film of solar cells [91] are attached on the top of the patch antenna, as shown in Fig. 7–22. The size of the solar panel is $64mm \times 37mm \times 0.2mm$, yielding an active area of $23cm^2$. As shown in Fig. 7–22, the DC+ and DC- of the solar panel are connected to the RFID using tiny wires.

The same system (TagFormance) that was used in the previous tag measurements is utilized here to evaluate the performance of the solar powered tag-based

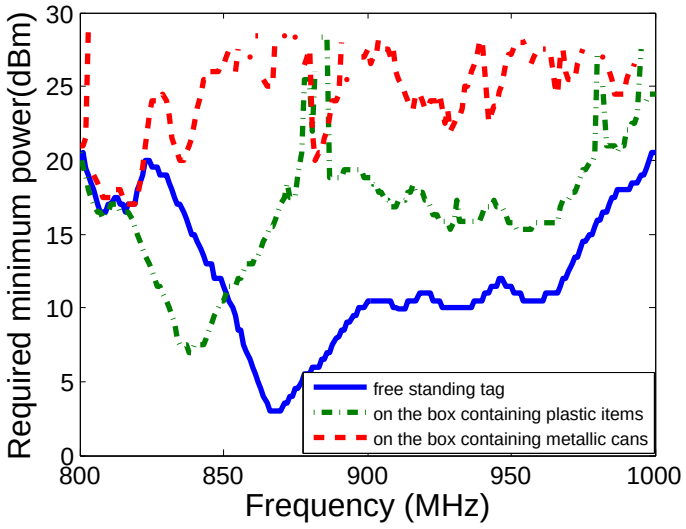

Figure 7–21: Measured required minimum power for the monopole tag antenna of Fig. 3–2 placed to the top of a box containing plastic and metallic items.

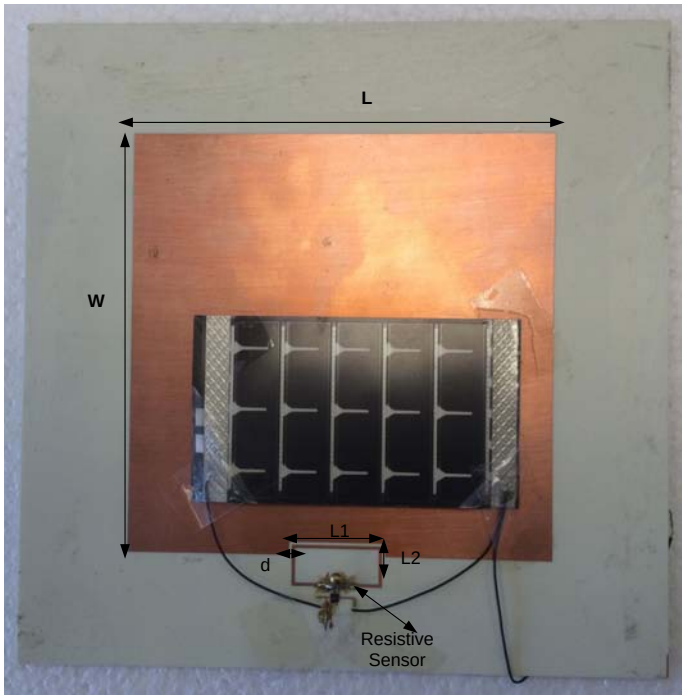

Figure 7–22: Picture of the prototyped solar powered RFID tag-based sensor.

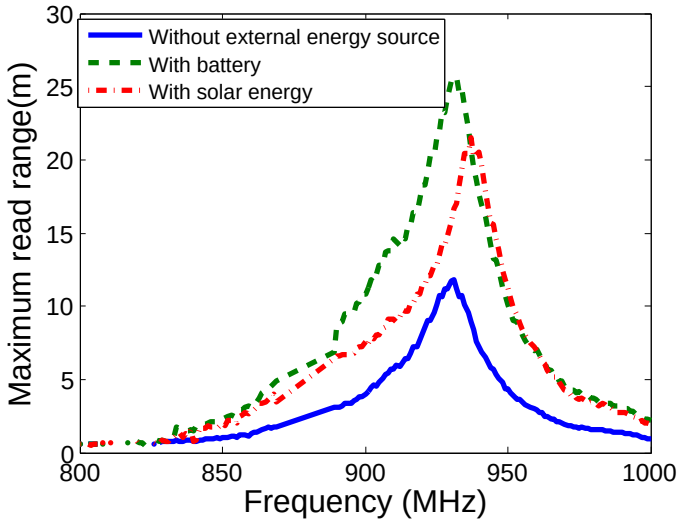

Figure 7–23: Maximum reading range of the reference port with and without external energy sources.

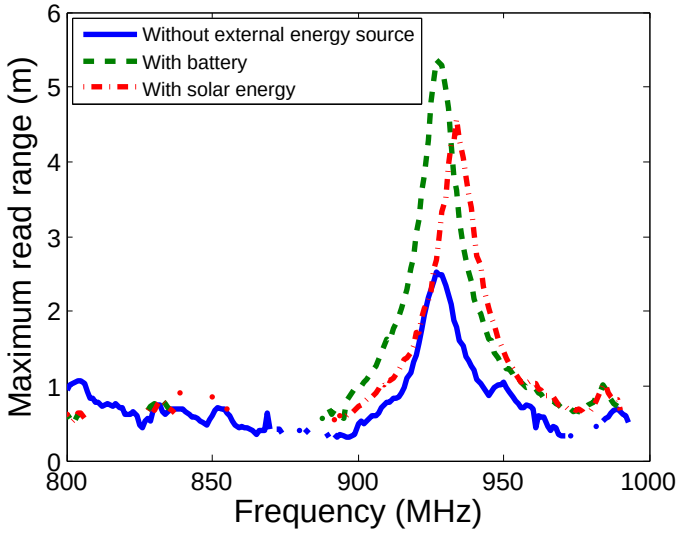

Figure 7–24: Maximum reading range of the sensor port with and without external energy sources.

sensor. In this test, the reading range for the reference and sensor ports are measured with and without connecting the solar energy source. First, the reading range of the RFID chip is measured without the external solar power source. Next, it is measured with two different external power sources connected, one at time: a small battery and the solar panel overlay. The measured reading range results for the reference port are presented in Fig.7–23. The maximum reading range without any additional energy sources is obtained at 932 MHz (11.2 m), while with a small battery the maximum reading range is 25.6 m at 932 MHz. When the solar panel is used to power up the RFID chip under typical indoor office illumination conditions, the maximum reading range of 21.5 is achieved at 937 MHz. Due to the loading effect of the solar panel the maximum reading range is shifted from 932 MHz to 937 MHz. Also, these measurement were repeated with a resistive thermal sensor, i.e., a Thermistor - NTCE100E3221JB0, connected in parallel with the RFID chip as shown in Fig. 7–22. The measured results of the maximum reading range are presented in Fig. 7–24. The reading range of the sensor port without an additional energy source is 2.4 m at 928 MHz. When the small battery and solar panel are used to power up the RFID chip, the reading ranges are 5.4 m at 928 MHz and 4.6 m at 934 MHz, respectively. It can be clearly observed that the effective reading range of the tag is almost doubled when an additional energy source is used to power up the RFID chip.

7.4 Summary

In this chapter, an RFID patch antenna is proposed for UHF RFID tag-based sensor applications. Single band antennas, operating at the 902-928 MHZ North

American frequencies and dual band antennas covering 865-868 MHz, (European frequency band) and 902-928 MHz frequency bands are presented. The proposed patch antennas are multi-port types and incorporate multiple RFID chips with a power sensitivity of -13 dBm and input impedances of $9.8 - j73\Omega$ and $8.2 - j61\Omega$ at the operation frequencies of 866.5 and 915 MHz, respectively. For maximum power transfer between the RFID chips and the antennas, inductively-coupled loop and inset feeds are integrated for each antenna layout. One port in each antenna is dedicated for attaching a resistive sensor as a load in parallel with the RFID chip. A few normal resistors are used as an alternative way to represent the resistive sensor in simulations and measurements. The proposed tags are fabricated and experimentally evaluated showing minimal sensitivity to the background material compared to previously discussed dipole-based tag designs. Further tests show that the designed RFID tag sensor can read resistance variation between 20Ω to $2K\Omega$, which is equivalent to the resistance's variation of a sample humidity sensor when the humidity changes from 20% to 80% or to that of a temperature sensor, e.g., NTC Thermistors, whose resistance changes from $1.9K\Omega$ (at 0^0C) up to 196Ω (at 60^0C). In comparison with the passive tag-based sensor in [101], the proposed tag is simple, since it only uses a one-layer substrate and can be integrated with different resistive sensors (e.g. temperature or humidity). Thus, the proposed multiport patch antennas equipped with resistive sensors are capable of serving as low-cost remote sensors for various applications, including supply chain operations and the transportation of sensitive items.

To improve the reading range of the sensor, solar powered RFID tag-enabled sensors are fabricated and experimentally evaluated. The measured results demonstrate that the reading range of a solar powered RFID tag-enabled sensor is increased by two times compared to a similar one prototyped without solar energy harvesting.

Chapter 8

RFID Tags for Transmission of Generic Sensors Data

8.1 Introduction

In Chapter 7 low-cost passive RFID tag-based sensors were successfully implemented and experimentally evaluated. However, from the evaluation results it can be clearly noted that these types of RFID tag-based sensor are limited in terms of their reading range and sensing accuracy. The reading range of the sensor port is strongly degraded due to the introduced mismatch between the RFID chip and the tag antenna. Moreover, the sensor's data is extracted from the ratio of the required minimum transmit power to the reference and sensor ports, which has a limited accuracy due to the impact of the sensor itself (as well as identification objects) on the tag antenna performance. Therefore, the previous types of sensors can be referred to as threshold passive sensor tags. These types of sensor tags can be useful for sensing heat and humidity in many applications, including supply chain operations and the transportation of various sensitive drugs and food items. Since the proposed

sensor tags are low cost, they can be placed on a large variety of common packages to qualify and display the quality status of these products.

The other promising technique is an RFID tag-enabled sensor for the transmission of generic sensor data. In this approach, an RFID tag transmits digitized sensor data in its RFID bit stream response back to the reader's query. Therefore, it is possible to design RFID tags separately for an enhanced and optimized reading range without any impact from an integrated sensing operation. A typical configuration of a tag-enabled sensor is composed of a passive RFID platform integrated with a low power microcontroller unit and generic sensors [9, 95–98, 115]. The microcontroller unit (MCU) is used to sample the output signal of the attached sensors and update the sensed data into certain bits of the ID code of the RFID chip. In this way, sensor data can be remotely recorded using standard commercial RFID readers. Several current research efforts are focused on developing ways to implement RFID tags that are able to operate independently in conjunction with digital sensors while transmitting sensor's data at a low cost and with long lifetime operation [9, 95–98, 98, 115]. At the state of the art, few RFID tag-based sensors have been implemented by integrating sensor circuits within the RFID chip [116, 117], where the sensor is powered by the RFID reader signal (passive-mode) or battery (active mode) and certain bits of the ID code of the RFID chip are used to transmit the sensed data. However, a fully integrated passive RFID-IC-sensor requires the sensor circuits to be both energy efficient and chip embeddable [116, 117]. Consequently, only a few kinds of sensors (e.g, temperature, light and pressure) satisfy these strict constraints [98, 116, 117]. Among the commercial fully integrated RFID-IC-sensors, the most attractive realizations are the SL900A tag-based sensor that is implemented

by IDS Mircochip [118], and the Esay2Log tag from CEN RFID [119]. However, the maximum reading range obtained by the SL900A in full passive operation is 1.5 m, while it is 5.2 m when it operates with a battery. Also, the reading range of the Esay2Log with a battery is approximately 10 m.

The other promising approach for implementation of RFID-based sensor utilizes Wireless Identification and Sensing Platform (WISP) that allows the use of an external sensor is presented in [95, 96]. The WISP is powered by standard Gen2 commercial readers, and thus the reported reading range for this system is up to approximately 3 m [95, 96]. An alternative realization of RFID tag-based sensors equipped with external sensors and using two antennas shows that they achieve a longer reading range (5 m) [115]. One of the antennas is connected to the RFID chip and is used to receive/transmit data from/to the reader. The other antenna is connected to an RF to DC rectifying circuit to produce the DC voltage for powering the digital circuit. To increase the reading range even further, a battery assisted RFID tag-enabled sensor is presented in [120].

From this overview of state-of-the-art technology it can be seen that the energy harvesting/supplying unit which should power up the sensors and the MCU plays a critical role in the performance, detection range and operating lifetime of RFID-tag sensors.

In the present chapter, this challenge has been addressed via solar energy harvesting incorporated with an overlay of solar cells on a patch antenna that is integrated with the new generation UHF I^2C-RFID chip, an MCU and an external sensor (i.e. thermal, humidity). In the following sections, single and multi port RFID patch tag antennas that are equipped with external sensors for transmission

of generic sensors data in wireless sensor networks are implemented. The operating power of the MCU and external sensor is provided by either using solar energy via the solar cells placed on top of the two-port patch antenna or by harvesting the ambient RF energy transmitted by the RFID reader (or other RF sources) through the second port of the tag antenna as will be described in the following sections.

8.2 Single Port Patch Tag Antenna for the Transmission of Generic Sensors Data

The system diagram of the proposed RFID tag-based sensor for the transmission of generic sensors data that could be used in wireless sensor networks is shown in Fig. 8–1. The system in general consists of an antenna for receiving and backscatteing the signal from and to the EPC Gen2 standard RFID readers, a low power microcontroller unit (MCU), analog or digital sensors, and energy sources. The microcontroller unit (MSP430 [121]) is used to sample the output signal of the attached sensor and update the sensor data into the ID code sequence of the RFID chip. In this manner, the sensor data can be remotly recorded using a standard commercial RFID reader. Different approaches can be used to harvest the energy needed to operate the sensor and the MCU.

8.2.1 RFID Tag Antenna Design

In this design, a single-port patch antenna is proposed to be integrated with the new generation UHF I^2C-RFID chip [33], the Microcontroller unit MSP430 [121] and an external thermal sensor as shown in Fig. 8–2. The MCU is connected to the surface mount analog temperature sensor LM940 ($-50^0C$to 70^0C with an accuracy of 1.8^0C) [122]. For simplicity of programming and its connecting to the system, the

MCU is placed on a socket. In this prototype, the required power for the sensor and the MCU is generated using the solar panel attached on top of the patch antenna as shown in Fig. 8–2. The RFID tag is fabricated using a Rogers RO4350B substrate ($\varepsilon_r = 3.66$and 1.524 thickness).The tag antenna is designed to operate at the North American operation bandwidth (902 MHz to 928 MHz) and the optimized length and width of the radiating patch are L=83mm and W= 82.8mm, respectively. An inductive loop feed design is used to match the RFID chip impedance of $(18.6 - j171\Omega)$ to the input impedance of the tag antenna for maximum power transfer. The optimized dimensions of the matching loop are L1=18.8mm, L2=8.5mm, d=0.6mm. A flexible thin-film solar cell panel (MPT3.6-75) with Voc=4.8 V, Isc=0.06 A and size of $(L \times W \times T = 74 \times 73 \times 0.2mm)$ [91] is attached on top of the patch antenna to generate the required power for the MCU and the external sensor. The solar panel with this size is able to produce the required minimum power to operate the sensor and the MCU in an indoor lighting condition. However, in full sun illumination (out door) intensity a flexible thin-film solar panel with the size of $(L \times W \times T = 64 \times 37 \times 0.2mm)$ (used in Chapter 6) can be used instead, to reduce the solar panel size. Thus, the compact patch antenna design presented in Chapter 5 can also be used for the realization of compact RFID tag-enabled sensor as well.

8.2.2 Simulated and Measured Results of the RFID Tag-Enabled Sensor

The simulated results of the input impedance of the tag antenna and the input impedance of the RFID chip are presented in Fig. 8–3. At the operating frequency of 915 MHz the input impedance of the chip, $18.6 - j171\Omega$, is conjugate matched to the input impedance of the tag antenna, $33.1 + j179.1\Omega$, using the printed inductive loop.

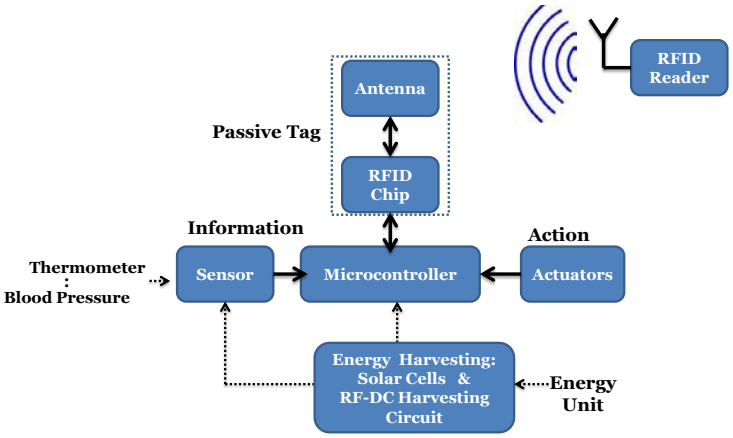

Figure 8–1: Block diagram of digital RFID tag-based sensors.

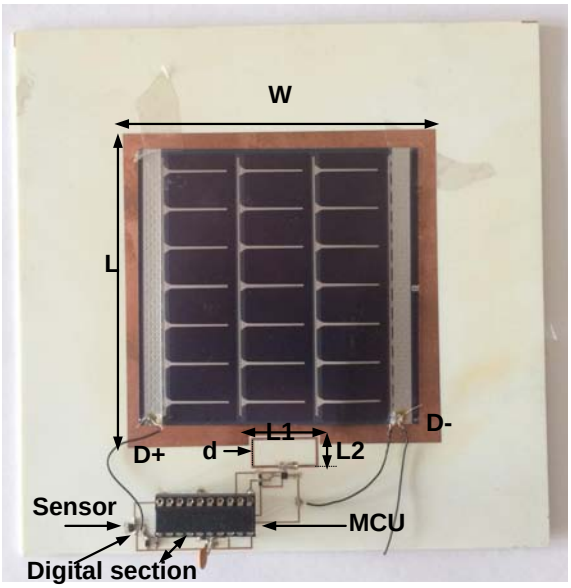

Figure 8–2: Prototyped single port RFID tag-based sensor.

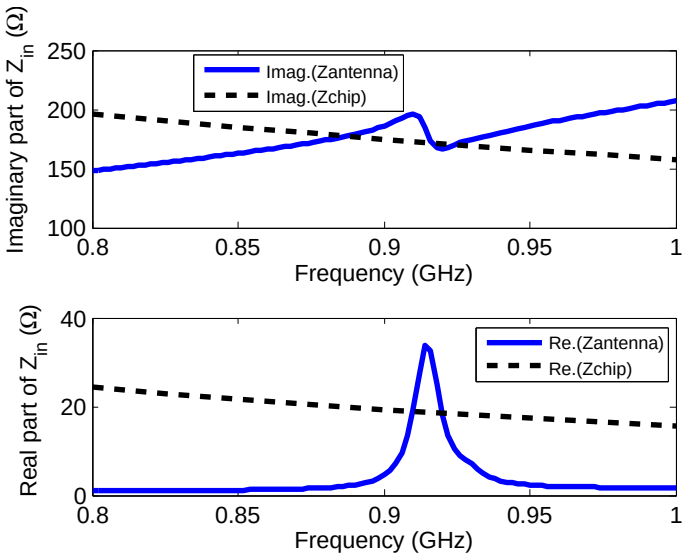

Figure 8–3: Simulated input impedance of the tag antenna shown in Fig. 8–2 and RFID chip.

A commercial RFID tag measurement system (Tagformance) [61] was used to evaluate the power sensitivity of the fabricated tag. The transmitter and receiver antennas in this measurement system are linearly polarized, providing a flat 6 dBi gain response at the frequency range of 800 to 1000 MHz. The distance between the reader and the tag in this commercial test system is 0.45 m. The measured required minimum power on tag to activate the RFID chip without and with a power source across the operation frequency band of 800 to 1000 MHz is presented in Fig. 8–4. Without an energy source, the tag operates like an ordinary RFID tag and the required minimum on-tag power at 928 MHz is -18.2 dBm to generate a response. When a small battery [123] or solar panel (inside the Lab under typical lighting conditions) is connected, the sensor is powered up and the sensed data is dynamically updated onto the RFID chip memory that has this additional power supply. Therefore, the required minimum on-tag power is reduced to -26.3dBm at 928 MHz and -25 dBm at 934 MHz, respectively. Note here there is a slight change in

the resonance frequency (shifted by 6 MHz) of the antenna that is powered with solar cells, due to the loading of the overlaying solar cells on the patch. The maximum reading range plot is presented in Fig. 8–5. When there is a small battery or solar energy harvesting, the proposed sensor achieves a maximum reading range of 30.9 m (with a battery) and 26.1m (with solar cells), while it exhibits a maximum reading range of 11.9 m without any additional energy source. To observe RFID-based wireless sensor performance when the sensor is powered by solar cells and exposed to extreme temperature variations (proximity to a hair dryer), different ID readings by an RFID reader (GAO RFID Inc. [20]) were recorded. As shown in Fig. 8–6, the readings of the commercial RFID reader were dynamically updated in the first four digits of the EPC ID of the RFID chip when the temperature changed. The integration of a digital sensor with dual functions (i.e. reading temperature and humidity) and the translating the original ID readings from Hexadecimal (Hex) representation into base ten notation will be described in detail in the following section.

8.3 A Multi-Port UHF RFID Tag Antenna for Enhanced Energy Harvesting of Self-Powered Wireless Sensors

This design takes a step further by incorporating two energy harvesting strategies to enable self-powered operation of the RFID tag-based sensor. Like a design of previous section a microcontroller unit is used to sample the output signal of the digital sensor a more elaborate one that is (able to measure both temperature and humidity) and write the pertinent data into the RFID chip. The required operating power of the MCU and the external sensor can be provided by either using solar

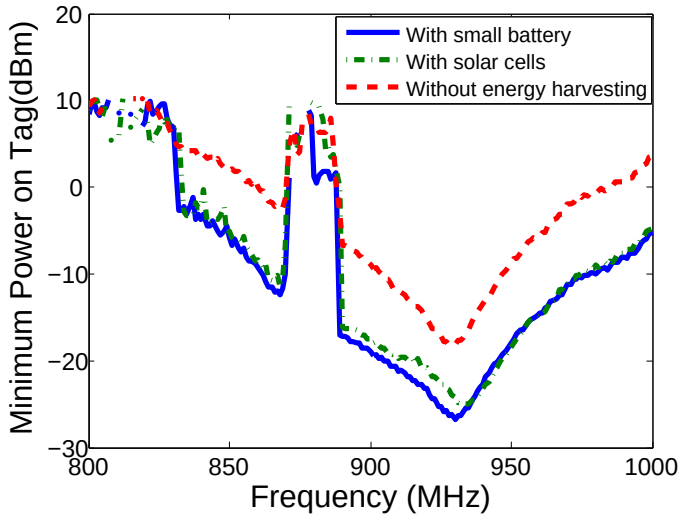

Figure 8–4: Measurement results of the power sensitivity of the RFID-enabled sensor with and without additional energy sources.

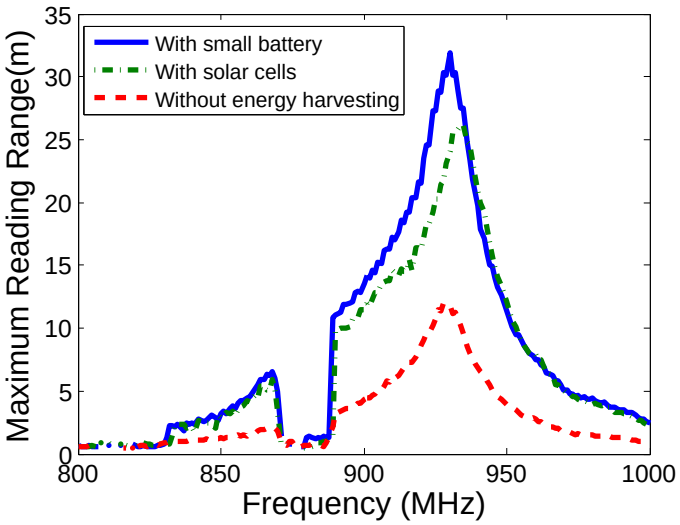

Figure 8–5: Measured results of maximum reading range of the RFID-enabled sensor with and without additional energy sources.

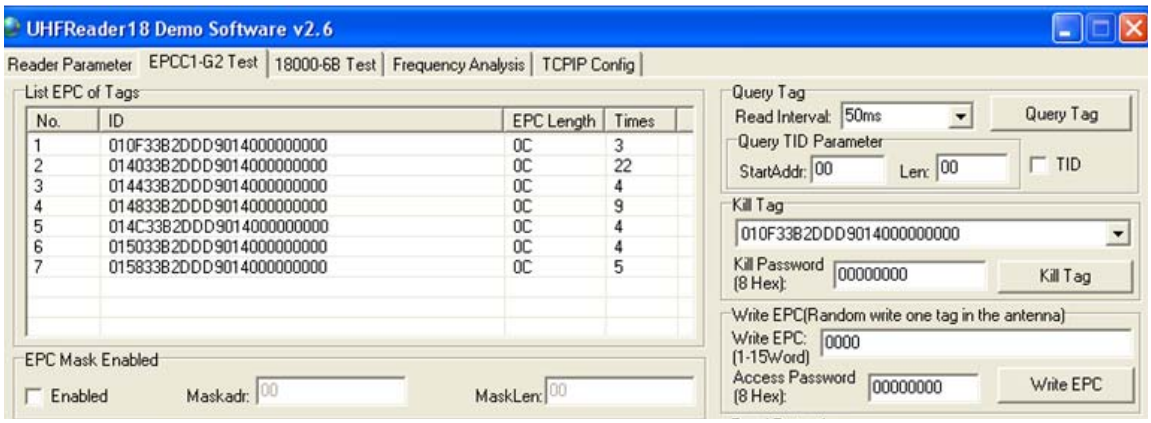

Figure 8–6: Remotely recorded IDs transmitted by the proposed RFID tag-enabled sensor using a commercial RFID reader.

energy via the solar panel placed on top of the two-port patch antenna or by harvesting the ambient RF energy transmitted by the RFID reader (or other RF sources) through the second port of the tag antenna. A preliminary RFID sensor prototype is fabricated using low-cost off-the-shelf discrete components and experimentally evaluated, as described in the following sections.

8.3.1 System Architecture

The block diagram of the proposed multi-port RFID-based sensor is presented in Fig. 8–7. The picture of the fabricated prototype is also shown in Figure 8–8. The part labeled as the digital section in the photograph is composed of the sensor and the MCU circuits. The block diagram shown in Fig. 8–7 and the energy harvesting method to power up the MCU and the sensor are thoroughly described in the following subsections, while the detailed features of the MUC, sensor, RFID chip and the communication protocols are provided in Table 8–1.

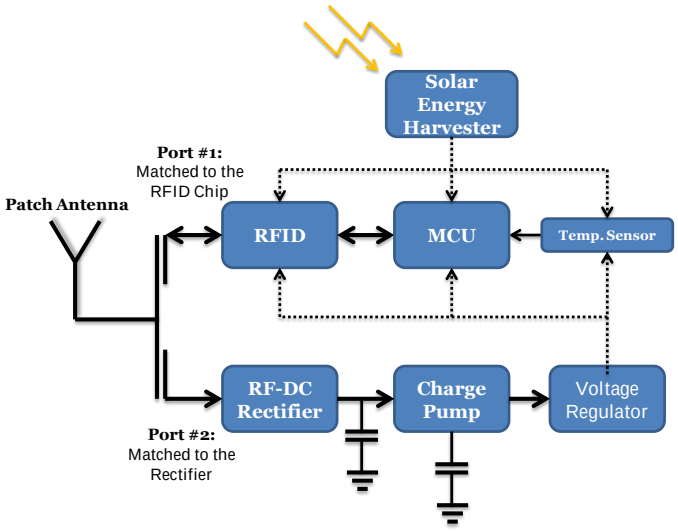

Figure 8–7: Block diagram of the proposed RFID-based sensor with a Multi-port patch tag antenna.

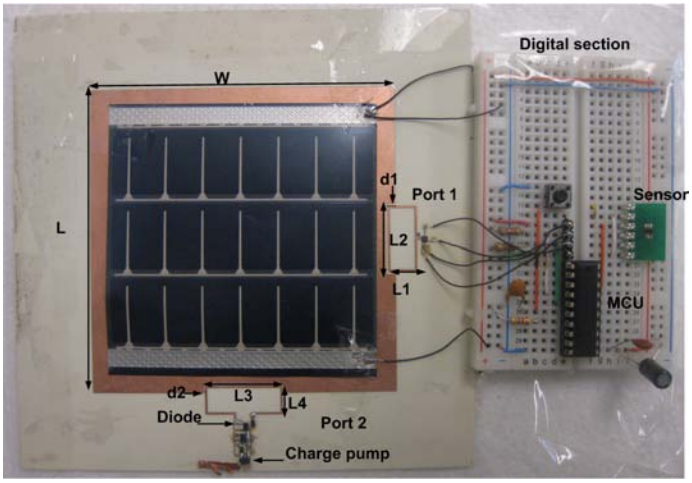

Figure 8–8: Prototyped RFID-based sensor with multi-port patch antenna tag and energy harvesting.

Table 8–1: Capabilities of the proposed sensor

Microcontroller	
Type	MSP430G2553
FRAM (kB)	16
Minimum operation (V)	1.8
Active current ($\mu A/MHz$)	230
Sleep current (μA)	0.5
Sensor on board	
Temperature	Digital output
Current	0.7 μA with 14 bit resolution
Humidity	Digital output
RFID Chip	
Type	Impinj Monza X
Memory	8Kbits
RFID Communication	
Operating frequencies	UHF band (860-960 MHz)
Data rate (kbits/s)	$40 \sim 640$
Modulation	Backscatter
R/W sensitivity (dBm)	-24 with energy harvesting -17 without energy harvesting
Active current (μA)	25
Sleep current (μA)	0
Interfaces	
Sensor with RFID chip	I^2C
Tag with reader	EPC class 1 Gen 2

8.3.2 Multi-Port Patch Antenna and RF Energy Harvesting Circuit

The tag antenna is designed to operate at the North American operation bandwidth (902 MHz to 928 MHz). A Rogers RO4350B substrate (ε_r = 3.66 and 1.524 thickness) was considered for implementing the tag antenna. At 915 MHz, the length and the width of the radiating patch is optimized by using the HFSS simulator yielding L=83mm and W= 82.8mm. The two ports of the patch are connected to two integrated circuits, i.e., the RFID chip at port 1 and the RF-DC rectifying circuit at Port2, with complex input impedances as shown in Fig. 8–8. Therefore, the inductive loop matching technique is used to feed both ports of the antenna. The dimensions of the inductive loops are optimized for conjugate matching, thus yielding L1=17.6mm, L2=7.9mm, L3=21.1mm, L4=7.9mm, d1=0.6mm and d2=0.2mm. The simulated results of the input impedance of Port 1 and the input impedance of the RFID chip are presented in Fig. 8–9. At the operating frequency of 915 MHz the input impedance of the chip ($18.6 - j171\Omega$) is conjugate matched to the input impedance of the tag antenna ($21.7 + j178.7\Omega$) using the designed printed inductive loop. Also, the simulated results of the input impedance at Port 2 and the input impedance of the rectifier circuit are presented in Fig. 8–10. At the operation frequency of 915 MHz, the input impedance of the rectifier ($81 - j227\Omega$) is conjugate matched to the antenna impedance of ($79.4 + j236\Omega$). To include the option of energy harvesting from ambient RF signals, an RF-DC rectifying circuit is designed and connected to the second port of the tag antenna. This circuit, which consists of a diode-based rectifier (operating at 915 MHz) followed by a charge pump and a voltage regulator as shown in Fig. 8–7, coverts the RF signal to a DC supply voltage. The HSMS-285C zero-bias Schottky diodes [124], which have high detection

sensitivity at UHF frequencies, are used in the rectifier. The Seiko S-882Z charge pump IC [125] is employed to boost the rectified DC output. The charge pump is suitable for ultra-low voltage applications. The oscillation in the charge pump starts with input voltages as small as 0.35V. Once the oscillation starts the storage capacitor charges up. When it reaches 2.4V, the internal supervisory circuitry discharges the capacitor into the load. The on time of the charge pump depends on the input voltage and value of the storage capacitor. The supply voltage harvested from the received RF signal via the second port provides an alternative means for powering up the sensor, the MCU and the RFID chip to achieve an extended reading range.

The design developed in this section also uses a solar energy as its primary source of energy. A flexible thin-film [91] (MPT3.6-75) with Voc=4.8 V and Isc=0.06 A was selected to harvest the required energy to power up the digital section (including the sensor). In this proposed design, the antenna and the solar panel share the same area, allowing for a more compact footprint. The solar panel of size ($L \times W \times T = 74 \times 73 \times 0.2mm$) is glued onto the top of the patch antenna. Its DC- and DC+ pads are routed out to power the digital section. The RFID chip DC- , DC+, SD and SCL (for I^2C communication) pins are also connected to the digital section. The impact of placing the solar cells on the patch antenna in terms of the resonance and feed design was found to be minimal via fullwave simulations (HFSS).

8.3.3 Digital Section and Sensor Programming

In order to use the RFID tag as a transmitter of sensor data, the new generation RFID-I^2C-chip, which provides the capability of writing information into its internal memory, is chosen as indicated earlier. To enable this feature, a low power microcontroller followed by a sensor (in this prototype a temperature/humidity sensor)

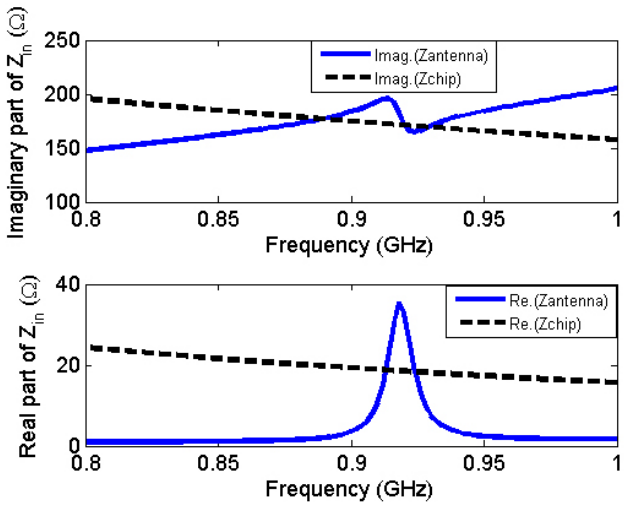

Figure 8–9: Simulated input impedance of Port 1 of tag antenna and RFID chip.

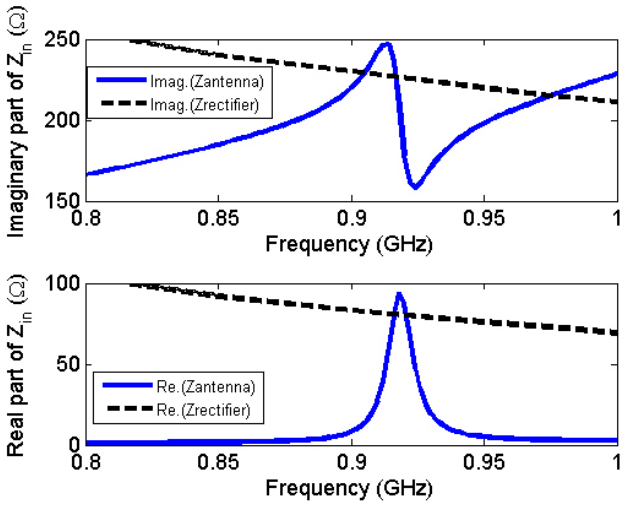

Figure 8–10: Simulated input impedance of Port 2 of tag antenna and the rectifier circuit.

are connected to the RFID chip. For simplicity in the integration, the testing different sensors and in programming the MCU, the whole digital circuit is implemented on a small Breadboard. As shown in Fig. 8–8, the surface mount digital temperature/humidity sensor (measures -40^0C to 125^0C with an accuracy of $\pm 0.25^0$C and relative humidity (RH) of 0 to 100%) is soldered onto a small printed circuit board and then connected to the Breadboard. The core of the digital subsystem is the ultra-low-power 16-bit MSP430G2553 MCU [121], with the power consumption characteristics of 230 μA/MHz at a supply voltage of 2.2 V in active mode and 0.5 μA/MHz in standby mode. To minimize the amount of hardware interfaces required for the system, communication with both the RFID chip and the digital temperature/humidity sensor is done using a single I^2C bus. For the purposes of energy-efficiency, the MCU is programmed to enter its active mode at a rate of 2.08 Hz in order to perform data capture operations. The MCU returns to standby mode once all necessary operations have been completed. In addition, the analog-to-digital conversion (ADC) in the digital sensor can be changed from a 14-bit representation to 8-bit to save on power consumption at the cost of bit resolution. When the supply voltage in the proposed sensor is provided via solar energy or an RF-DC harvester, the digital sensor can use the 14-bit representation. The operations performed by the MCU in active mode involves: polling the digital sensor for new data, formatting the raw data into a human readable form, and transmitting the formatted data into the EPC memory banks of the RFID chip. New temperature and humidity data are read from the digital sensor by the MCU in a raw data format. An initial conversion to degrees Celsius and percentage relative humidity is required using the conversion equations associated with the digital sensor. Further formatting is performed by

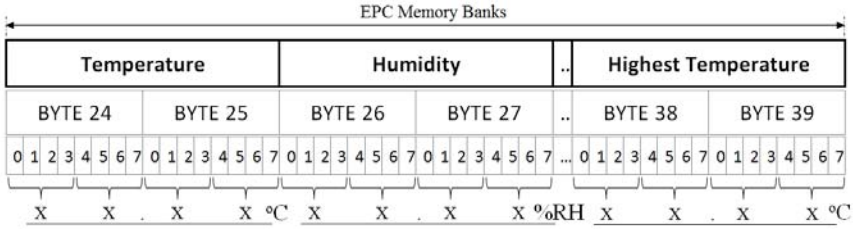

Figure 8–11: Organization of the sensor readings into RFID chip memory.

individually isolating the tens, ones, tenths, and hundredths digits of the converted temperature/humidity values and storing each digit in four bits. Essentially translating the original values from Hex representation into readable base ten notation. The formatted data is then written to the start of the EPC memory banks as seen in Fig. 8–11. As an additional feature, the highest recorded temperature is retained by the MCU, and is also written to the end of the EPC memory banks at an asynchronous rate, based on when the highest temperature value is updated. In this way, the sensor data, along with the highest experienced temperature value, can be directly read by scanning the EPC of the RFID tag. Ultimately, the signal transmitted to the reader has the detected sensor data that is remotely recorded by a standard Gen2 commercial RFID reader.

8.4 Measured Results

8.4.1 Power Sensitivity and Reading Distance Measurements

A commercial RFID tag measurement system (Tagformance) [61] was used to evaluate the power sensitivity of the fabricated tag. The transmitter and receiver antennas in this measurement system provide a flat 6 dBi gain response at the frequency range of 800 to 1000 MHz. The transmit power was incremented by 0.1 dB

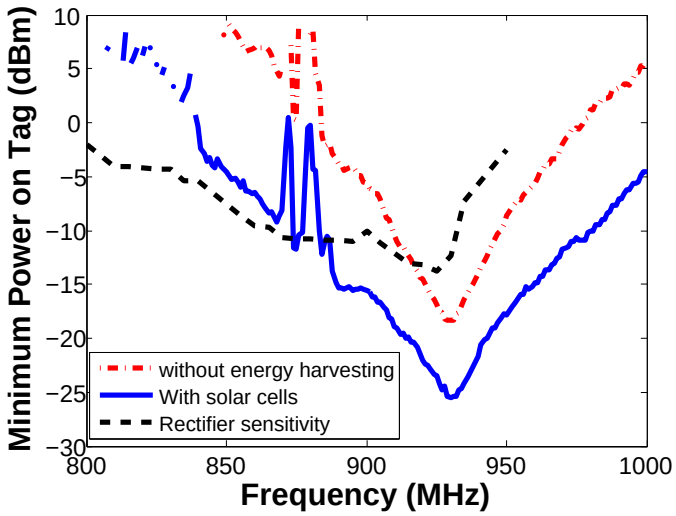

Figure 8–12: Measurement power sensitivity results for the RFID-based sensor with solar energy harvesting, without any energy harvesting method along with the rectifier's sensitivity.

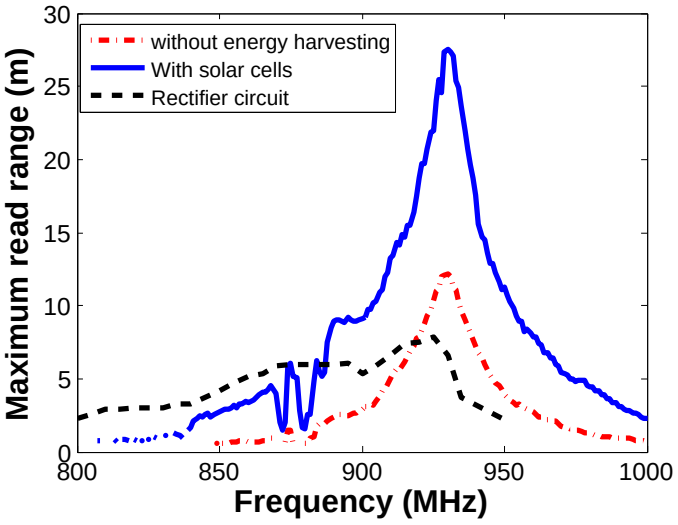

Figure 8–13: Measured maximum reading range of the RFID-based sensor with solar energy harvesting and without any energy harvesting method, along with the reading range of rectifier circuit.

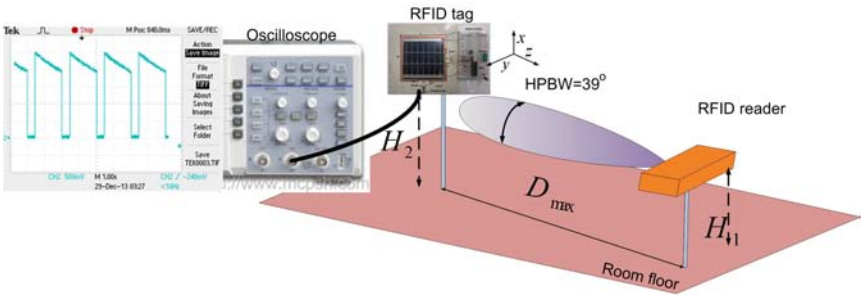

Figure 8–14: Schematic of the setup used for measuring tag's power sensitivity and maximum reading range with RF-DC energy harvesting.

steps (starting from 0 dBm) at each test frequency across the 800 MHz to 1000 MHz bands to detect the minimum power required to obtain a correct tag response. The distance between the reader and the tag in this commercial test system is 0.45 m. The required minimum power on tag to activate the RFID chip with and without solar energy are measured. The obtained power sensitivity results are presented in Fig. 8–12. Without any energy-harvesting source, the tag operates like an ordinary RFID tag and the required minimum on-tag power at 930 MHz is -18.27 dBm to generate a response. When the solar panel is connected, the sensor is powered up and the sensed data is dynamically updated into the RFID chip memory that has this additional power supply, and the required minimum on-tag power is reduced to -25.34 dBm at 932 MHz. The measurement is carried out inside the Lab under typical indoor lighting conditions. The maximum reading range is presented in Fig. 8–13. When there is solar energy harvesting, the proposed sensor achieves a maximum reading range of 27 m, while it exhibits a maximum reading range of 12.1 m without any additional energy source. To evaluate the RF energy harvesting circuits, the sensitivity of the rectifier is measured by sweeping the transmit power across the selected frequency band using the system setup shown in Fig. 8–14. The minimum power required to activate the charge pump and to obtain the output voltage of

2.4V at each frequency point is then recorded as shown in Fig. 8–12. As can be seen in the figure, the best sensitivity is achieved at 925MHz and is -13.8dBm. The power sensitivity of the rectifier circuit is less than the power sensitivity of the RFID tag in ordinary identification mode. Since the voltage generated from the rectifier circuit powers up the sensor, the MCU and the RFID chip, the reading range can be determined by the test setup shown in Fig. 8–14. The commercial RFID reader was mounted on a base at the height of H1=1.3 m above the ground. The tag also, as Fig. 8–14 demonstrates, was placed on a mast with the height of H2=1.3 m. By increasing the distance between the tag and the reader while observing the output voltage on an oscilloscope, the pertinent reading range is determined while an output of 2.4 V is achieved. The results are presented in Fig. 8–13. At the operating frequency of 932MHz, the maximum reading of 7.48 m was obtained. Beyond this distance the tag was not able to generate the voltage required to power up the sensor and the MCU. It should be noted that the allowed maximum transmit power of the reader is determined by the effective isotropic radiated power (EIRP) of 3.2 W (ERP 2 W) recommended by the European Telecommunications Standards Institute (ETSI) [17]. For other countries that allow 4 W EIRP, a 10.43% should be added to the reading range results. In addition, Table 8–2 presents a comparison between the performance of the proposed sensor and pertinent designs from the literature employing different antenna configurations and energy harvester systems (referred in section 8.1 of this Chapter). It can be seen that the proposed sensor achieves superior performance in terms of maximum communication distance from the reader and with the integration of energy harvester systems.

Table 8–2: Comparison between the the proposed sensor and pertinent designs from literature.

	Tag Antenna	Supply Energy	Reading Range
[120]	Single antenna	Battery	22 m
[115]	Dual antenna	RF-DC harvester	5 m
[95]	Single antenna	Solar cells	22 m
		RF-DC harvester	3 m
Proposed sensor	Multi feed antenna	Solar cells	27 m
		RF-DC harvester	7.48 m

8.4.2 Temperature and Humidity Measurements

To verify RFID-based wireless sensor capabilities to perform environmental sensing (temperatures and humidity), the following experiments were conducted in a climate chamber which was available at the time of measurement. The RFID sensor was placed close to the RFID reader antenna at distance of 0.5 m, which is in the far field region of the antenna. A commercial reader (GAO 216010) [20], with the operation frequency band of 902-928 MHz, was used to interrogate the RFID sensor and collect the sensor data at the host PC. The nominal temperature range of the climate chamber was from 4^0C to 45^0C (no light inside the chamber) and 10^0C to 45^0C (with light inside the chamber) with $\pm 0.5^0$C tolerance. The humidity range of the chamber was from ambient to a maximum of 85% RH at 28^0C with an error of 3% RH. In this measurement, the chamber was programmed to change temperature from 20^0C to 30^0C, and then to go back to 25^0C in 90 minutes. Every 5 minutes the RFID reader interrogated the RFID sensor and collected sensor data at the host PC. The measured results from the proposed sensor in conjunction with measured results of the wired probe thermometer are plotted in Fig. 8–15. The measured results of the proposed sensor show excellent agreement with those of a wired probe thermometer. Also, the relative humidity of the climate chamber was swept 50% to 80% RH in 200

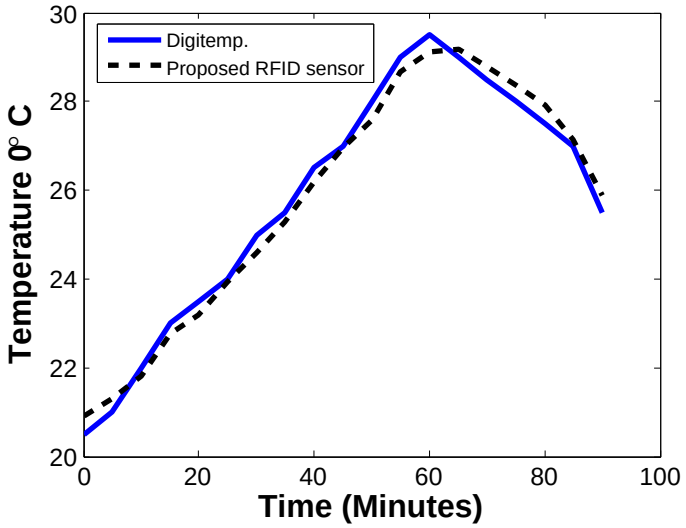

Figure 8–15: Comparison between a wired Digitemp probe Thermometer and proposed RFID-based sensor.

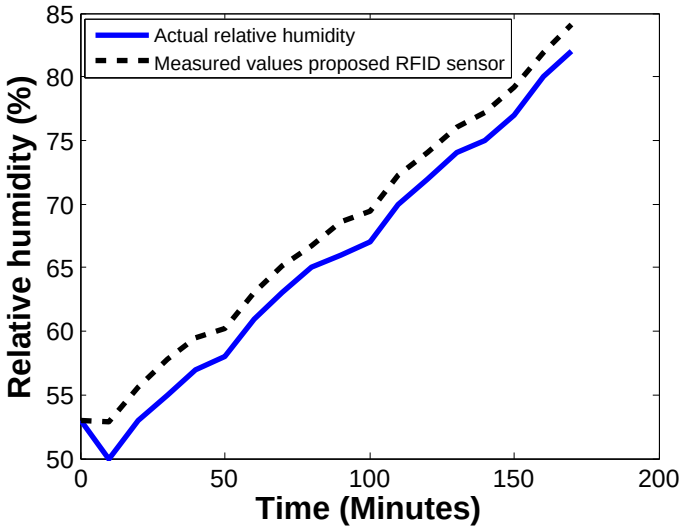

Figure 8–16: Comparison between actual relative humidity values and received values from the proposed sensor.

minutes. The measured results are plotted in Fig. 8–16, showing excellent agreement within the error tolerance range of the chamber. The actual relative humidity in comparison with the ambient humidity were read from the chamber's indicator.

8.5 Summary

RFID tag-enabled sensors for the transmission of generic sensor data were successfully implemented and experimentally evaluated. In this chapter first, a single-port RFID tag antenna was integrated with an I^2C-RFID chip along with a microcontroller unit (MCU) and a sensor to implement a low-cost wireless temperature sensor using a commercial RFID reader. The MCU was used to sample the output signal of the temperature sensor and write the pertinent data into the RFID chip. The required operating power of the MCU and the external sensor was generated by using solar energy via the solar cells placed on top of the patch antenna. The measurements of the fabricated tag-based sensor demonstrated that a maximum sensing/reading range of 26 m was achieved when all the circuits were powered using solar energy. When the tag was operated as a simple RFID tag with no energy harvesting employed to power up the passive RFID chip, a 11.9 m reading range was obtained.

Second, a two-port RFID tag antenna integrated with a new generation I^2C RFID chip was also presented in this chapter. Dual energy-harvesting sources were incorporated in the tag design to support operation of the sensor and of the MCU as well as extending the reading range of the RFID tag. The enabling feature of this tag design is a two-port patch antenna with inductive loop feeds for connection to the RFID chip and RF to DC energy harvesting circuitry. Also, solar panel was used to power up the sensor and support the MCU, resulting in a maximum reading range of 27 m for the RFID tag sensor, while a reading range of 12.1 m was achieved when no energy-harvesting was used. The maximum reading range achieved with the RF-DC energy harvesting technique was 7.48 m. However, with this option,

the reading range can be further increased by implementing more efficient RF-DC converter circuit an optimal port placement. To observe the RFID-based wireless sensor performance, the RFID sensor was evaluated in a climate chamber. The measured results demonstrated that the sensor data was successfully recorded with an excellent accuracy using a commercial RFID reader.

Chapter 9

Conclusions

9.1 Thesis Summary and Conclusions

In this thesis various miniaturized RFID tag antennas and tag-enabled sensors for passive UHF RFID system were investigated and implemented. Three compact printed monopole antennas were fabricated for use in UHF RFID tags that contain a chip with an input impedance of $8.2 - j61\Omega$. A method for measuring the radiation pattern of the passive RFID tag was presented using a network analyzer and by determining a calibrated S_{21}. Using the proposed method the radiation pattern of an assembled tag antenna including the chip can be measured without he use of probes or cables directly connected to the antenna. This is important, as it represents how the tag is used in practice. The radiation pattern of the prototyped meander monopole tag was obtained using the proposed test method and the measured results show very good agreement with the simulated results using an EM simulator (HFSS). The power sensitivity of the designed RFID tags was also measured by sweeping the power and determining the minimum power level needed for generating a correct response to a command. The experimental results also demonstrated that

the maximum readable range of the proposed folded, 2D and 3D meander monopole tags are 6.38 m, 5.39 m and 5.24 m, respectively, with an EIRP of 3.28 W. A tunable compact printed folded monopole tag antenna was also presented. The proposed tag antenna was integrated with an RFID chip whose operational frequency covers the global regulated UHF RFID bands. For size reduction and tuning, a tunable inductor was incorporated in the tag antenna, resulting in an area reduction of 36.5% comparing with a conventional folded monopole tag antenna. The tag was fabricated and experimentally evaluated; the frequency response was measured with the proposed new method using a network analyzer, and by determining a calibrated S_{11}. Other parameters, such as power sensitivity, differential radar cross section and reading range were also evaluated via a commercial RFID measurement system. All the measured results demonstrate that the tag can be tuned to operate efficiently at any desired UHF RFID band by using the tunable inductor. With a maximum effective isotropic radiated power of 3.28 W from the reader, the tag can be correctly identified within a distance of approximately 6 m in any region in the world (6 m in Japan and 5.9 m in North America, 6.1 m in Europe and China). The developed compact passive tag proves to be a viable solution that can be marketed globally for a variety of UHF RFID applications. To reduce tag sensitivity to the identification object, a miniaturized patch antenna using embedded electromagnetic band gap structures was presented in this thesis. Compared to a conventional microstrip patch antenna, the size of the proposed antenna is reduced by 29.11%. The antenna was fabricated for use in UHF RFID tags that contain a chip with an input impedance of $8.2 - j61\Omega$. For conjugate matching, the embedded inset feed was employed. Experimental results demonstrate that the proposed tag works efficiently in free space and

when placed on a metal plate. In both cases, a maximum readable range of almost 11m was achieved. Moreover, a printed meander monopole tag antenna incorporating a 4 cells by 4 cells AMC surface for UHF RFID applications was proposed. The designed tag antenna is integrated with an RFID chip with an input impedance of $8.2 - j61\Omega$. The T-matching technique was utilized in the antenna layout for conjugate matching. The achieved maximum reading ranges in free space and when tag was directly attached to a metal sheet were 10 m and 8.3 m, respectively. To improve the reading range of the passive tag, an enhanced passive tags (EPT) was designed and fabricated. A single feed patch antenna integrated with a new generation (Monza X) RFID chip was proposed and implemented. In this implementation, a thin film solar panel was used to provide a portion of the tag's operating power (in addition to harvesting RF energy) to extend the reading range. The measured results of the EPT demonstrate that the effective read range is increased by two times compared to an ordinary RFID tag. Another design was also proposed herein for extending the reading range which utilized a multiple-port RFID chip with multi-antennas to receive more than one copy of the signal from the reader. The measured results of the proposed dual tag antenna demonstrates superior performance in terms of communication range in comparison with a conventional single tag antenna.

Implementations of compact modern RFID tags that transmit data from on-board sensors were presented in this thesis as well. Various RFID tag-enabled sensors were designed and fabricated. First, RFID tags incorporating low-cost passive resistive sensors were implemented and experimentally evaluated. The proposed tag sensors contain multi-feed patch antennas with integrated resistive sensors. Single band antennas, operating at the 902-928 MHz (North American) frequencies, and

dual band antennas covering 865-868 MHz (European frequency band) and 902-928 MHz frequency bands were presented. The measured results demonstrate that the sensed data can be extracted using a commercial RFID reader, from the difference in the reader's output power for activating the two RFID chips integrated at two ports of a single tag antenna. Also, the tag was placed on a typical package containing consumer products and was experimentally evaluated. The measured results demonstrate that the proposed tag-based sensor is less sensitive to the loading effects of various commercial packages compared to a conventional RFID tag. It can be concluded that the proposed multi-port patch antennas equipped with resistive sensors are capable of serving as low-cost remote sensors for various applications including supply chain operations and transportation of sensitive items.

Finally, an RFID tag-enabled sensor for the transmission of generic sensor data was also successfully implemented and experimentally evaluated. A single-port RFID tag antenna was integrated with an I^2C-RFID chip along with a microcontroller unit (MCU) and an active sensor to implement a long-range wireless sensor system using a commercial RFID reader. A microcontroller unit was used to sample the output signal of the external active sensors and write the pertinent data into the RFID chip. The required operating power of the MCU and the external sensor was generated by using solar energy via a solar panel placed on top of the patch antenna. In addition, a novel multi-port UHF RFID tag antenna for enhanced energy harvesting of self-powered wireless sensors was proposed. The key and enabling feature of the tag design is a two-port patch antenna with inductive loop feeds for connection to the RFID chip, and RF to DC energy harvesting circuitry. Solar cells were also attached on top of the tag antenna to provide an alternative means for powering up

the sensor and supporting the MCU integrated with the tag. The measured results demonstrate that a maximum reading range of 27 m for the RFID tag sensor with solar energy was obtained, while a range of 12.1 m was achieved when no energy-harvesting was used to power the RFID chip. The achieved maximum reading range with the RF-DC energy harvesting technique was 7.48 m. The proposed sensor with dual energy harvesting achieves a longer reading distance and lifetime compared to similar battery-assisted sensor-enhanced RFID tags. Moreover, the prototyped RFID-tag sensor was tested in a climate chamber and showed excellent agreement with actual temperature and humidity measurements.

9.2 Future Work Recommendations

The works presented in this thesis focused on antenna design and energy harvesting to improve the power sensitivity and reading range of the tag as well as exploring new sensor applications. However, enhancement of modulated backscattring signals and reader sensitivity need to be investigated.Utilizing a PSK modulator based on a low-power consumption multi-port (four ports) receiver in tag's RFID chip that is proposed by the author in [126] can be investigated for implementation in UHF RFID system.

The design and implementation of RF-DC conversion circuits in multi-port UHF RFID tag antennas for enhanced energy harvesting of self-powered wireless sensors as presented in Chapter 7 can be extended to improve the reading range. Currently, the generated power from RF-DC circuitry is limiting the reading range of the sensor. To increase the communication range even further, the energy-harvesting capabilities of more sophisticated RF-DC converters can be integrated in future work. Also,

the digital circuit printed on the breadboard (of the digital section) is considerably bulky and could be miniaturized if integrated in the antenna layout. To expand the application of the proposed sensor in Chapter 8, the microcontroller unit (MCU) can be programmed to update the lowest or highest value of the sensor readings and compare it with the threshold value of the tagged packages. This feature can be used in tracking sensitive items that require a controlled climate environment and exceeding a threshold temperature or humidity will damage the packaged items. In addition, this data can be updated into the password-protected user memory of the RFID Gen2 chip. Consequently, only authorized RFID readers can wirelessly access the stored sensor data. Programming the reader to send a warning to the base station if the tag exceeds the threshold value can be considered as a next step for this type of application as well.

REFERENCES

[1] R. Want, "An introduction to RFID technology," *Pervasive Computing, IEEE*, vol. 5, no. 1, pp. 25–33, Jan 2006.

[2] J. Griffin and G. Durgin, "Complete link budgets for backscatter-radio and RFID systems," *Antennas and Propagation Magazine, IEEE*, vol. 51, no. 2, pp. 11–25, 2009.

[3] J.-W. Lee, D. H. T. Vo, Q.-H. Huynh, and S.-H. Hong, "A fully integrated HF-band passive RFID tag IC using 0.18 CMOS technology for low-cost security applications," *Industrial Electronics, IEEE Transactions on*, vol. 58, no. 6, pp. 2531–2540, 2011.

[4] D. Lee, S. Kim, H. Kim, and N. Park, "Mobile platform for networked RFID applications," *Information Technology: New Generations (ITNG), 2010 Seventh International Conference on*, pp. 625–630, 2010.

[5] Y. Zuo, "Survivable RFID systems: issues, challenges, and techniques," *Systems, Man, and Cybernetics, Part C: Applications and Reviews, IEEE Transactions on*, vol. 40, no. 4, pp. 406–418, 2010.

[6] G. Jadhav and S. Hamedi-Hagh, "UHF class-4 active two-way RFID tag for a hybrid RFID-based system," *RF and Microwave Conference (RFM), 2011 IEEE Internationa*, pp. 337–342, 2011.

[7] L. Zhang and X. Li, "A new resonant frequency tunable RFID tag antenna design," in *Microwave and Millimeter Wave Technology, 2008. ICMMT 2008. International Conference on*, vol. 3, 2008, pp. 1222–1225.

[8] O. technologies. RFID tag pricing guide. [Online]. Available: http://www.sii-ic.com

[9] L. Catarinucci, R. Colella, and L. Tarricone, "A cost-effective UHF RFID tag for transmission of generic sensor data in wireless sensor networks," *Microwave Theory and Techniques, IEEE Transactions on*, vol. 57, no. 5, pp. 1291–1296, 2009.

[10] A. E. Abdulhadi, D. Yi, M. Parvizi, and R. Abhari, "Multi-port UHF RFID tag antenna for enhanced energy harvesting of self-powered wireless sensors," in *Microwave Symposium Digest (IMS), 2014 IEEE MTT-S International*, 2014, pp. 1–4.

[11] G. Orecchini, L. Yang, M. Tentzeris, and L. Roselli, "High directivity passive UHF RFID tag with dual-radiating-body antenna," in *Antennas and Propagation Society International Symposium (APSURSI), 2010 IEEE*, 2010, pp. 1–4.

[12] Z. Su, S.-C. Cheung, and K.-T. Chu, "Investigation of radio link budget for UHF RFID systems," in *RFID-Technology and Applications (RFID-TA), 2010 IEEE International Conference on*, 2010, pp. 164–169.

[13] W. B. A. Chau T. C. and E. W. R, "Analysis and characterization of transponder antennae for radio frequency identification (RFID) systems," in *Packag. Technol. Sci.*, vol. 19, no. 1, 2006, pp. 33–44.

[14] A. Abdulhadi and R. Abhari, "Compact printed monopole tag antennas for UHF RFID applications," in *Antennas and Propagation Society International Symposium (APSURSI), 2010 IEEE*, 2010, pp. 1–4.

[15] L. Yang, S. Serkan Basat, and M. Tentzeris, "Design and development of novel inductively coupled RFID antennas," in *Antennas and Propagation Society International Symposium 2006, IEEE*, 2006, pp. 1035–1038.

[16] A. Abdulhadi and R. Abhari, "Tunable compact printed monopole antenna for passive UHF RFID tags," in *Antennas and Propagation Society International Symposium (APSURSI), 2012 IEEE*, 2012, pp. 1–2.

[17] K. V. S. Rao, P. Nikitin, and S. Lam, "Antenna design for UHF RFID tags: a review and a practical application," *Antennas and Propagation, IEEE Transactions on*, vol. 53, no. 12, pp. 3870–3876, 2005.

[18] A. Abdulhadi and R. Abhari, "Design and experimental evaluation of miniaturized monopole UHF RFID tag antennas," *Antennas and Wireless Propagation Letters, IEEE*, vol. 11, pp. 248–251, 2012.

[19] G. R. Inc. RFID reader,GAO216010. [Online]. Available: http://www.gaorfid.com/RFID-PDF/216010.pdf

[20] ——. RFID reader,GAO216010. [Online]. Available: http://www.gaorfid.com/RFID-PDF/216010.pdf

[21] A. Abdulhadi, H. M. Tehran, and R. Abhari, "Design and characterization of a miniaturized patch antenna for passive UHF RFID applications," in *Microwave Symposium Digest (MTT), 2012 IEEE MTT-S International*, 2012, pp. 1–3.

[22] H.-K. Ryu and J.-M. Woo, "Miniaturisation of rectangular loop antenna using meander line for RFID tags," *Electronics Letters*, vol. 43, no. 7, pp. 372–374, March 2007.

[23] J.-S. Kim, W. Choi, and G. young Choi, "Ceramic patch antenna for UHF RFID tag embedded in metallic objects," in *Antennas and Propagation Society International Symposium, 2009. APSURSI '09. IEEE*, June 2009, pp. 1–4.

[24] M. Lai and R. Li, "Broadband UHF RFID tag antenna with parasitic patches for metallic objects," *Microw. Opt. Technol. Lett.*, vol. 53, no. 7, pp. 1467–1470, Julyl 2011.

[25] A. Suntives and R. Abhari, "Miniaturization and isolation improvement of a multiple-patch antenna system using electromagnetic bandgap structures." in *Microw. Opt. Technol. Lett.*, vol. 55, no. 7, July 2013, pp. 1609–1612.

[26] I. Mayordomo, R. Berenguer, I. Fernandez, I. Gutierrez, W. Strauss, and J. Bernhard, "Simulation and measurement of a long-range passive RFID system focused on reader architecture and backscattering communication," in *Microwave Conference, 2008. EuMC 2008. 38th European*, 2008, pp. 1058–1061.

[27] U. Karthaus and M. Fischer, "Fully integrated passive UHF RFID transponder ic with 16.7- mu;w minimum RF input power," *Solid-State Circuits, IEEE Journal of*, vol. 38, no. 10, pp. 1602–1608, 2003.

[28] A. Vaz, A. Ubarretxena, D. Pardo, I. Sancho, and R. Berenguer, "Design methodology of a voltage multiplier for full passive long range UHF RFID," in *RFID Systems and Technologies (RFID SysTech), 2007 3rd European Workshop on*, 2007, pp. 1–4.

[29] J.-W. Lee and B. Lee, "A long-range UHF-band passive RFID tag IC based on high- Q design approach," *Industrial Electronics, IEEE Transactions on*, vol. 56, no. 7, pp. 2308–2316, 2009.

[30] B. Nilsson, L. Bengtsson, B. Svensson, U. Bilstrup, and P. Wiberg, "An active backscatter wake-up and tag identification extraction protocol for low cost and low power active RFID," in *RFID-Technology and Applications (RFID-TA), 2010 IEEE International Conference on*, 2010, pp. 86–91.

[31] H.-C. Liu, M.-C. Hua, C.-G. Peng, and J.-P. Ciou, "A novel battery-assisted Class-1 Generation-2 RF identification tag design," *Microwave Theory and Techniques, IEEE Transactions on*, vol. 57, no. 5, pp. 1388–1397, May 2009.

[32] A. Georgiadis and A. Collado, "Improving range of passive RFID tags utilizing energy harvesting and high efficiency Class-E oscillators," in *Antennas and Propagation (EUCAP), 2012 6th European Conference on*, March 2012, pp. 3455–3458.

[33] I. D. IC. Impinj Monza X- dura IC. [Online]. Available: http://www.impinj.com

[34] Q. Sheng, X. Li, and S. Zeadally, "Enabling next-generation RFID applications: Solutions and challenges," *Computer*, vol. 41, no. 9, pp. 21–28, Sept 2008.

[35] S.-W. Wang, W.-H. Chen, C.-S. Ong, L. Liu, and Y.-W. Chuang, "RFID application in hospitals: A case study on a demonstration RFID project in a Taiwan hospital," in *System Sciences, 2006. HICSS '06. Proceedings of the 39th Annual Hawaii International Conference on*, vol. 8, Jan 2006, pp. 184a–184a.

[36] G. Venkataramani and S. Gopalan, "Mobile phone based RFID architecture for secure electronic payments using RFID credit cards," in *Availability, Reliability and Security, 2007. ARES 2007. The Second International Conference on*, April 2007, pp. 610–620.

[37] L.-N. Albert, "RFID design fundamental and applications," *CRC Press*, 2011.

[38] L. Harvey, "RFID design principles," *ARTECH HOUSE*, 2008.

[39] B. Mioderag, S. David, and S. Ivan, "RFID systemes," *WILEY*, 2010.

[40] K. Nemai, "Handbook of smart antennas for RFID system," *WILEY*, 2010.

[41] P. Nikitin, K. V. S. Rao, and R. Martinez, "Differential RCS of RFID tag," *Electronics Letters*, vol. 43, no. 8, pp. 431–432, April 2007.

[42] A. Abdulhadi and R. Abhari, "Dual printed meander monopole antennas for passive UHF RFID tags," in *Antennas and Propagation (APSURSI), 2011 IEEE International Symposium on*, 2011, pp. 988–991.

[43] P. Nikitin and K. V. S. Rao, "Performance of RFID tags with multiple RF ports," in *Antennas and Propagation Society International Symposium, 2007 IEEE*, June 2007, pp. 5459–5462.

[44] G. Seigneuret, E. Bergeret, C. Moreaux, T. Deleruyelle, and P. Pannier, "Influence of multiantenna tag on the read range of a passive UHF RFID system," *Antennas and Wireless Propagation Letters, IEEE*, vol. 10, pp. 1174–1177, 2011.

[45] K. Noguchi, T. Moroya, M. Mizusawa, S. Betsudan, S. Makino, and T. Sasaki, "Broadband matching of a RFID antenna by using a T-type circuit," in *Antenna Technology, 2009. iWAT 2009. IEEE International Workshop on*, March 2009, pp. 1–4.

[46] S. Serkan Basat, S. Bhattacharya, L. Yang, A. Rida, M. Tentzeris, and J. Laskar, "Design of a novel high-efficiency UHF RFID antenna on flexible LCP substrate with high read-range capability," in *Antennas and Propagation Society International Symposium 2006, IEEE*, July 2006, pp. 1031–1034.

[47] K. Penttil, L. Sydnheimo, and M. Kivikoski, "Implementation of Tx/Rx isolation in an RFID reader," in *Int. J. Radio Freq. Identification Technol. Appl.*, vol. 1, no. 1, pp. 74–79.

[48] K. Payandehjoo and R. Abhari, "Employing EBG structures in multiantenna systems for improving isolation and diversity gain," *Antennas and Wireless Propagation Letters, IEEE*, vol. 8, pp. 1162–1165, 2009.

[49] R. Bhattacharyya, C. Floerkemeier, and S. Sarma, "RFID tag antenna based sensing: Does your beverage glass need a refill," in *RFID, 2010 IEEE International Conference on*, April 2010, pp. 126–133.

[50] J. Gao, J. Siden, and H.-E. Nilsson, "Printed electromagnetic coupler with an embedded moisture sensor for ordinary passive RFID tags," *Electron Device Letters, IEEE*, vol. 32, no. 12, pp. 1767–1769, 2011.

[51] Z. Yan, T. Laurence, and C. Jiming, "RFID and sensor networks," *CRC Press*, 2010.

[52] V. Chawla and D.-S. Ha, "An overview of passive RFID," *Communications Magazine, IEEE*, vol. 45, no. 9, pp. 11–17, 2007.

[53] H. Choo and H. Ling, "Design of electrically small planar antennas using inductively coupled feed," *Electronics Letters*, vol. 39, no. 22, pp. 1563–1565, 2003.

[54] K. Chung. Low cost and reliable RFID tags for all frequencies. [Online]. Available: http://www.avantetech.com

[55] C. Cho, H. Choo, and I. Park, "Broadband RFID tag antenna with quasi-isotropic radiation pattern," *Electronics Letters*, vol. 41, no. 20, pp. 1091–1092, Sept 2005.

[56] H.-W. Son and C.-S. Pyo, "Design of RFID tag antennas using an inductively coupled feed," *Electronics Letters*, vol. 41, no. 18, pp. 994–996, Sept 2005.

[57] K. S. Leong, M. L. Ng, and P. Cole, "Miniaturization of dual frequency RFID antenna with high frequency ratio," in *Antennas and Propagation Society International Symposium, 2007 IEEE*, June 2007, pp. 5475–5478.

[58] J. Griffin, G. Durgin, A. Haldi, and B. Kippelen, "RF tag antenna performance on various materials using radio link budgets," *Antennas and Wireless Propagation Letters, IEEE*, vol. 5, no. 1, pp. 247–250, Dec 2006.

[59] M. Ritamaki, A. Ruhanen, V. Kukko, J. Miettinen, and L. H. Turner, "Contactless radiation pattern measurement method for UHF RFID transponders," *Electronics Letters*, vol. 41, no. 13, pp. 723–724, June 2005.

[60] L. Ukkonen and L. Sydanheimo, "Threshold power-based radiation pattern measurement of passive UHF RFID tags," *PIERS Online*, vol. 6, no. 6, pp. 523–526, June 2010.

[61] V. Ltd. tagformance. [Online]. Available: http://www.voyantic.com/index.php?trg=home

[62] F. Paredes, G. Zamora, F. Herraiz-Martinez, F. Martin, and J. Bonache, "Dual-band UHF-RFID tags based on meander-line antennas loaded with spiral resonators," *Antennas and Wireless Propagation Letters, IEEE*, vol. 10, pp. 768–771, 2011.

[63] J. Dacuna and R. Pous, "Low-profile patch antenna for RF identification applications," *Microwave Theory and Techniques, IEEE Transactions on*, vol. 57, no. 5, pp. 1406–1410, May 2009.

[64] H.-W. Liu, C.-F. Yang, and C.-H. Ku, "Novel miniature monopole tag antenna for UHF RFID applications," *Antennas and Wireless Propagation Letters, IEEE*, vol. 9, pp. 363–366, 2010.

[65] Z. L. Ma, L. J. Jiang, J. Xi, and T. Ye, "A single-layer compact HF-UHF dual-band RFID tag antenna," *Antennas and Wireless Propagation Letters, IEEE*, vol. 11, pp. 1257–1260, 2012.

[66] B. Braaten, "A novel compact UHF RFID tag antenna designed with series connected open complementary split ring resonator (OCSRR) particles," *Antennas and Propagation, IEEE Transactions on*, vol. 58, no. 11, pp. 3728–3733, Nov 2010.

[67] B. Braaten, M. Reich, and J. Glower, "A compact meander-line UHF RFID tag antenna loaded with elements found in right/left-handed coplanar waveguide structures," *Antennas and Wireless Propagation Letters, IEEE*, vol. 8, pp. 1158–1161, 2009.

[68] B. Braaten and M. Aziz, "Using meander open complementary split ring resonator (MOCSRR) particles to design a compact UHF RFID tag antenna," *Antennas and Wireless Propagation Letters, IEEE*, vol. 9, pp. 1037–1040, 2010.

[69] A. Abdulhadi and R. Abhari, "Tunable compact printed monopole antenna for passive UHF RFID tags," in *Antennas and Propagation Society International Symposium (APSURSI), 2012 IEEE*, July 2012, pp. 1–2.

[70] M. Hirvonen, K. Jaakkola, P. Pursula, and J. Saily, "Dual-band platform tolerant antennas for radio-frequency identification," *Antennas and Propagation, IEEE Transactions on*, vol. 54, no. 9, pp. 2632–2637, 2006.

[71] L. Zhang and X. Li, "A new resonant frequency tunable RFID tag antenna design," in *Microwave and Millimeter Wave Technology, 2008. ICMMT 2008. International Conference on*, vol. 3, April 2008, pp. 1222–1225.

[72] S. Manzari, S. Pettinari, and G. Marrocco, "Miniaturized and tunable wearable RFID tag for body-centric applications," in *RFID-Technologies and Applications (RFID-TA), 2012 IEEE International Conference on*, Nov 2012, pp. 239–243.

[73] coilcraft inc. Tunable inductor. [Online]. Available: http://www.coilcraft.com

[74] T. Instruments. SMT EPC Gen2 IC, RI-UHF-IC116-00,. [Online]. Available: http://media.digikey.com/pdf/Data/RI-UHG-IC116-00.pdf

[75] S.-L. Chen, K.-H. Lin, and R. Mittra, "A measurement technique for verifying the match condition of assembled RFID tags," *Instrumentation and Measurement, IEEE Transactions on*, vol. 59, no. 8, pp. 2123–2133, Aug 2010.

[76] V. Kronverger, R. Wienstroer and B. Friedmann, "Gain determination of small UHF RFID antenna structures," in *International Symposium on Antenna and Propagation (ISAP)*, November 2010, pp. 23–26.

[77] Y. Choi, U. Kim, J. Kim, and J. Choi, "Design of modified folded dipole antenna for UHF RFID tag," *Electronics Letters*, vol. 45, no. 8, pp. 387–389, April 2009.

[78] M. Lai and R. Li, "A low-profile broadband RFID tag antenna for metallic objects," in *Microwave and Millimeter Wave Technology (ICMMT), 2010 International Conference on*, May 2010, pp. 1891–1893.

[79] T. V. Koskinen, H. Rajagopalan, and Y. Rahmat-Samii, "A thin multi-slotted dual patch UHF-band metal-mountable RFID tag antenna," *Microw. Opt. Technol. Lett.*, vol. 53, no. 1, pp. 40–47, Julyl 2011.

[80] L. Mo, H. Zhang, and H. Zhou, "Broadband UHF RFID tag antenna with a pair of U slots mountable on metallic objects," *Electronics Letters*, vol. 44, no. 20, pp. 1173–1174, September 2008.

[81] A. Abdulhadi and R. Abhari, "Passive UHF RFID printed monopole tag antenna for identification of metallic objects," in *Antennas and Propagation Society International Symposium (APSURSI), 2012 IEEE*, July 2012, pp. 1–2.

[82] R. Abhari and G. Eleftheriades, "Metallo-dielectric electromagnetic bandgap structures for suppression and isolation of the parallel-plate noise in high-speed circuits," *Microwave Theory and Techniques, IEEE Transactions on*, vol. 51, no. 6, pp. 1629–1639, June 2003.

[83] D. Kim and J. Yeo, "Low-profile RFID tag antenna using compact AMC substrate for metallic objects," *Antennas and Wireless Propagation Letters, IEEE*, vol. 7, pp. 718–720, 2008.

[84] B. Gao and M.-F. Yuen, "Passive UHF RFID packaging with electromagnetic band gap (EBG) material for metallic objects tracking," *Components, Packaging and Manufacturing Technology, IEEE Transactions on*, vol. 1, no. 8, pp. 1140–1146, Aug 2011.

[85] D. Kostka and R. Abhari, "Experimental evaluations of printed circuit board and on-chip inductors backed by AMC surfaces," *Antennas and Wireless Propagation Letters, IEEE*, vol. 8, pp. 720–723, 2009.

[86] D. M. Dobkin, "Radio basics for UHF RFID," in *in The RF in RFID: Passive UHR RFID in Practice, 1st ed. Burkington, MA: Newnes*, 2007, pp. 51–101.

[87] P. Nikitin and K. V. S. Rao, "Performance limitations of passive UHF RFID systems," in *Antennas and Propagation Society International Symposium 2006, IEEE*, July 2006, pp. 1011–1014.

[88] N. Tran, B. Lee, and J.-W. Lee, "Development of long-range UHF-band RFID tag chip using schottky diodes in standard CMOS technology," in *Radio Frequency Integrated Circuits (RFIC) Symposium, 2007 IEEE*, 2007, pp. 281–284.

[89] H.-C. Liu, Y.-F. Chen, and Y.-T. Chen, "A frequency diverse Gen2 RFID system with isolated continuouswave emitters," *J. Networks*, vol. 2, no. 5, pp. 54–60, Sep. 2007.

[90] A. Sample, J. Braun, A. Parks, and J. Smith, "Photovoltaic enhanced UHF RFID tag antennas for dual purpose energy harvesting," in *RFID (RFID), 2011 IEEE International Conference on*, April 2011, pp. 146–153.

[91] P. INC. Flexible thin-film. [Online]. Available: http://www.powerfilmsolar.com

[92] K. Lee and Y. C. Chung, "High gain Yagi-Uda UHF RFID tag antennas," in *Antennas and Propagation Society International Symposium, 2007 IEEE*, June 2007, pp. 1753–1756.

[93] J. Gao, J. Sidn and H.-E. Nilsson, "Printed temperature sensors for passive RFID tags," *in Proc. 27th Conf. PIERS, 2010*, pp. 845–849, 2010.

[94] J. Gao, J. Siden, H. Nilsson, and M. Gulliksson, "Printed humidity sensor with memory functionality for passive RFID tags," *Sensors Journal, IEEE*, vol. 13, no. 5, pp. 1824–1834, 2013.

[95] A. Sample, D. Yeager, P. Powledge, A. Mamishev, and J. Smith, "Design of an RFID-based battery-free programmable sensing platform," *Instrumentation and Measurement, IEEE Transactions on*, vol. 57, no. 11, pp. 2608–2615, 2008.

[96] M. Philipose, J. Smith, B. Jiang, A. Mamishev, S. Roy, and K. Sundara-Rajan, "Battery-free wireless identification and sensing," *Pervasive Computing, IEEE*, vol. 4, no. 1, pp. 37–45, Jan 2005.

[97] L. Catarinucci, R. Colella, and L. Tarricone, "Sensor data transmission through passive RFID tags to feed wireless sensor networks," in *Microwave Symposium Digest (MTT), 2010 IEEE MTT-S International*, 2010, pp. 1772–1775.

[98] ——, "Enhanced UHF RFID sensor-tag," *Microwave and Wireless Components Letters, IEEE*, vol. 23, no. 1, pp. 49–51, 2013.

[99] J. Siden, X. Zeng, T. Unander, A. Koptyug, and H.-E. Nilsson, "Remote moisture sensing utilizing ordinary RFID tags," in *Sensors, 2007 IEEE*, 2007, pp. 308–311.

[100] Y. Jia, M. Heiss, Q. Fu, and N. Gay, "A prototype RFID humidity sensor for built environment monitoring," in *Education Technology and Training, 2008. and 2008 International Workshop on Geoscience and Remote Sensing. ETT and GRS 2008.*, vol. 2, 2008, pp. 496–499.

[101] A. Babar, S. Manzari, L. Sydanheimo, A. Elsherbeni, and L. Ukkonen, "Passive UHF RFID tag for heat sensing applications," *Antennas and Propagation, IEEE Transactions on*, vol. 60, no. 9, pp. 4056–4064, 2012.

[102] G. Marrocco, L. Mattioni, and C. Calabrese, "Multiport sensor RFIDs for wireless passive sensing of objects-basic theory and early results," *Antennas and Propagation, IEEE Transactions on*, vol. 56, no. 8, pp. 2691–2702, 2008.

[103] J. Siden, J. Gao, and B. Neubauer, "Microstrip antennas for remote moisture sensing using passive RFID," in *Microwave Conference, 2009. APMC 2009. Asia Pacific*, 2009, pp. 2375–2378.

[104] Z. Jiang and F. Yang, "Reconfigurable RFID tag antenna for wireless temperature monitoring," in *Antennas and Propagation Society International Symposium (APSURSI), 2012 IEEE*, 2012, pp. 1–2.

[105] S. Caizzone, C. Occhiuzzi, and G. Marrocco, "Multi-chip RFID antenna integrating shape-memory alloys for detection of thermal thresholds," *Antennas and Propagation, IEEE Transactions on*, vol. 59, no. 7, pp. 2488–2494, 2011.

[106] G. Marrocco and F. Amato, "Self-sensing passive RFID: From theory to tag design and experimentation," in *Microwave Conference, 2009. EuMC 2009. European*, 2009, pp. 001–004.

[107] G. Manzi and M. Feliziani, "Impact of UHF RFID IC impedance on the RFID system performances in presence of dielectric materials," in *Electromagnetic Compatibility - EMC Europe, 2008 International Symposium on*, 2008, pp. 1–6.

[108] A. Cataldo, G. Monti, E. De Benedetto, G. Cannazza, and L. Tarricone, "A noninvasive resonance-based method for moisture content evaluation through microstrip antennas," *Instrumentation and Measurement, IEEE Transactions on*, vol. 58, no. 5, pp. 1420–1426, 2009.

[109] P. Soontornpipit, C. Furse, Y. C. Chung, and B. Lin, "Optimization of a buried microstrip antenna for simultaneous communication and sensing of soil moisture," *Antennas and Propagation, IEEE Transactions on*, vol. 54, no. 3, pp. 797–800, 2006.

[110] R. Bhattacharyya, C. Floerkemeier, and S. Sarma, "RFID tag antenna based temperature sensing," in *RFID, 2010 IEEE International Conference on*, 2010, pp. 8–15.

[111] P. Nikitin, K. V. S. Rao, and R. Martinez, "Differential RCS of RFID tag," *Electronics Letters*, vol. 43, no. 8, pp. 431–432, 2007.

[112] B. C. Vishay. Thermistors - NTC NTC 680ohms. [Online]. Available: http://www.vishay.com/sensors-temperature/ntc/

[113] S. Caizzone and G. Marrocco, "RFID grids: Part II -experimentations," *Antennas and Propagation, IEEE Transactions on*, vol. 59, no. 8, pp. 2896–2904, 2011.

[114] G. Marrocco, "RFID grids: Part I: Electromagnetic theory," *Antennas and Propagation, IEEE Transactions on*, vol. 59, no. 3, pp. 1019–1026, 2011.

[115] D. De Donno, L. Catarinucci, and L. Tarricone, "Enabling self-powered autonomous wireless sensors with new-generation I2C-RFID chips," in *Microwave Symposium Digest (IMS), 2013 IEEE MTT-S International*, 2013, pp. 1–4.

[116] A. Vaz, A. Ubarretxena, I. Zalbide, D. Pardo, H. Solar, A. Garcia-Alonso, and R. Berenguer, "Full passive UHF tag with a temperature sensor suitable for human body temperature monitoring," *Circuits and Systems II: Express Briefs, IEEE Transactions on*, vol. 57, no. 2, pp. 95–99, 2010.

[117] J. Virtanen, L. Ukkonen, T. Bjorninen, and L. Sydanheimo, "Printed humidity sensor for UHF RFID systems," in *Sensors Applications Symposium (SAS), 2010 IEEE*, 2010, pp. 269–272.

[118] T. I. Sensor. UHF RFID Gen2 SL900a. [Online]. Available: http://www.caenrfid.it.

[119] C. RFID. Esaytlog rfid tag. [Online]. Available: http://www.ids-microchip.com.

[120] D. De Donno, L. Catarinucci, and L. Tarricone, "A battery-assisted sensor-enhanced RFID tag enabling heterogeneous wireless sensor networks," *Sensors Journal, IEEE*, vol. 14, no. 4, pp. 1048–1055, April 2014.

[121] T. Instruments. microcontroller unit MSP430. [Online]. Available: http://www.ti.com/.

[122] ——. temperature sensor LM940. [Online]. Available: http://www.ti.com/.

[123] MicrowBattery. Lithium battery 3v. [Online]. Available: http://www.microbattery.com/s.nl/sc.2/category.9/.f

[124] A. Technologie. HSMS-285c schottky diodes. [Online]. Available: http://www.avagotech.com

[125] S. Seiko. Seiko S-882Z charge pumps. [Online]. Available: http://www.sii-ic.com

[126] A. Abdulhadi, A. Suntives, and R. Abhari, "Design of a SIW-based data communication system using a SIW six-port receiver," in *Electrical Performance of Electronic Packaging and Systems, 2009. EPEPS '09. IEEE 18th Conference on*, Oct 2009, pp. 151–154.